An analysis of recent extensive air shower data from the Durham array

Stewart, Thomas R.

AN ANALYSIS OF RECENT EXTENSIVE AIR SHOWER DATA FROM THE DURHAM ARRAY

by

Thomas R. Stewart, B.Sc.

A Thesis submitted to the
University of Durham for the degree
of Master of Science

Department of Physics
University of Durham

October, 1980

A B S T R A C T

A small sea level air shower array, consisting of 14 plastic scintillators providing both density and directional information, is described. The data collection electronics are described, and any recent improvements implemented during the period 1975 - 1977 are outlined.

The offline treatment of the data, from initial data checking to final analysis is described, and a quantitative assessment of the performance of the analysis programmes using simulated data, is presented.

The differential shower size spectrum slope, based on a sample of 650 events has been calculated as

$$\gamma = 2.95 \pm 0.2 \text{ for } 6.3 \times 10^5 < N < 2 \times 10^6$$

Finally, some discrepancies between the analysis of real and simulated data are presented, and some possible causes discussed.

PREFACE

The work described in this thesis was carried out during the period 1975 - 1977 while the author was working under the supervision of Dr. M. G. Thompson, in the Cosmic Ray Group of the Physics Department in the University of Durham.

During this time the author has been responsible for the specification and implementation of necessary improvements in the Durham extensive air shower array, and the running of an experiment to collect and analyse air shower data, yielding useful results in the region $5 \times 10^5 - 2 \times 10^6$ particles. The author has also been responsible for the writing of the air shower data simulation programme, and its use in testing the performance of both the experiment and the analysis programmes.

C O N T E N T S

CHAPTER 1

THE COSMIC RADIATION

1.1 INTRODUCTION

The discovery of cosmic rays over 60 years ago initiated a continuing investigation into the fundamental processes of nature, through their study, on both a microscopic and macroscopic level. Significant advances in the field of nuclear physics have occurred through the study of the interactions of the energetic particles in the past, and while particles with energies of up to 1500 GeV may currently be created in accelerator experiments, it is likely that the field of cosmic rays will play an important continued role in the testing of nuclear models at extrapolated energies of up to 10^{20} eV. Cosmic radiation consists of X rays, gamma rays, electrons and energetic nuclei, and covers a large range of primary energies. The study of the information that they carry, their origin, and their mass and energy spectra, provides the only direct knowledge about matter originating outside the solar system.

1.2 THE DISCOVERY OF THE RADIATION

At the turn of the century, experiments on the conductivity of shielded gases, by Elster and Geitel (Elster and Geitel 1899), revealed the presence of an ionising background radiation, thought at that time to originate from radioactive materials on earth. However, in 1912, Hess (Hess 1912) concluded from experiments involving airborne ionisation chambers, that the radiation was of extraterrestial origin, and that the sun was not the source of the majority of the radiation. These observations were given further proof by work performed by Millikan and Cameron (Millikan and Cameron 1926) using submerged sealed electroscopes to measure ionisation.

Initially the radiation was believed to be gamma rays, but experiments using Geiger Müller counters, performed by Bothe and Kolhörster (Bothe

and Kolhörster 1928) indicated the presence of charged particles in cosmic radiation at ground level. Work at this time on the latitude effect by Clay (Clay 1927) and Millikan and the discovery of the East-West effect by Johnson and Street (Johnson and Street 1933), in 1933, indicated that not only were cosmic ray primaries charged, but that the overall charge was positive.

Significant discoveries of new particles were made in cosmic ray study during the following twenty years. Anderson and Neddermeyer, (Anderson and Neddermeyer 1936) discovered the electron positron pair, already predicted by Dirac's relativistic quantum mechanics, and during the next decade the discovery of the meson and observation by Rochester and Butler of the Λ^{o} through its decay to positive and negative particles in a cloud chamber, were important early contributions to the field of particle physics.

1.3 THE PRIMARY COSMIC RAYS

The observed energy spectrum is best illustrated from a summary by Wolfendale (Wolfendale 1973) in Figure 1.1, together with the type of experiment which provides information about each energy range. One important feature of the energy spectrum is a change in slope at approximately 10^{16} eV, occurring over a small energy range. There have been various interpretations of this 'knee' in the primary spectrum; Kempa et al (1974) and Karakula et al (1974) have suggested that this may be the result of cosmic rays from discrete sources superimposed on a normal cosmic ray background, whereas Juliusson (Juliusson 1975) interprets this change in slope as the gradual breakdown in the retention of low charge particles by the galactic magnetic field.

The mass spectrum of the primaries may be measured directly at low energies, below $\sim 10^{12}$ eV/nucleon, by balloon borne or satellite experiments, with the accuracy decreasing with increasing energy. Recent results, reviewed by Bell (1974 b), suggest that beyond an energy of ~2 Gev/nucleon, the slope of the energy spectrum of lighter elements is steeper than that of heavier elements, indicating that at EAS

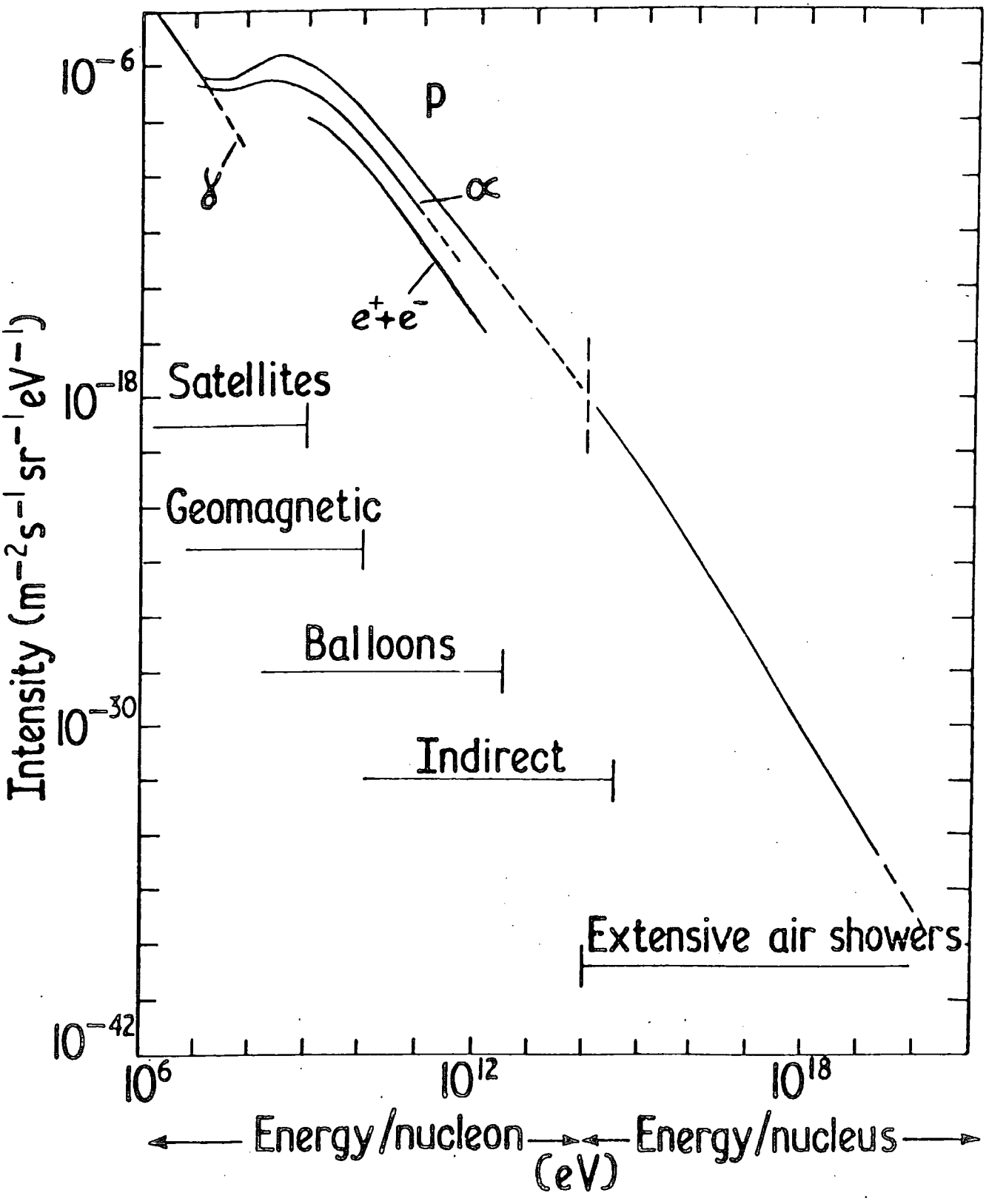

Figure 1.1: Primary cosmic ray spectra.
(After Wolfendale, 1973)

Energy	Total No. Of Events	% Protons and Neutrons	% α Particles	% Heavier Particles
3.7 x 10"eV	46	80	13	7
Universal Composition	-	99	<1	$<.02$

Table 1.1: Mass distribution of primary cosmic rays obtained from a balloon borne experiment flown at an atmospheric depth of approximately 22 gcm^{-2}. (Malhotra et al 1966).

energies, the heavier elements would dominate in the primary particles.

Table 1.1 illustrates the mass distribution obtained by Malhotra et al (Malhotra et al 1966) at an energy of 3.7×10^{11} eV/nucleon. At particle energies above approximately 10^{12} eV/nucleon, there is no direct information concerning the mass composition, although conclusions may be drawn from multiple muon studies (Elbert et al 1975), which indicate that at energies of approximately 10^{14} eV/nucleon, there may be an enrichment of heavier nuclei . In this energy region, the primary spectrum is estimated indirectly by the assumption of interaction models to relate the primaries to the ground level observations. The mass composition at these higher energies is not only important in the studies of the origin of cosmic rays, but also has important astrophysical implications, since the composition of the primary beam places severe constraints on the structure and strength of the Galactic magnetic field.

Work by Greisen (Greisen 1966), Roll and Wilkinson (Roll and Wilkinson 1966), and Strong (Strong et al 1974), has indicated that a cutoff in cosmic ray intensity should occur around 10^{20} eV, due to interaction with the 2.7 K background radiation. However, the expected resultant steepening of the primary spectrum has not been observed in results from both Sydney (Bell et al 1974) and Haverah Park (Edge et al 1973) arrays. Local containment by magnetic fields of the very high energy charged particles, in the region of galactic clusters may explain this) but clearly a more accurate spectrum estimation in this region is required.

1.4 THE EXTENSIVE AIR SHOWER

The Extensive Air Shower (EAS) has been the subject of detailed study for approximately 40 years. The early experiments (Auger et al 1939) Kolhörster (1938) were concerned with establishing the main characteristics of the EAS and linking the effect to the already well known electromagnetic cascades produced by the passage of high energy

electrons and photons through matter. The early ground level experiments studying the electromagnetic components used widely spaced counters to detect the simultaneous arrival of charged particles over hundreds of square metres, a sampling technique similar to that used by the majority of modern particle arrays.

Other experiments at this time (Fromen and Stearns 1938) indicated the presence of a 'hard' component capable of passing through 15 cm of lead without interaction, proving that the electromagnetic cascade theory alone was not the full explanation of the development of EAS. Later balloon work using nuclear emulsions discovered the presence of protons and heavier nuclei in the primary radiation. Spurred by the fact that EAS were the result of the interactions of the highest energy cosmic ray primaries, interest in EAS increased and gradually, during the last three decades, a standard model of the generation of EAS in the atmosphere has been developed.

Extensive air showers are initiated by the interaction of a primary cosmic ray particle with an air nucleus at an average depth of 80 gm/cm^{-2} in the earths atmosphere. The primary particle is assumed to lose approximately half its energy in this and subsequent interactions, producing from each, secondary particles, which are mostly pions, π^+, π^-, and π^o in roughly equal numbers. The multiplicity, energy and transverse momentum distributions of these secondary pions are the subject of considerable current interest. The description of pion production in the proton-proton (p-p) interaction has been divided up broadly into two models; the 'Standard Model', and the 'Scaling Model'.

The main features of the 'Standard model', arose empirically from accelerator data available in the mid 1960's for primary energies up to approximately 3×10^{10}eV. The pion multiplicity is assumed to vary with primary energy Ep as Ep^{α}, the mean transverse momentum, $\langle P_t \rangle$, rising slowly with Ep, from a value of 0.4 GeV/c at $Ep = 10^{12}$eV, and the pion energy spectrum according to the empirical formulae of Cocconi, Koester and Perkins, (1961).

Recent pion production data, however, obtained from the CERN Intersecting Storage Rings, for primary energies up to 1.5×10^{12}eV are consistent with the predictions from the 'Scaling' hypothesis of Feynman (1969), indicating a logarithmic rise of the pion multiplicity with Ep, near constancy of $\langle P_t \rangle$, and the distribution of fractional energy taken by the secondary pions from the interaction independent of proton energy, in the region 10^{10} - 10^{12}eV. From a comparison of the pion multiplicities predicted from the 'Scaling' hypothesis, with those derived from cosmic ray experiments, 'Scaling' appears to break down at energies greater than approximately $Ep = 10^{14}$eV; but some agreement may be restored if the mean mass of primary cosmic ray particles is assumed to increase sharply for $E_p > 10^{15}$ eV

The charged pions either interact again to continue the nuclear active cascade, or decay to weakly interacting muons, which usually survive to sea level, carrying with them much more information about the early shower development than the electromagnetic component. The nuetral pions decay immediately

into pairs of photons, which in turn, may initiate electromagnetic cascades, the superposition of which, coupled with scattering through the atmosphere, constitute the bulk of the particles observed as the shower at ground level. As the available energy in the shower is distributed among an increasing number of secondaries, mainly electrons, the mean particle energy is reduced, until the energy transfer through Bremsstrahlung becomes less important than the energy loss through ionisation. At this energy, approximately 84 MeV for electrons, the number of particles in the shower starts to decrease. The mean depth in the atmosphere of shower maximum development, together with the fluctuations in this quantity are regarded as important parameters in determining the primary mass composition; a heavy primary having smaller fluctuations in a decreased depth of shower maximum. It is thought that future experiments studying the Cerenkov light emitted by showers during their passage through the atmosphere, will provide important high quality experimental data on this subject.

1.5 THE EAS COMPONENTS

As has been discussed above, the various components found in EAS may be broadly classified into three groups; the electron, muon and nucleon components. The electron component is by far the most numerous component in an extensive air shower. The lateral spread of electrons may be described well over a large range of radii and shower size, by a density distribution function, commonly referred to as the structure function, which may be approximated by the expression due to Greisen (Greisen 1960)

$$f\left(\frac{r}{r_1}\right) = C(s)\left(\frac{r}{r_1}\right)^{s-2}\left(\frac{r}{r_1}+1\right)^{s-4.5}$$

where s is the so called cascade age parameter, r_1 is the scattering length for electrons in air, frequently called the Molière unit with a

——— Catz $\rho(N,r) = \frac{0.0157\ N \exp(-r/120)}{(r+1)^{1.62}}$

— — — NKG $\rho(N,r) = \frac{0.45\ N}{r_1^2}\left(\frac{r_1}{r}\right)^{.75}\left(\frac{r_1}{r+r_1}\right)^{3.25}$

— · — Hasegawa $\rho(N,r) = \frac{N}{2\pi(120\pi)^{\frac{1}{2}}}\frac{\exp(-r/120)}{r^{1.5}}$

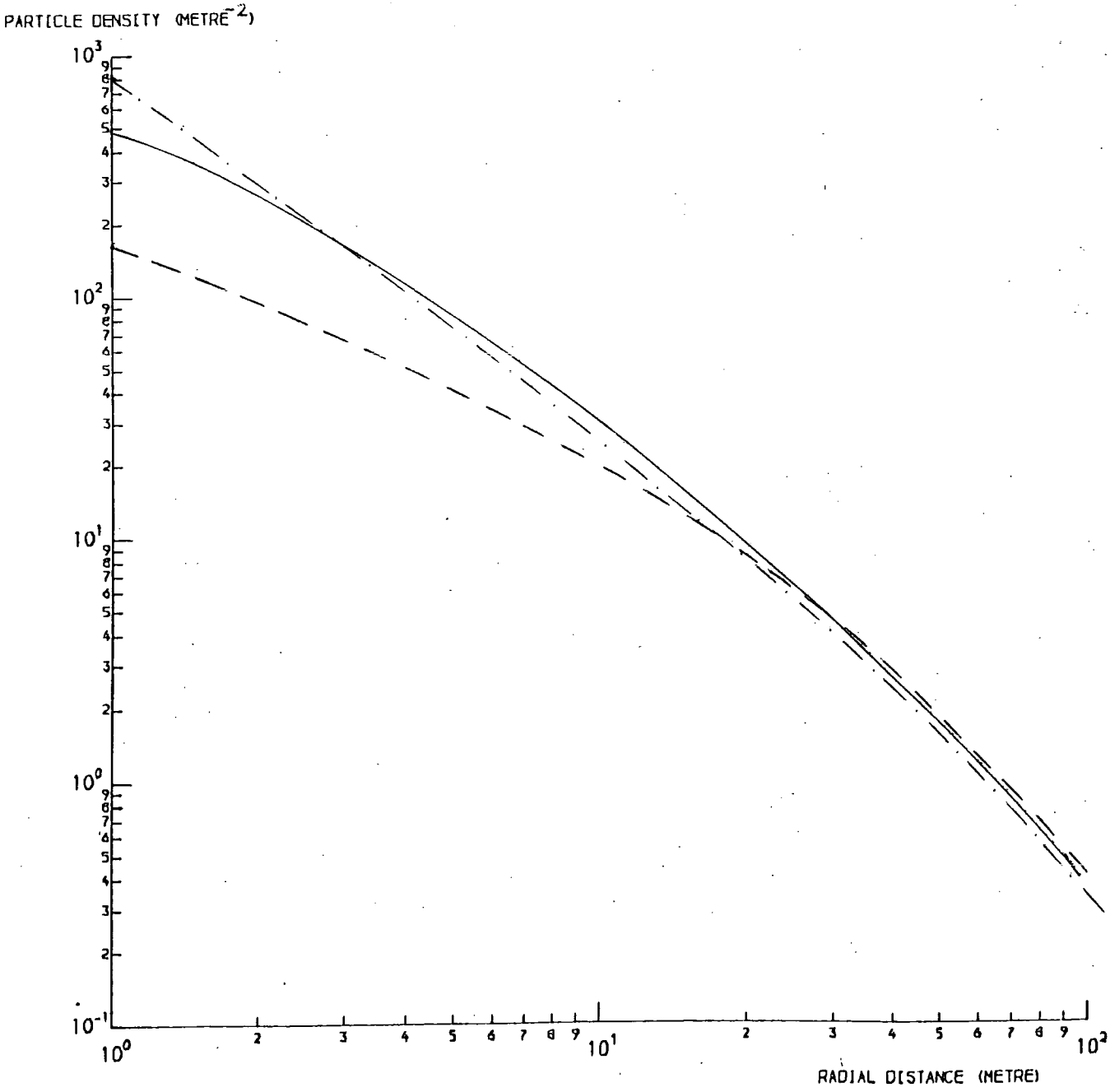

FIGURE 1.2 The lateral structure function obtained by several authors, normalised to N = 10^5 particles.

value of 79 m at sea level, C(s) is a normalising factor and

$$f(r) = \frac{r_1^2 \rho(r)}{N}$$

where $\rho(r)$ is the particle density at radius r and N is the total number of particles in the shower. The age parameter, over the range 10^3 - 10^9 particles, appears to be virtually constant in the range 1.2 - 1.25, contrary to the behaviour expected from a single pure electromagnetic cascade. It has been noted (Hasegawa 1962) that the structure function often depends on the method of detection of the EAS, plastic scintillators producing a slightly steeper function than Geiger Müller counters, due to the dependence of the scintillator response on the energy spectrum of the electromagnetic component. To examine the sensitivity of the experiment to this effect, two other structure functions have been considered for use in this work; the function due to Hasegawa and that due to Catz (Catz et al 1975). As illustrated in Figure 1.2, there is still good agreement between them in the range 10 - 100 metres.

Muons are able to provide more direct data about the early stages of shower development, since they interact weakly, and because of the fact that they are not appreciably scattered in the earth's atmosphere, their arrival direction reflects the direction of emission of the parent particle. Studies of muons in showers may be broadly divided into two energy regions; low energy at $\sim$10 GeV and high energy at $\sim$1000 GeV. The study of the low energy muon structure function, tied in with shower development models, yields valuable information about the multiplicity of pion production in the very first interactions in the shower. Recent models give muon lateral distributions narrower than those observed experimentally using shielded detectors, indicating that either the assumed pion production mean transverse momentum is too low, or that the muons should be

produced higher in the atmosphere. Recent work on high energy muons (Adcock 1970, 1971) in Utah, has produced some interesting results on both pion production multiplicity and mean transverse momentum at production energies of around 10^{14} - 10^{15} eV. Measurement of muon decoherence curve undergound, together with theoretical predictions for various mean transverse momenta, indicate a mean value of $P_T = 0.6 \pm .05$ GeV/c, while the measured ratio of multiple muon rates recorded in a large area detector, support a pion production multiplicity of $n_s = 2.7\ E^{\frac{1}{4}}$ where E is the nucleon energy in GeV.

Hadrons, comprising the nuclear active component of a shower, are far less numerous than the other particles, but because of their large energies and strong interaction with matter, are responsible for the generation and sustenance of the other shower components . The number of Hadrons in a shower correlate strongly with the total number of electrons almost independently of primary energy, clearly reflecting this role. From observations of the multicore structure of EAS (Dake et al 1971) conclusions have been drawn about the existence of hadrons with very high transverse momenta, about 10 GeV/c. There is inconsistency, however, between different experiments, and recent work by Greider (1977) suggests that the lateral distribution may be adequately described up to 1000 TeV, with only a small increase in transverse momentum.

Clearly there is still a requirement for investigation of EAS, perhaps by recording simultaneous measurements of each shower by different experiments. Any deductions made from the data rely on the quality of the measurement and the understanding of the assumptions made in the analysis. This thesis contains an account of the steps taken to achieve this aim.

CHAPTER 2
THE EXPERIMENT

2.1 INTRODUCTION

Chapter 1 has illustrated the existence of several areas of interest about which the further study of EAS may shed some additional light. Many arrays have been built in the past 20 years in pursuit of this aim, with very different geometries, at different altitudes, and with different detecting elements, ranging from scintillation counters, to arrays of Geiger Muller Tubes, to estimate the local particle density.

The Durham array, the particle detectors, their calibration, and the laboratory electronics, are described.

2.2 THE DURHAM ARRAY

Preliminary work began on the Durham array in 1973 and during the following three years, all of the fourteen plastic scintillator detectors originally planned, were completed. The array was intended not only to provide information on EAS in the form of shower size, direction and core position in a 'Stand Alone' mode, but also to provide shower data for the other EAS experiments in Durham, such as MARS, the Muon Automated Research Spectrograph (described in detail in Ayre 1971 and Whalley 1974), and the Hadron Chamber (Cooper 1974).

The array was therefore built to provide a flexibility in operational modes and fast data collection, with the storage of air shower event information in a digital form, for subsequent computer analysis. Work by Smith (Smith 1976) showed that the array geometry and the detector density measuring range adopted would provide useful extensive air shower information in the range 10^4 to 10^7 particles. A plan view of the array is shown in Fig. 2.1. The approximate symmetry along the main arms C-33, C-53 and C-13 is not important for the method

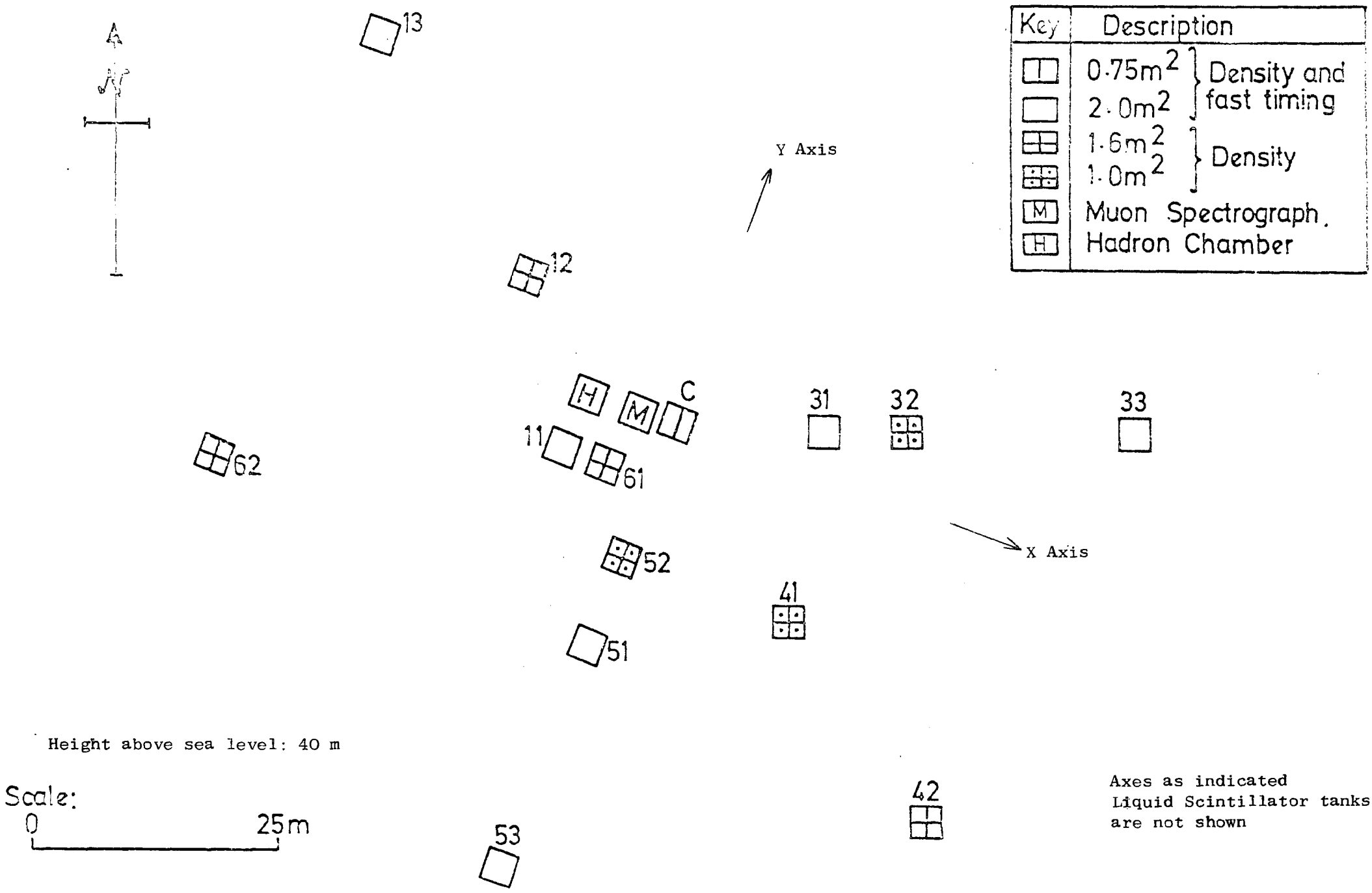

Figure 2.1: The Durham Extensive Air Shower Automated Research Array (After Treasure 1980)

of shower analysis adopted, but is useful in daily detector monitoring and fault finding procedures.

2.2.1 The Detectors

The detectors are of two types: Liquid Scintillator Tanks (a full description of these detectors and calibration may be found in Shaat 1979), and plastic scintillators of various designs housed in electrically screened light proof wooden boxes, raised from the ground on a metal frame and protected from the weather by a wooden hut, the total thickness of absorber above the scintillator being around $2g/cm^2$. The main characteristics of the plastic scintillators are shown in Table 2.1 and a schematic of each construction in Figure 2.2.

The output from each plastic scintillation detector is taken from a high input impedance, low output impedance amplifier situated at each detector site and this provides a density measurement in the range of from 1 to 80 particles/m^2. Note that the timing information from each of the timing detectors (C, 11, 13, 31, 33, 51, 53) is provided by an additional independent fast photomultiplier tube, one on each scintillator slab. Details of the photomultiplier linearity, base circuits, head amplifier design, and EHT distribution, may be found in Smith 1976.

2.2.2 Calibration of the Plastic Scintillator Density Detectors

Each detector used during the period of data collection relevant to this thesis, has been individually calibrated. It was decided, for ease of calibration, to adjust each density detector 'Single particle response' to $\pm$ 20% of the values tabled in Smith 1976, and to reduce the variation further in the analysis treatment. A similar method to that described in Smith 1976 was used to calibrate each detector; a

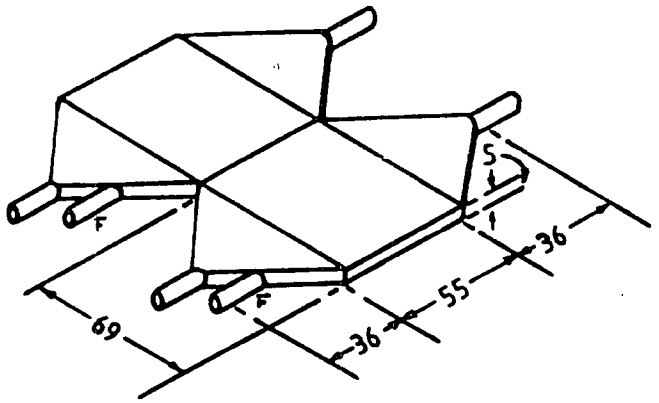

(a) The central detector (NE102A).

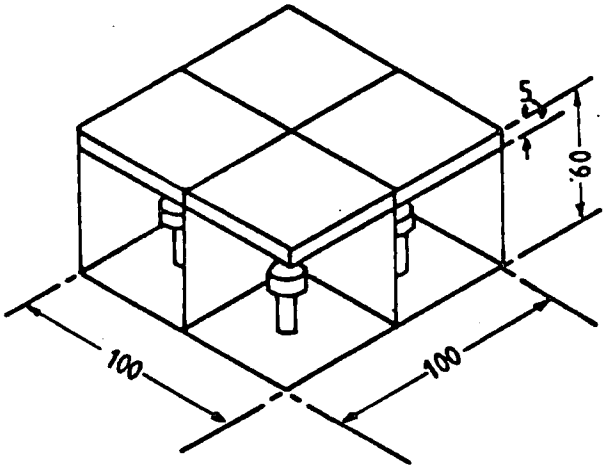

(b) A 1·0 m^2 detector (composition unknown).

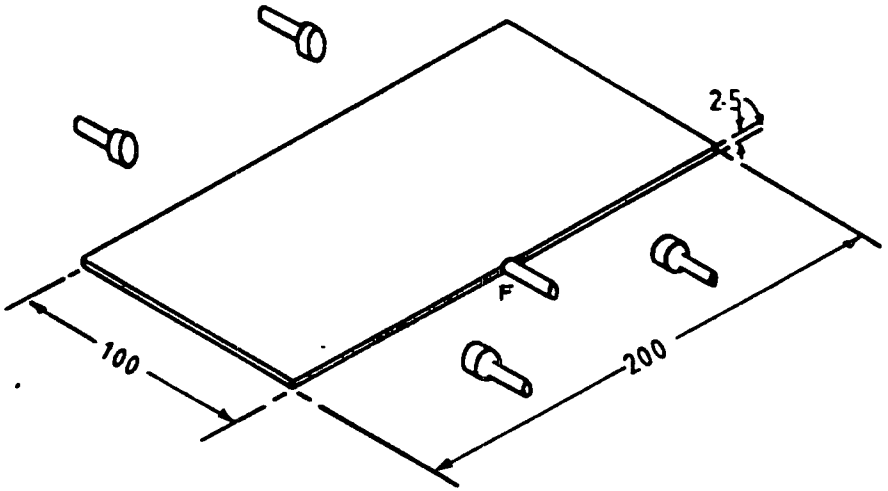

(d) A 2·0 m^2 detector (NE110).

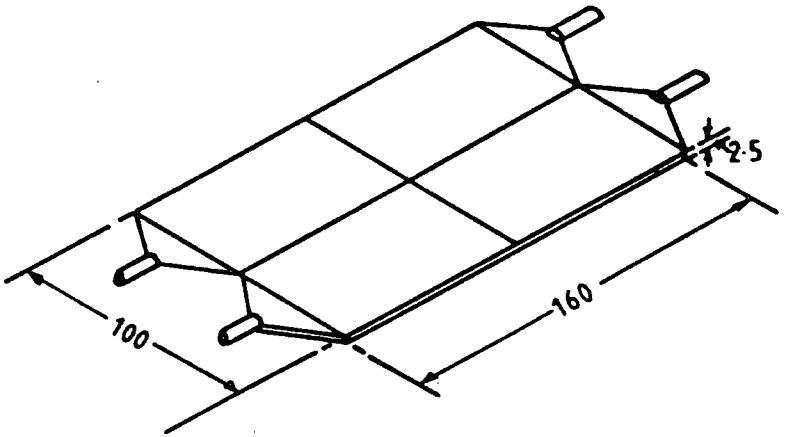

(c) A 1·6 m^2 detector (NE102A).

Figure 2.2: Schematic diagrams of detectors used in Durham array. (After Shaat 1979)
Fast photomultiplier tubes marked 'F'

Table 2.1: Main Characteristics of Each of the 4 Types of Plastic Scintillator Detectors Used in the Durham Array

Detector	Total Area (m^2)	Number of Slabs of Scintillator	Number of Photomultipliers Viewing Each Slab	Fast Timing
C	0.76	2	2	Yes
11,13,31,33, 51,53	2.00	1	4	Yes
12,42,61,62	1.6	4	1	No
32,41,52	1.0	4	1	No

Table 2.2: Calibration Information For The Plastic Scintillator Detectors

Detector	Ratio of Pulse Height at Calibration Point to Mean Pulse Height Over Whole Area (g)	Millivolt Corresponding to 1 particle/m^2 for each detector
C	0.89	89
11	1.41	69
13		74
31		67
33		81
51		65
53		71
12	1.0	62
42		134
61		79
62		93
32	1.0	117
41		97
52		95

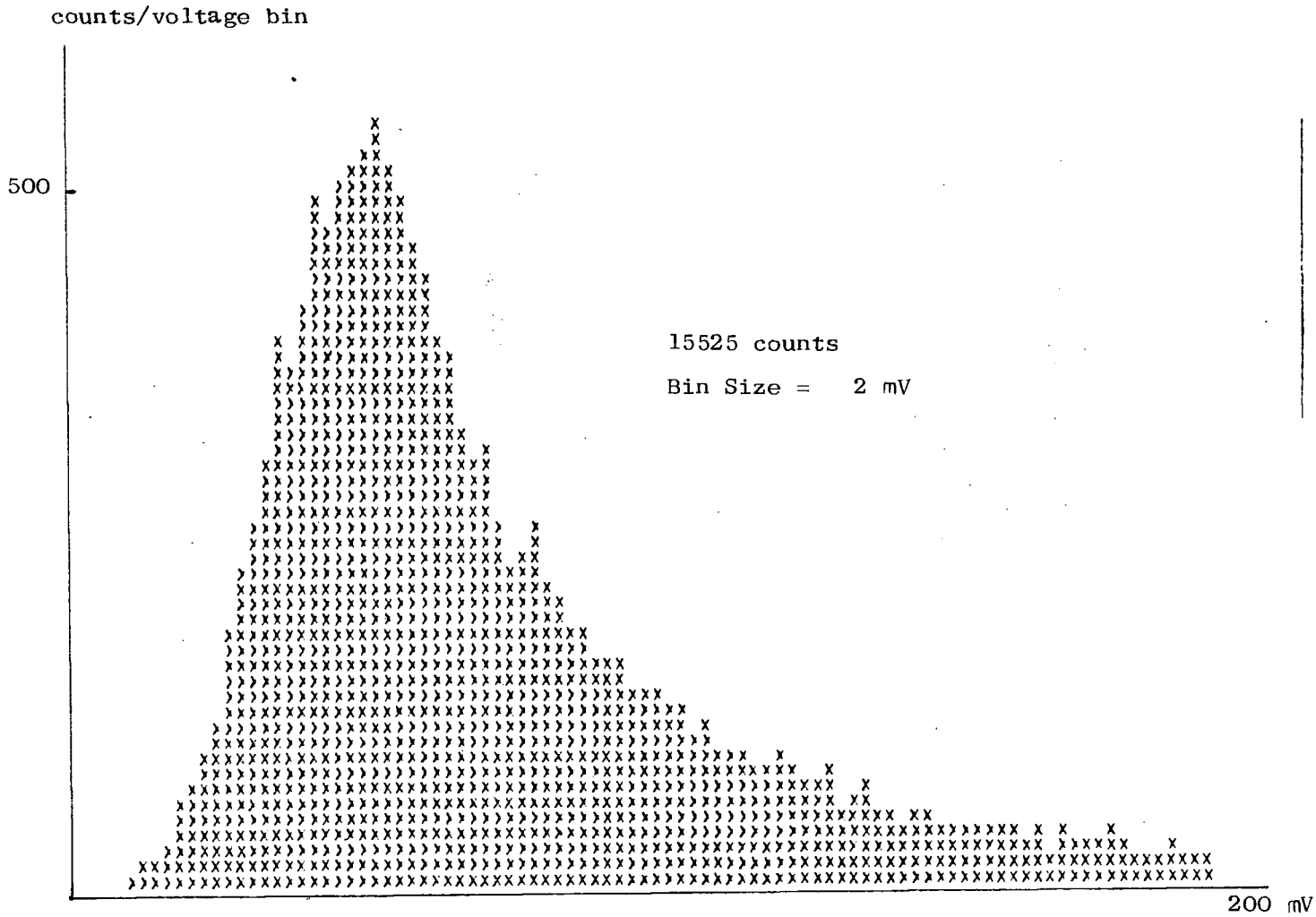

Figure 2.3: Typical 'Single particle distribution' obtained from one quarter of detector 61, during calibration. The amplifier and photo-multiplier noise has been excluded at the low end.

23 cm x 23 cm x 3 cm plastic scintillator telescope was used as a gate for a pulse height analyser (PHA), measuring the voltage pulses from the detector under examination. The resultant calibration distributions, one for each piece of plastic scintillator were then stored on paper tapes for further processing. Figure 2.3 shows a typical 'Single particle distribution' for one quarter of detector 61 obtained in this manner.

2.3 PROCESSING OF THE CALIBRATION COEFFICIENTS

The distribution shown in Figure 2.3 represents a single particle response, polluted by a small fraction of multiple particles, obtained at a particular localised position in one of the slabs of scintillator, and is produced by particles arriving at all angles within the solid angle of acceptance of the telescope and scintillator. The value of interest for conversion from observed voltage to particle density is the mean of 1 vertical particle/m^2 averaged over the whole detector. This number was obtained for each detector, starting from the distributions measured in § 2.23 according to the steps outlined in Figure 2.4. Each of the assumptions made is discussed below. No attempt was made to obtain the actual shape of the final distribution of interest.

2.3.1 Effect of Multiple Particles

The pollution of the distributions, of the type shown in Figure 2.3, by multiple particles was neglected. Smith (Smith 1976) showed this to be of the order of 3% for the present detectors, an error which is much less than that produced by other sources.

2.3.2 Detector Uniformity

The uniformity of each type of detector was measured by Treasure (Treasure 1980) as follows. The 'Single particle' distribution mean

Figure 2.4: Processing of Calibration Information For Each Detector

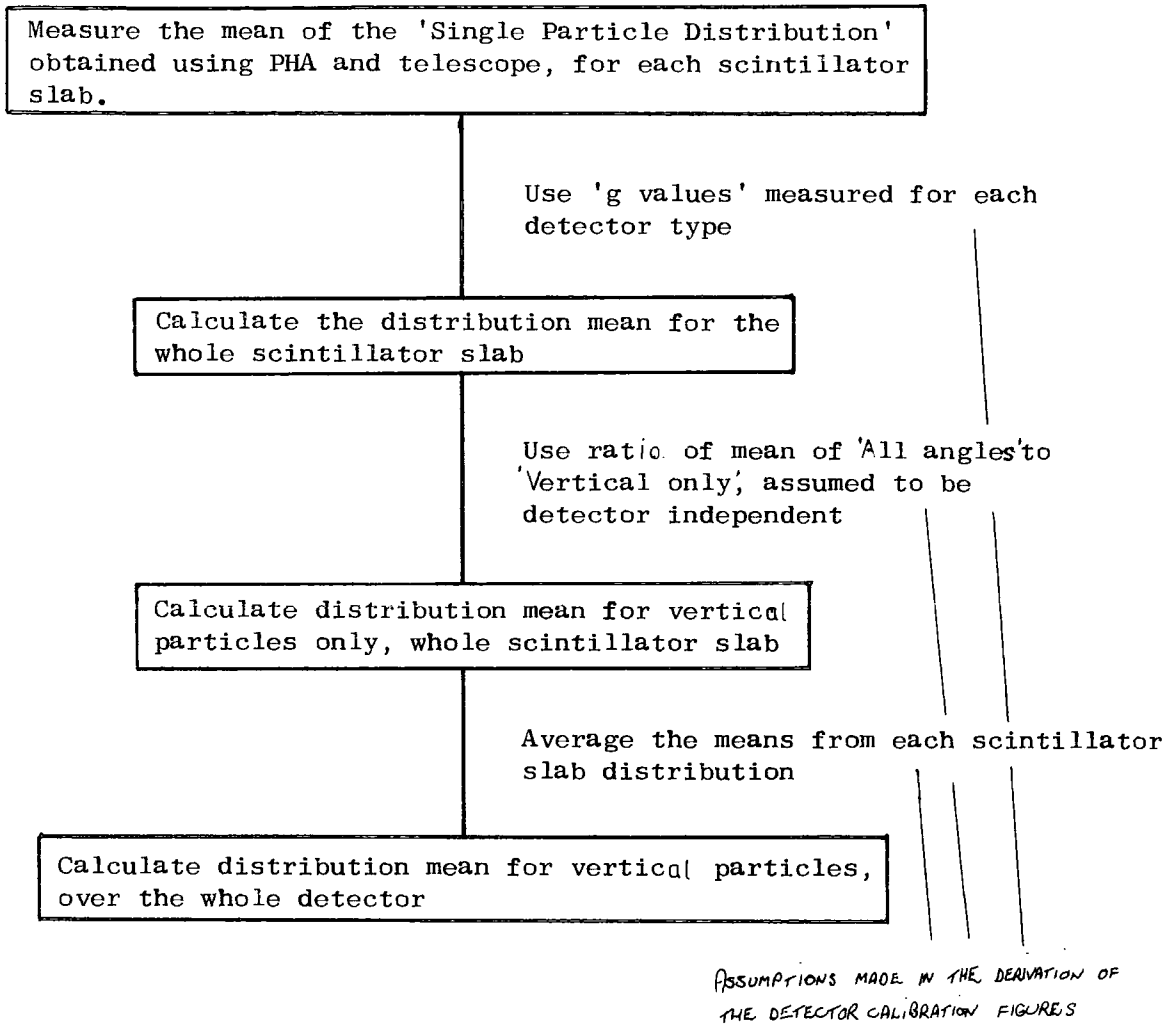

was measured using one 23 cm x 23 cm telescope at selected areas of the scintillator. A uniformity map was then plotted, and the average response, obtained by integration over the area of the detector, was compared to the response at the calibration point. The resultant 'g' values (the response at the calibration point/average response) are shown in Table 2.2.

2.3.3 'All Angles' to Vertical Ratio

The 'Single particle distribution' was obtained at the calibration point using one 23 x 23 cm telescope. A second similar telescope was placed $1\frac{1}{2}$ m vertically above the first and the two telescopes were used in a coincidence mode to gate the density pulses from the detector into a PHA. The resultant ratio of 'all angle' to 'vertical only' response was assumed to be constant for all detectors calibrated using similar telescopes positioned at equal distances above the scintillator.

2.3.4 Whole Detector Response

The mean of the whole detector, single particle response, was obtained by averaging the individual means obtained from each scintillator forming the detector. This is permissable since the areas of each scintillator slab in any one detector are equal.

2.3.5 Errors in the Final Calibration Figures

No attempt was made to calculate the final vertical particle, whole detector distribution shapes, but it has been assumed, for the purposes of simulation, that they have a similar shape to that shown in Figure 2.3. This is reasonable, since the parameters of each distribution added in § 2.3.4 were approximately equal in any one detector.

The final voltage to particle density conversion figures are shown in Table 2.2. The error in each is estimated to be 15 per cent, arising primarily from the error on the measurement of the detector uniformity and the estimation of the mean of the single particle distributions themselves. This is the result of artificially inserting cut off points in the distributions: one at the lower end to exclude photomultiplier and head amplifier noise, and a second at the upper end, set by the range of the PHA.

2.4 THE DATA HANDLING ELECTRONICS

The data from an air shower event arrives in the laboratory in the following form: the density information as a set of voltage pulses, and the timing information as time differences between pulses from different detectors. The technique used is to convert all the measured parameters describing the air shower, (the density pulses and directional information) to a digital form, usually binary. These binary numbers are then stored together with 'book-keeping' information, such as array trigger mode, event number, run number and time of event, in a magnetic memory, which is serviced periodically by a computer. This form of data collection is fast, and allows treatment of high event rates with very low dead time.

Figure 2.5 illustrates our experimental set up. Each section will now be described in detail.

2.4.1 Timing Information

The timing information arrives into the laboratory on 50 Ω cable as a set of 5 ns wide gaussian pulses directly from the fast photomultiplier tubes on each of the timing detectors. These pulses, arising from both photomultiplier tube noise and the detection of real particles,

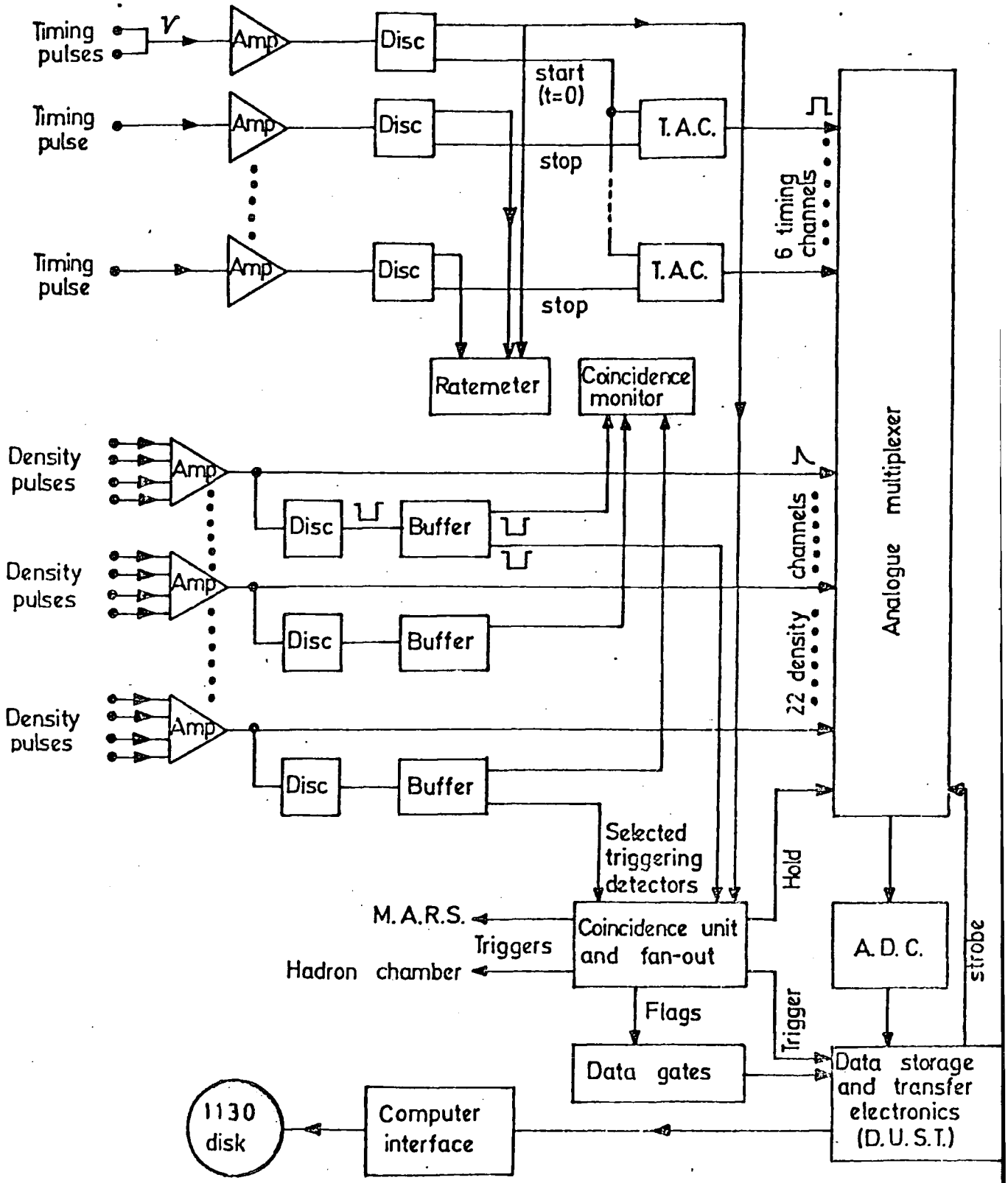

Figure 2.5: Block diagram of the array electronics

are amplified and discriminated, to produce a rate of 200 pulses/second approximately. This rate was regarded by the author to be high enough to produce good timing efficiency statistics, (the percentage of events with timing information), but low enough to keep the number of spurious readings, misinterpreted by the array as real data, to an acceptable level.

The cable lengths from each of the detectors have been arranged such that the fast pulse from detector C always arrives in the laboratory first, with the pulses from each of the other detectors delayed by an amount dependent on the cable length difference relative to detector C, the detector coordinates and the shower direction. These positive time differences are then converted to 5 μs wide 0 - 5 V pulses using time to amplitude convertors (TAC's), 5 V corresponding to around 500 ns. The fast pulse from detector C is used to start all 6 TAC's supported by the array electronics. Each TAC is stopped by a fast pulse from its own dedicated timing detector. The resulting analogue outputs are delayed and are available for measurement at the multiplexer inputs, 2 - 3 μs after the stop pulse has occurred. Each TAC used in the experiment has been calibrated individually, and the resultant curves of time difference against output voltage have been included in the analysis and simulation programmes.

2.4.2 The Density Information

The density information arrives in the laboratory along 50 Ω cable as a set of 300 ns rise time, 20 μs decay time, exponential pulses, each pulse height being related to the measured density at each detector. After an event has been established, these pulses are sampled at the input to the analogue multiplexer. For monitoring

purposes, the pulses are buffered and discriminated at 400 mV for detector C and 200 mV for all other detectors. The rates of these discriminated pulses are measured, both individually and in predefined coincidences, to provide daily detector fault diagnostics.

2.4.3 The Analogue Multiplexer and Digital Storage

The shower information arrives in the laboratory in parallel, the TAC information and density pulses all within 2 μs time spread. Each of the TAC outputs and the 22 density measurements is sampled and held at the input to an analogue multiplexing system on receipt of a 'Hold' command. The pulse is generated by the coincidence unit (§ 2.5.1) and occurs approximately 3 μs after the shower passes through the central detector. Each of the multiplexer inputs is then strobed through a common 10 bit analogue to digital convertor (ADC) and stored together with digital book-keeping information as an 'Event', a series of 88 8 bitwords, in a Mullard MM1501 core store. This buffer may contain up to a maximum of 11 events before it requires servicing by the online 1130 computer, which transfers the contents of the core store to magnetic disc.

The conversion and storage of one event takes less than 2 ms, the rate determining step being the ADC conversion time. The 1130 computer takes approximately 300 ms to complete the transfer of data. More details of DUST, the device to control the process of writing the digital information into core, may be found in Smith 1976. During both event storage and transfer of data to the 1130, the data acquisition electronics is inhibited.

The Analogue Multiplexer unit was custom designed for use with the array by Nuclear Enterprises Limited, and consists of 3 x 8 input Nim standard analogue multiplexers (MPXR). The first MPXR is a 'master' unit containing the logic to operate up to 11 'Slave' units. The master and slave units also contain logic to generate an internal 'Hold' command

from a user defined coincidence of input signals, set on the front panel of each unit. This logic however is not used. It was decided, therefore, that an additional compatible MPXR unit could be designed very simply and added to the current system, providing 8 inputs for the planned liquid scintillator tanks.

2.4.4 The Liquid Scintillator Tank MPXR

Figure 2.6 shows a schematic diagram of the operation of the MPXR unit, built by the author to provide 8 additional data inputs for the liquid scintillator tanks added to the array in 1976 (Shaat 1979).

The unit was built on 'Veroboard' and housed in a NIM standard module. The design is simple; a low leakage 100 pF polystyrene capacitor samples the input pulse at around 10 MHZ. On receipt of a Hold pulse, the FET switch opens, and the charge on the capacitor leaks to earth with a long time constant through the parallel resistances of the FET switch 'off'resistance and the source follower input impedance. The value of the signal on each input at 'Hold' time may then be measured by strobing each serially through the analogue 8 to 1 line multiplexer chip by supplying sequential 3 bit addresses.

This MPXR was found to be much poorer in performance than the commercially built units in characteristics such as offset, linearity, droop and sample to hold offset. All of these limitations in performance, however, may be taken into account in the calibration of the laboratory electronics (§ 4.5.2).

2.5 MODIFICATIONS TO THE LABORATORY ELECTRONICS PRIOR TO THE DATA COLLECTION PERIOD

Several errors were found in array data collected immediately before May 1977. These took the form of a deviation of approximately 10 per cent from the expected 100 per cent efficiency of a triggering

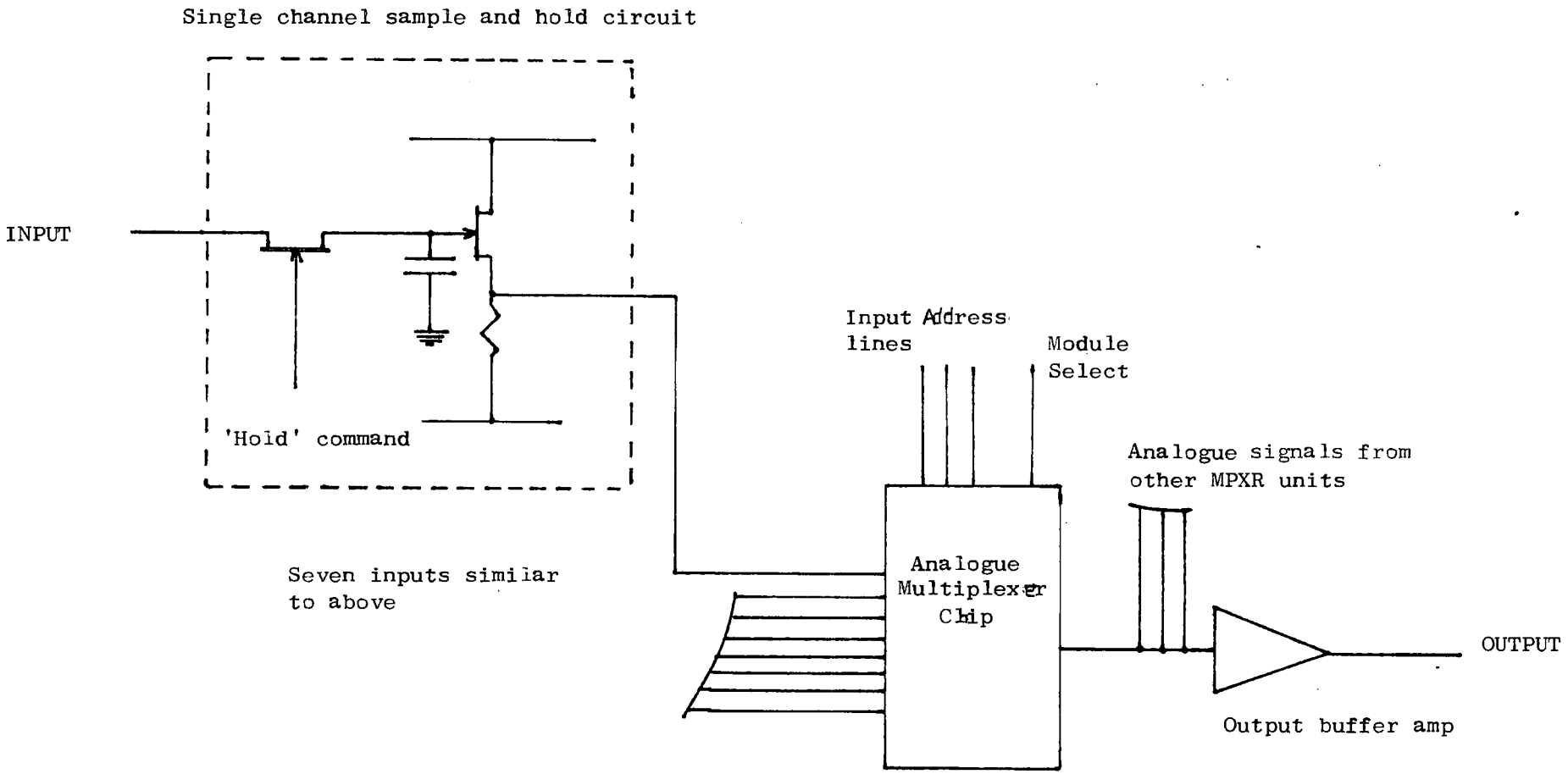

Figure 2.6: Schematic diagram of operation of analogue MPXR unit

detector. The measures adopted to cure this fault are outlined below.

2.5.1 The Coincidence Unit

It was thought that the error in the efficiency of the triggering detectors may be the result of pick-up in the coincidence unit which established an event. A replacement unit was designed and built by the author, and used during the collection of the data presented in this thesis.

The unit was designed to operate in either of two modes: X 8 or 2 X 4

X 8 Mode - An 'n fold' coincidence may be demanded between detectors selected by front panel switches. One trigger and flag are provided.

2 X 4 Mode - Two groups of detectors (with one common detector) may be selected, each with a separate trigger and flag.

It was envisaged that the unit would finally be used in the 2 X 4 mode, providing array triggers from both outer and inner ring coincidences, (C 13, 33, 53 and C 11, 31, 51 respectively).

One other requirement in the design was that the final coincidence TRIG OUT pulse should have a narrow time spread with respect to the time of the shower passing through the central detector. By using the fast pulse from C as a time marker, the time jitter of the output pulse was reduced from 1 μs to 75 ns. Figure 2.7 shows the operation of the unit, with the function of each section labelled. Coincidences are formed in the normal manner, either X 8 or 2 X 4 depending on the front panel switch setting. The 500 ns, delayed fast central detector pulse is used as a time marker to provide the required TRIG OUT and flag pulses. Should a fast pulse not arrive, as may happen in less than 2 per cent of the events, the unit defaults to normal operation

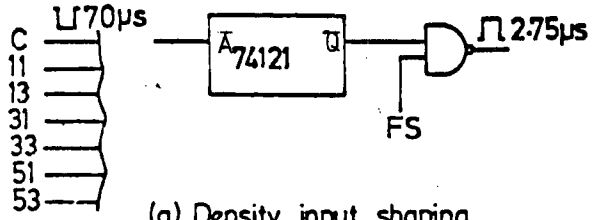

(a) Density input shaping

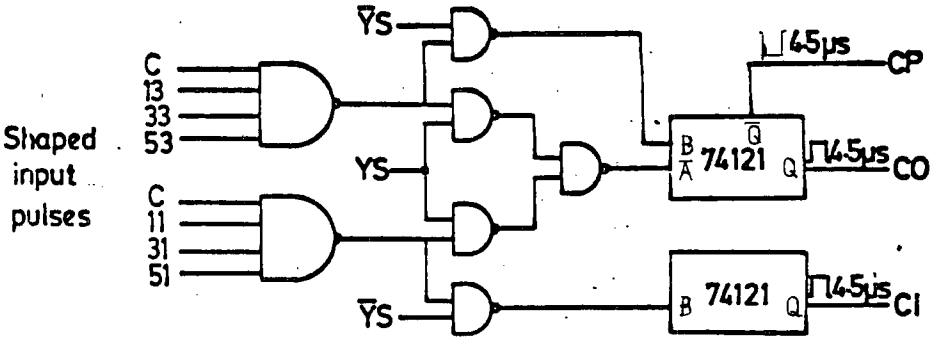

(b) Density coincidence

FAST C pulse in

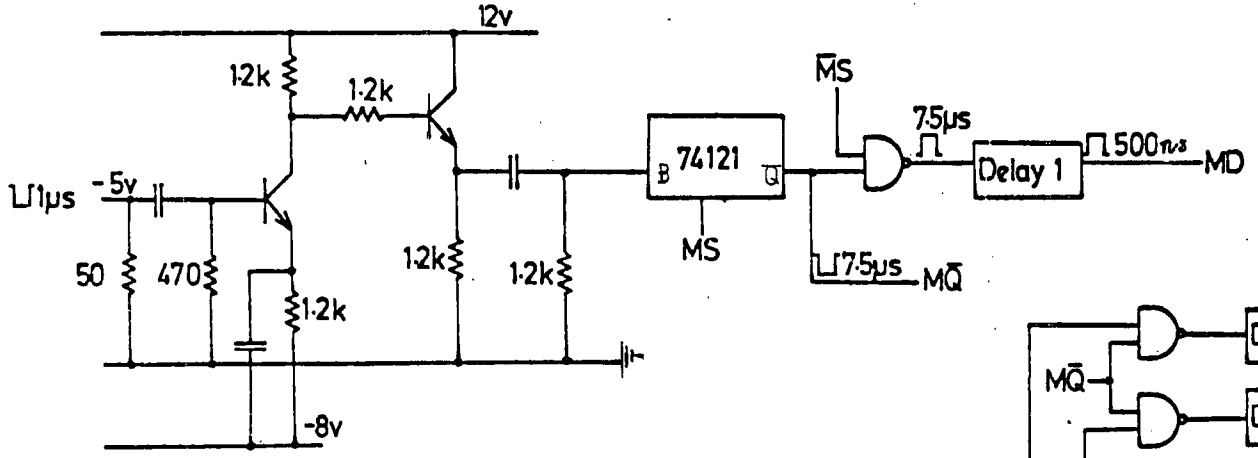

(c) Marker

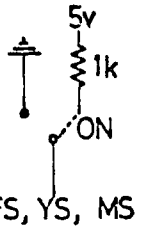

(e) All switches

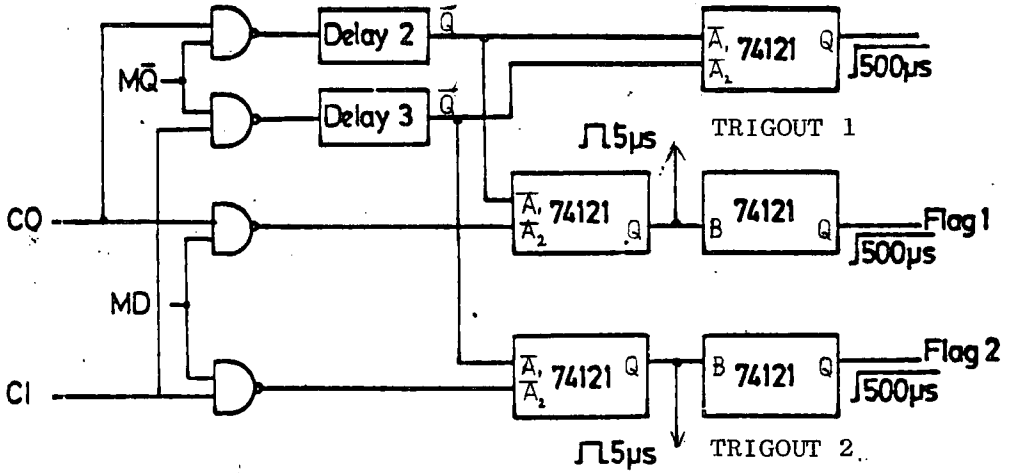

(d) Delay and flags

Figure 2.7: The array coincidence unit

Switch 'YS' is x8 or 2 x 4 selector

74121

INPUTS		OUTPUTS	
$\overline{A_1}, \overline{A_2}$	⌊	Q	⌈
B	⌈	$\overline{Q}$	⌊

providing a 'default flag'. A trigger is provided through delays 2 and 3. Delays 1, 2 and 3 were adjusted to be long enough ($3.2_{\mu}s$) to allow all TAC pulses to be correctly stored.

2.5.2 Buffer Amp

It was found that the array ADC returned an 0 value for input voltages above 5 V on the setting used. It was thought that this may be a possible cause of the efficiency errors in the array data. A buffer amp of gain 1 was built, input impedence approximately 1 KΩ, low output impedence, saturating at 4.8 V output. This was inserted between the MPXR output and the ADC input.

2.5.3 Standard Voltage Level

A standard voltage level was measured at each event and the result was stored with the event data using a spare multiplexer input, in an attempt to monitor any overall change in gain of the system. It was decided to make this reference more accurate than the standard TTL pulse used up to this point. A 6.2 V Zener diode, driven by a constant current of around 1 mA was used. The whole circuit was enclosed in a constant temperature bath at 75^{o} C. This level was measured at the start of each run, and was found to be constant at 6.84 $\pm$ .01 V.

SUMMARY

This chapter has described the Durham EAS array, from the detectors, through to the raw data on computer disc. Each assumption in the derivation of the detector calibration coefficients has been discussed. Limitations of the laboratory electronics have been outlined. It is hoped that the biases in the data introduced by the measuring electronics are well enough understood to be taken out in the treatment of the data at the analysis stage.

CHAPTER 3
THE DATA CHECKS

This chapter describes techniques which have been used to verify that collected data is error free.. The checks are all performed on 'Raw' data, prior to analysis.

3.1 INTRODUCTION

Data from any complex experiment may not be finally analysed until months after the collection date. Because of this long turnaround time, it is important that data errors should be detected at an early stage in the data collection/analysis sequence, and that the experiment should run under well defined circumstances, with as many critical variables as possible being measured during the data collection period. Online data collection is particularly suited to this approach, since the fault coverage of simple checking routines may be considerably increased by the manipulation of the stored collected data by computer programme.

3.1.1 Data Collection Periods

The data presented in this thesis have been divided into two batches containing approximately equal numbers of events. The conditions under which each batch was collected are shown in Table 3.1. The main difference between the two groupings is the inclusion in the second batch of the inner ring 2 m^2 detectors, 11, 31, 51 providing additional density and timing information. A second array trigger is also provided from the coincidence C, 11, 31, 51, increasing the event rate from 5 to 15 events per hour.

The data checking procedures can be divided into three types;checking for trivial errors, checking of data collected in each 12 hour run, and checking of groups of 1500 - 2000 events.

3.1.2 Checking for Trivial Faults

The data were collected in batches, each of approximately 12 hours duration. Before startup of each run, the operation of the laboratory electronics was checked by storage and readout of both book-keeping and

TABLE 3.1

DATA COLLECTION CONDITIONS

COLLECTION PERIOD	NOV'76 - MAY'77	MAY'77 - AUG'77
OPERATIONAL UNITS	Density C, 13, 33, 53, 32, 41, 42, 52 61, 62	C, 11, 13, 31, 33, 51, 53 12, 32, 41, 42, 52, 61, 62
	Timing 11, 13, 31, 33 53	11, 13, 31, 33, 53
ARRAY TRIGGER	C, 13, 33, 53 (outer ring)	C, 11, 31, 51 (inner ring) C, 13, 33, 53 (outer ring)
RUN NUMBERS	112 - 117	121 - 126
TOTAL NUMBER OF EVENTS COLLECTED	8388	10,185

analogue data. The density detector rates above a preselected discriminator threshold were measured, and the rates of the fast discriminated pulses from each timing detector were measured and adjusted to less than 200 counts/sec if necessary. This sequence of checks was found to locate the majority of trivial errors. The storage of events on 1130 disc and checking programmes run on these data will now be described.

3.2 THE 1130 DATA

Section § 2.4.3 has described how data are digitised and finally written onto magnetic disc. The digitised data from the array appear on 1130 disc as a sequential file containing events interspersed with various identifier and end codes. A typical example of an air shower event is shown in Figure 3.1 with core identifiers deleted for clarity. The data are in hexadecimal format. Each group of four digits represents a 16 bit word which would be stored in two sequential addresses in the array core store.

3.2.1 Daily Checking

After each data collection period containing around 100 events, checks are run on the data before final storage on disc. These are done by a programme running on the IBM 1130. The checks are listed below.

(a) 'Failed events' are printed. (Any event in which a value of 0 volts has been measured at a triggering detector is termed a 'Failed event').

(b) Array trigger flag combinations are printed. If the array may be triggered in several modes, useful diagnostics may be obtained by careful daily monitoring of the rates of each trigger.

(c) Histograms of the data collected at each multiplexer input during the run, are printed. The statistics are normally not good enough to provide information about detector calibration drift; but useful information may be obtained about detector efficiency, drift of ADC gain and pickup on any unused input.

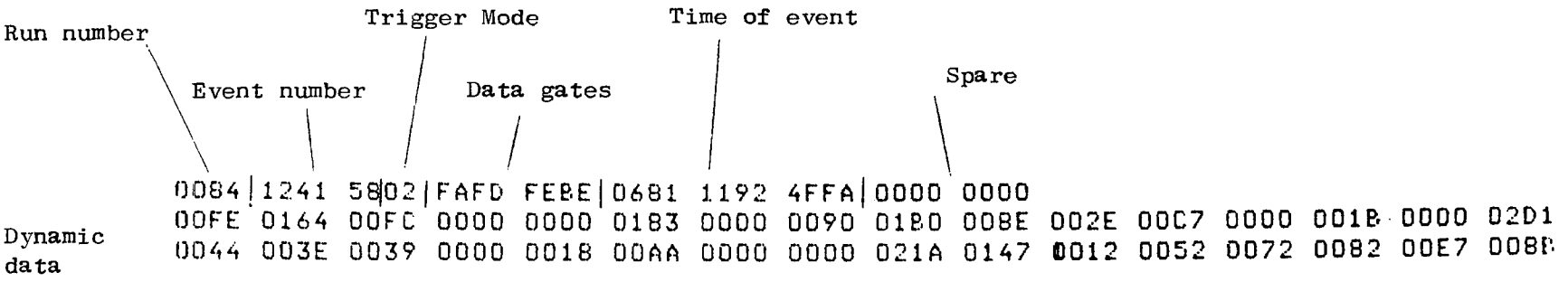

Dynamic data consists of timing and density information grouped into 8 words/MPXR in the following order:

Timing	11,13,31,33,51,53, spare, spare
Density	C,11,13,31,33,51,53, standard pulse 12,32,41,42,52,61,62, spare 8 liquid scintillator tanks.

Figure 3.1: A typical air shower event in hexadecimal format. The event is an inner ring trigger from Run 132.

3.3 BULK CHECKING OF MTS FILES

Groups of events which have passed the two levels of checks described above, are finally transferred to the Northumbrian University Multiple Access Computer (NUMAC) running under the Michigan Terminal System(MTS) for off line analysis. Events collected under similar run conditions may be conveniently grouped into MTS files, containing 1500-2000 events. This number is a compromise between statistical accuracy and computer storage limitations. At this point a more accurate estimation may be made of the detector efficiencies, mean pulse heights and ADC drift. In addition, parameters for later use by both the analysis and simulation programmes may be ascertained. This is done by a checking programme using the raw data MTS files as input. The main features of the programme are discussed below.

3.3.1 Analysis of Flag Combinations

Figure 3.2 illustrates a typical output showing the flag combinations from a file of data collected using two array triggers; outer ring (04 flag) and inner ring (02 flag). As expected, the number of 'outer ring only triggers' is low, since each outer ring trigger would be expected to trigger the inner ring. The percentage of fast timing default flags is less than 2 per cent of the majority of defaults occurring with inner ring only triggers. The programme has been written to allow various trigger flag combinations to be selected either in a flag prescence or exact flag combination mode.

3.3.2 MPXR Input Pulse Height Distributions

Information may be obtained by plotting histograms of both timing and density data values collected throughout a run of around 2000 events. Figure 3.3 shows a distribution of timing values obtained from detector 53 over a collection period of several weeks, under the

Figure 3.2: BULK FLAG CHECK ON A RAW DATA FILE CONTAINING 1584 EVENTS COLLECTED UNDER AN OUTER AND INNER RING TRIGGER

1584 EVENTS IN THIS FILE

RUN. NOS. 121 122

EVENT NOS. 1170616 1172214

FLAG COMBINATIONS FOR 1584 EVENTS

0 1562 316 65 0 . . .

Analysis of 'Flag Presence' in trigger words of input events (01,02,04,08 . . .)

0 1214 0 20 0 . . .

Exact arithmetic combination of trigger mode data gates of input events. (1,2,3,4,5 . . .)

INNER RING TRIGGER: 02 FLAG

OUTER RING TRIGGER: 04 FLAG

FAST TIMING DEFAULT FLAG: 08 FLAG

TOTALS REPRESENT THE NUMBER OF TIMES EACH ARITHMETIC COMBINATION OF TRIGGER FLAGS APPEARS IN THE TRIGGER WORDS IN THE DATAFILE, IE. AN OUTER RING (04 FLAG), AND INNER RING (02 FLAG) TRIGGER EVENT, WITH A TRIGGER WORD OF 0110 0...., WOULD PRODUCE AN ARITHMETIC COMBINATION OF 5.

TOTALS REPRESENT THE NUMBER OF OCCURRENCES OF EACH FLAG IN THE TRIGGER WORDS IN THE DATA FILE.

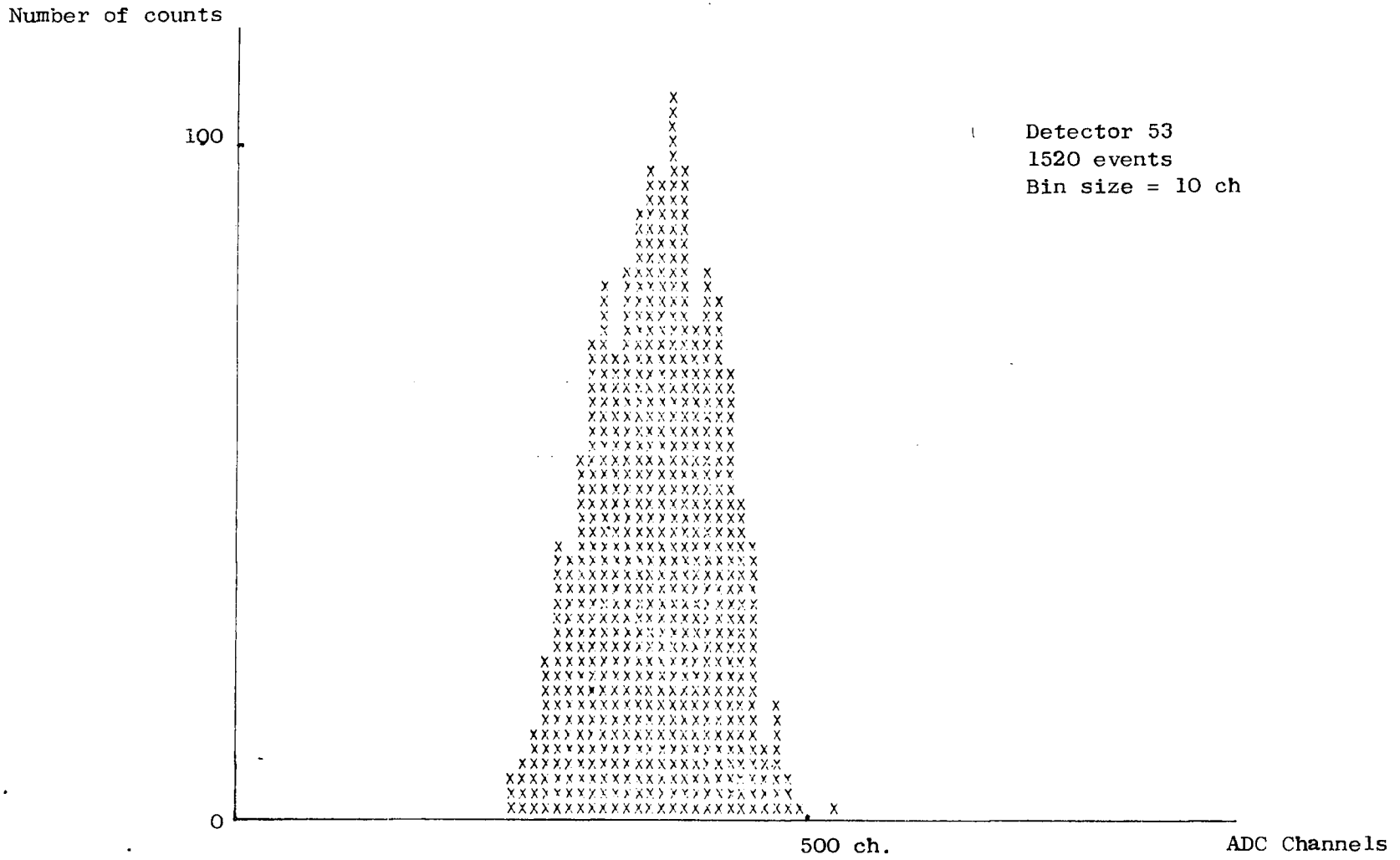

Figure 3.3: Distribution of Timing Values Obtained from Detector 53 TAC, for Run 113
A Time Difference of 1 ns Corresponds to Approximately 1 Channel

conditions shown. Smith (Smith 1976) has shown that the mean of this distribution is related to the difference in cable delays between detector 53 and detector C and to the Z coordinate difference between these detectors. The shape of the histogram is dependent primarily on the angular distribution of showers triggering the array, but the shape is slightly modified by the array triggering probability and the shower size spectrum. The distribution must however lie within the bounds dictated by the maximum and minimum physical time differences for the detector pair C and 53.

The mean and standard deviations of timing distributions would be expected to be constant throughout a run where data are collected under constant conditions. Figure 3.4 shows the timing means of detector 53 for sequential runs, each comprising approximately 1000 events, collected over a period of eight months. The timing means of all other timing detectors were found to be constant over this period within experimental error.

Figure 3.5 shows a histogram of the density values obtained from detector 33 during run 115,collected under an outer ring trigger. Figure 3.6 shows a histogram of data from detector 33 collected under both inner and outer ring trigger during run 124. The flag demand in Figure 3.6 is '02 presence'. The means of the distributions are dependent on detector calibration, triggering probability and shower size spectrum, but would be expected to be constant throughout a run for a constant detector calibration. Figure 3.7 shows the density means calculated for detector 33 from runs 112 to 117. All other detectors used in data analysis were found to be constant throughout this period within experimental error.

3.3.3 Detector Saturation Values

The head amplifier at each detector was found to saturate at a

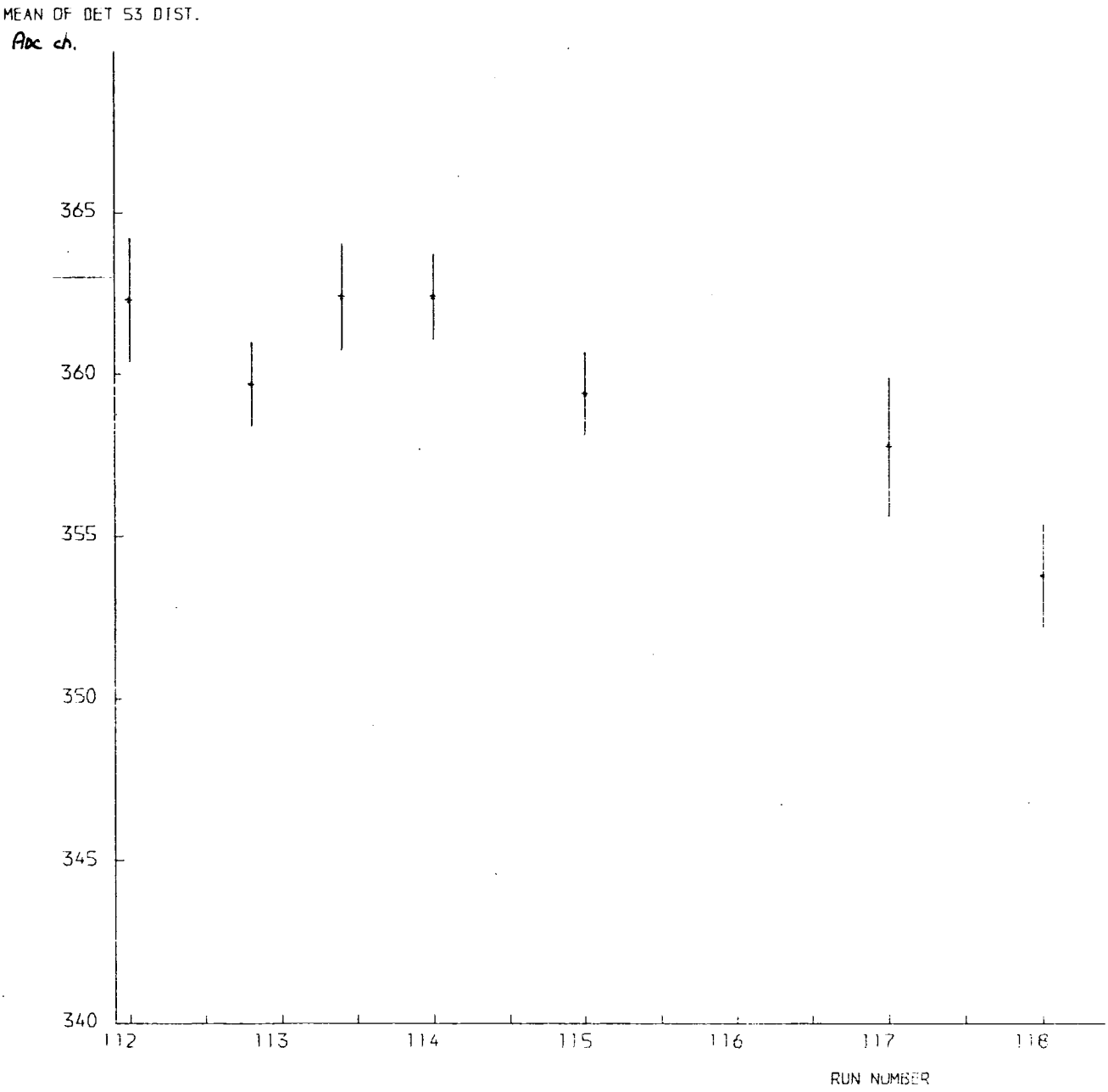

FIG 3.4 MEAN OF TIMING DET. 53 VS RUN NUMBER

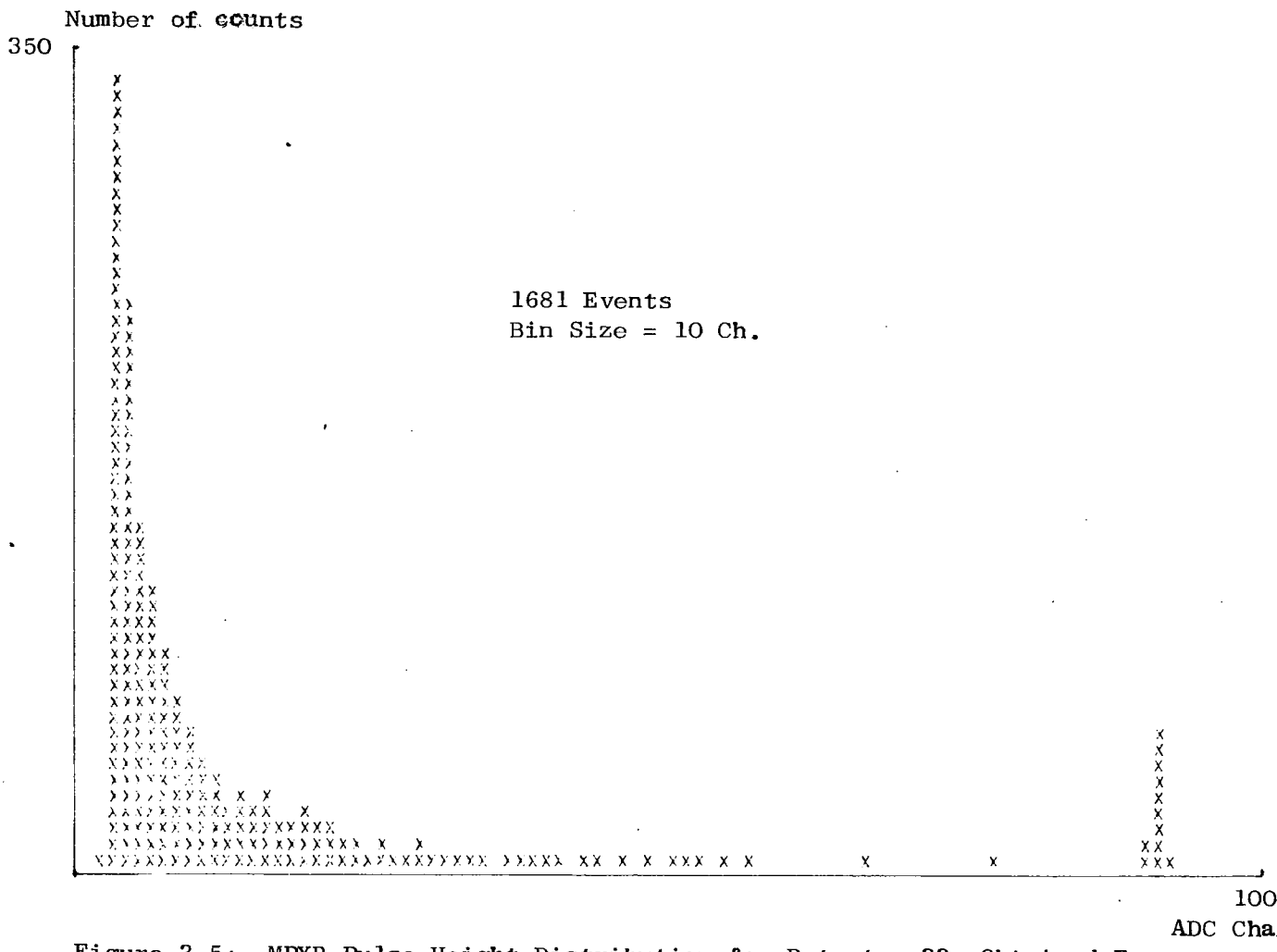

Figure 3.5: MPXR Pulse Height Distribution for Detector 33, Obtained From Run 113 Under an Outer Ring Trigger. 1ch ~ 10mV

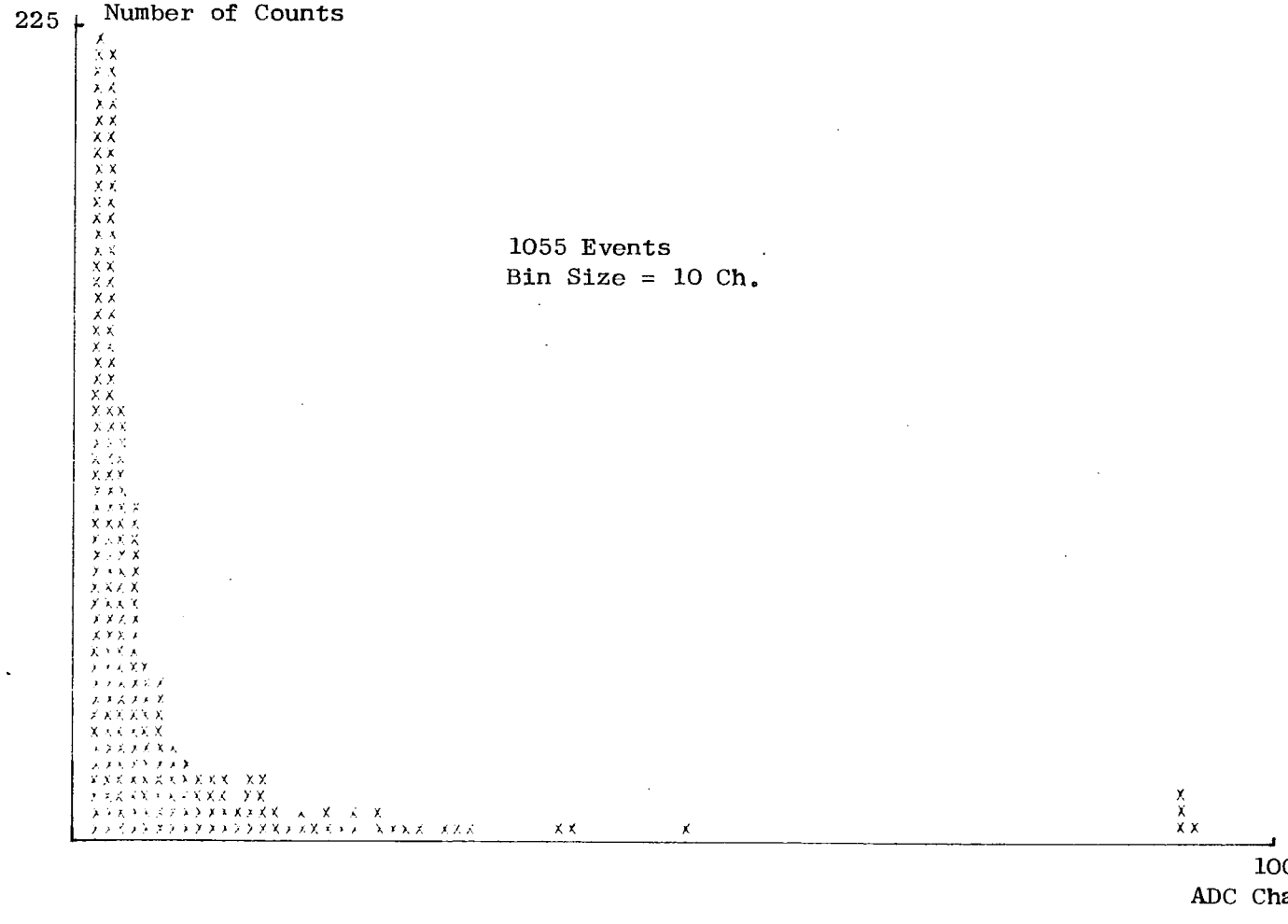

Figure 3.6: MPXR Pulse Height Distribution for Detector 33, Obtained From Run 124 Under an Inner and Outer Ring Trigger. 1ch ~ 10mV

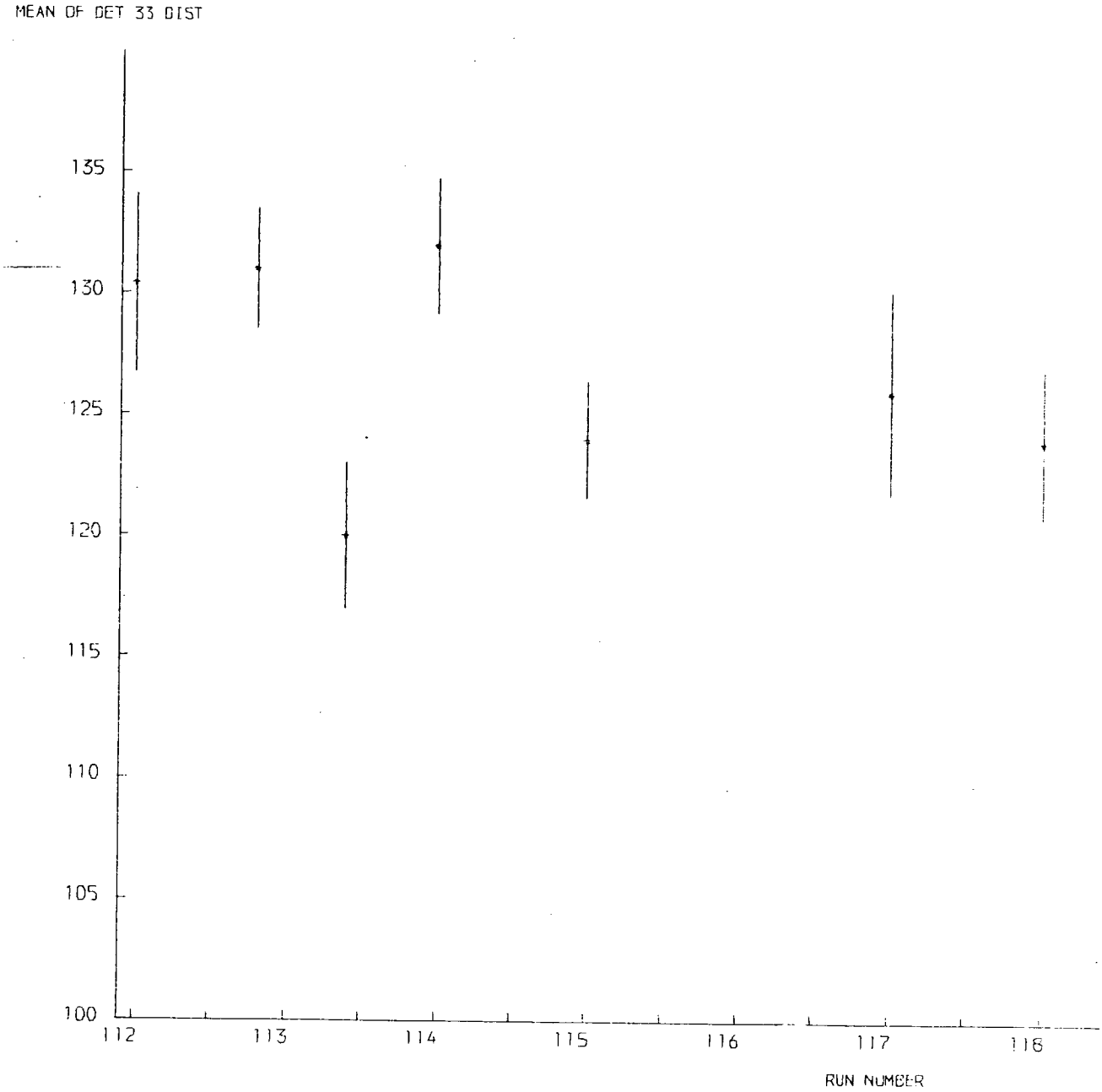

FIG 3.7 MEAN OF DENSITY DET 33 VS RUN NUMBER

different value dependent on supply voltage and amplifier gain. It is important that this value should be constantly monitored throughout the data collection period since the misinterpretation of a saturated detector measurement for real data could cause significant errors during analysis.

At the saturation output voltages of each head amplifier, piling up of pulses will occur. Figure 3.8 shows an expanded view of the top end of the histogram obtained from detector 33 where this effect may be easily seen. This provides a continuous automatic check on each detector saturation value, accurate to $\pm$ 15 channels, which is independent of detector calibration and trigger mode. Saturation values for each detector were obtained as follows. The position of the equivalent peak shown in Figure 3.8 was obtained for each detector from the expanded histogram. The saturation value of each detector was then arbitrarily assigned a value of 15 channels below this. This was necessary because of the finite width of the peaks and in addition ensures that no saturated measurement would ever be used as a real measurement in the analysis. Where different saturation values have been calculated for any detector during a long series of runs, the minimum value calculated was chosen.

3.3.4 Discrimination Level Check

Figure 3.9 shows an expanded view of the lower end of the histogram shown in Figure 3.5. For a triggering detector, no pulses should occur below that detector's discrimination level and a sharp cut-off edge should occur. In practice this edge is rounded because of measurement noise which reduces the accuracy of this technique to 30 mV approximately. Since the detector discrimination levels may be measured to better than 5 mV in the laboratory, it was decided that this histogram method would be used as a visual check only.

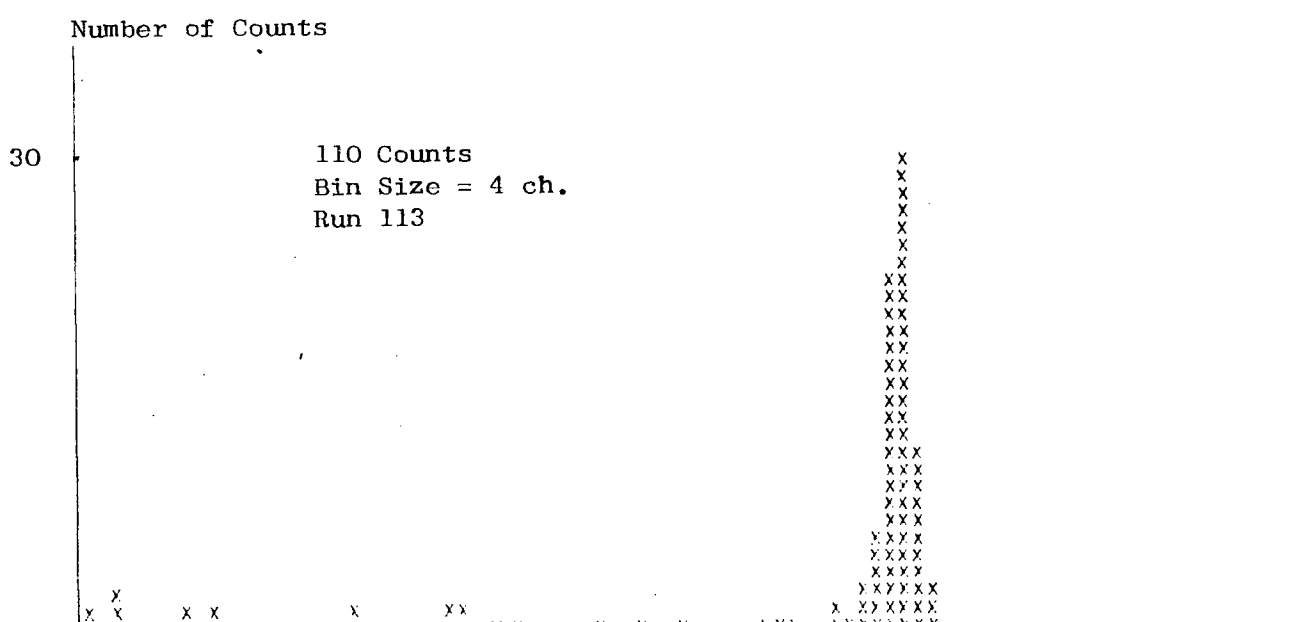

Figure 3.8: Expanded View of Saturation Limit of MPXR Distribution for Detector 33. 1ch ~ 10mV

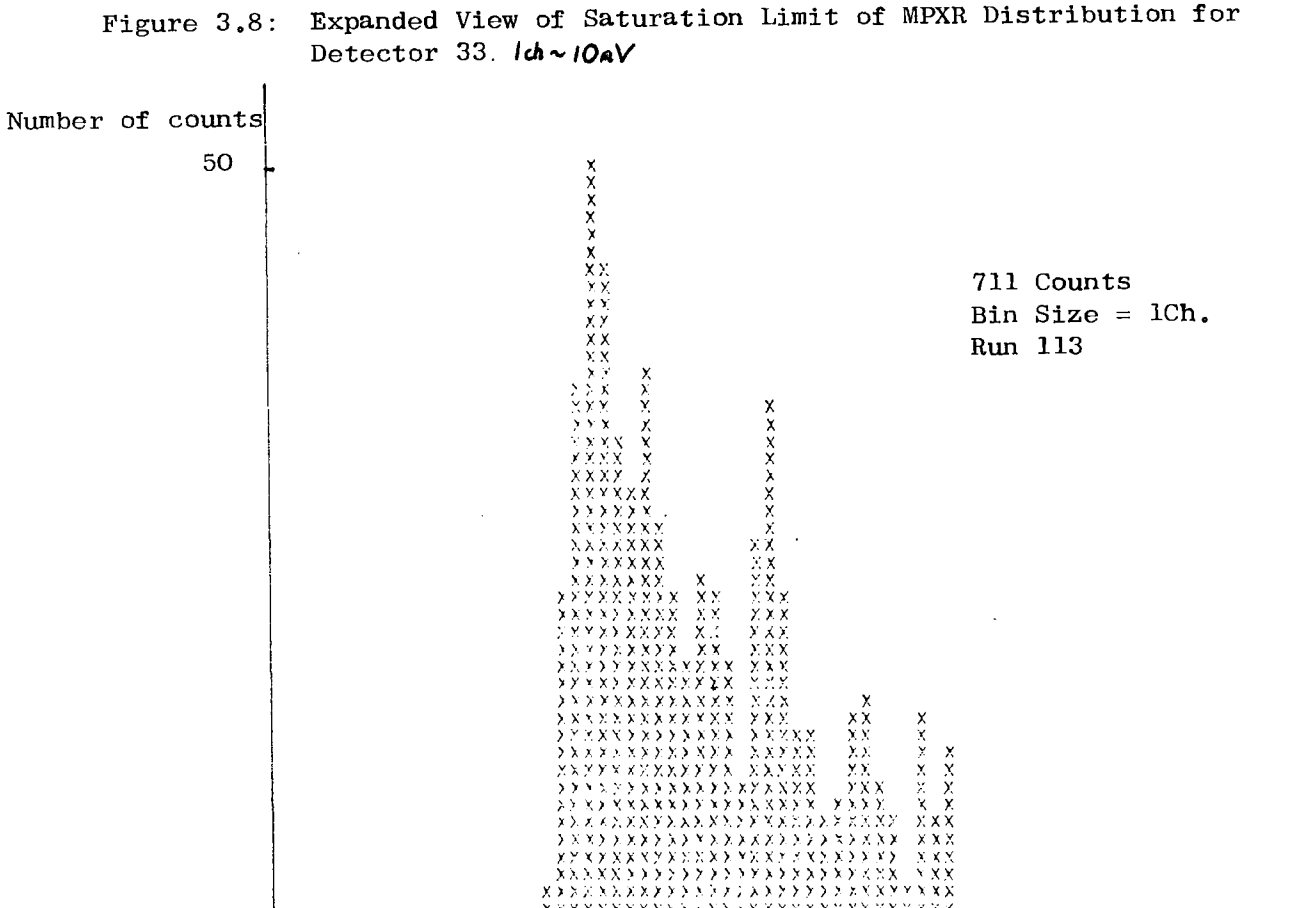

Figure 3.9: Expanded View of Lower Limit of MPXR Distribution For Detector 33. 1ch ~ 10mV

3.3.5 Fast Timing Probability

Fast timing pulses from each detector are provided by an independent fast photomultiplier tube. The probability of generating a fast pulse during an event depends on the density measured by the detector and the efficiency of the fast tube. Curves of this probability versus density measured were obtained as follows. By scanning raw data, density values obtained from any timing detector were grouped into bins. For each bin, the percentage of events containing TAC pulses from that detector, was obtained. An example of a curve obtained for detector 53 from raw data comprising RUN 113 is shown in Figure 3.10. This method assumes that fast detector C is 100 per cent efficient. The shape of each fast detector probability curve obtained in this manner may be used as input to the simulation programmes, described in Chapter 5.

3.3.6 Time of Event Information

The 'Time of Event' is contained in each event in the raw data. In addition to checking for negative time difference errors, this allows automatic plotting of a measured variable against time, useful in long term fault investigations. Histograms of the time difference between events may also be plotted. Figure 3.11 shows one such histogram from events comprising runs 113 - 114 collected under an outer ring trigger. The percentage of events lost by any other experiment with a long dead time, running in conjunction with the array may be estimated from this plot.

3.4 SUMMARY

Intermediate checking of data obtained from a complex experiment is necessary to detect errors which may otherwise cause corruption of large amounts of data. Checks done on the array data have been described,

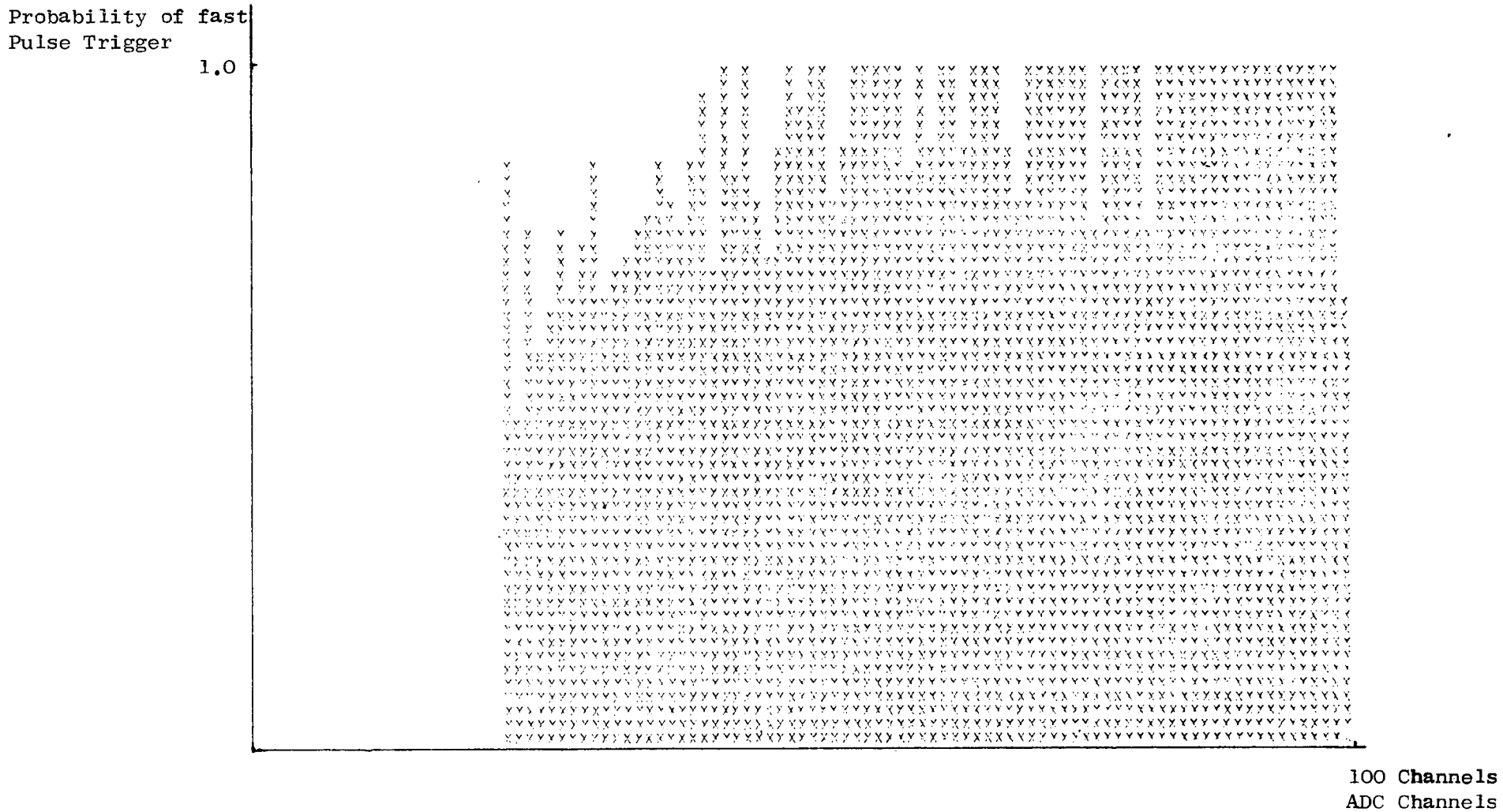

Figure 3.10: Probability of Obtaining a Fast Pulse vs. Slow Density, for Detector 53
The Data is Taken From Run 113 and is Based on 1180 Events. 1ch ~ 10mV

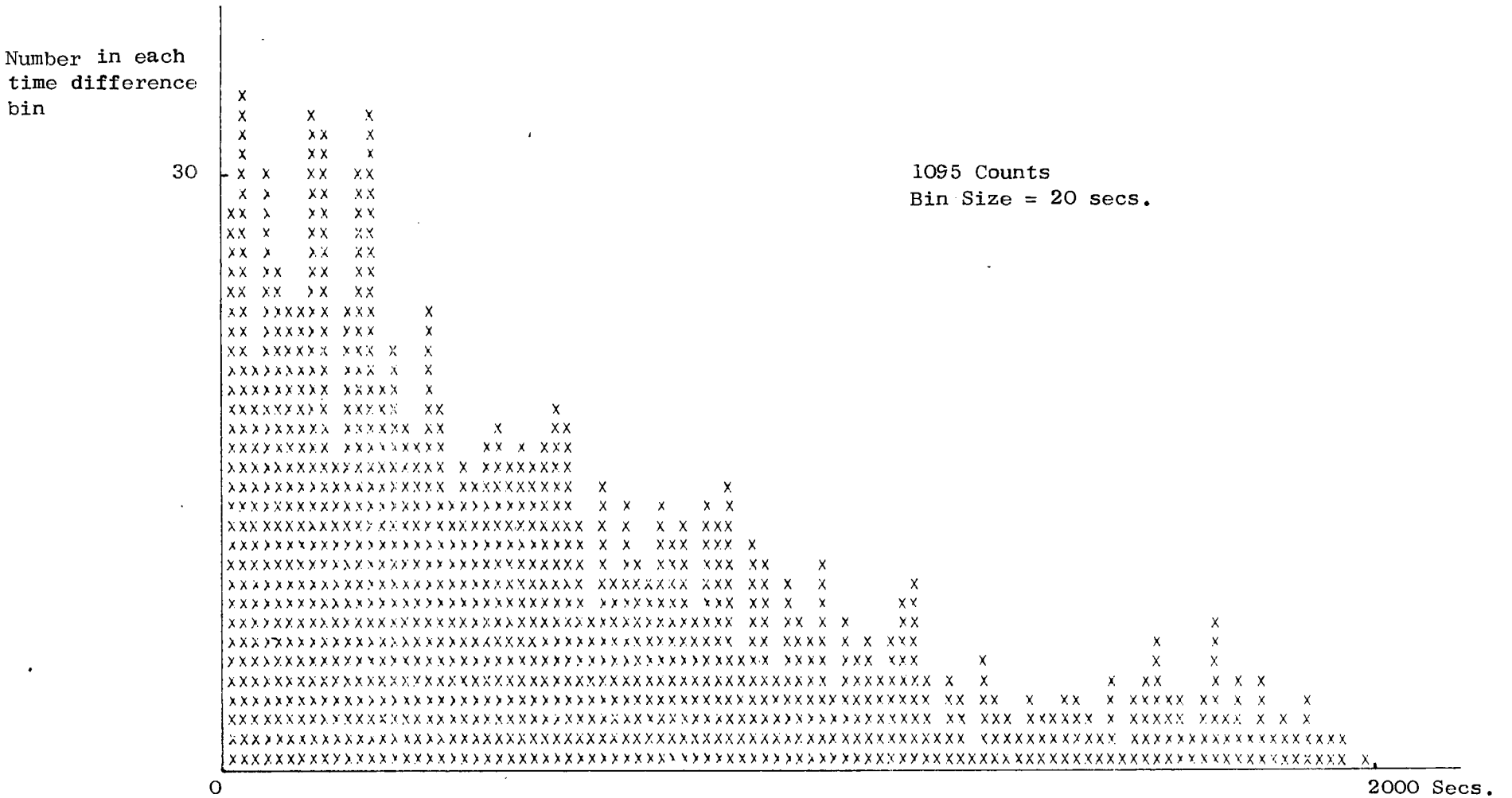

Figure 3.11: Distribution of Time Difference Between Events Comprising Runs 113-114

from simple daily manual checks, to computerised bulk checking of data collected over periods of weeks. This bulk checking also provides essential parameters for input to both the simulation and analysis programmes.

CHAPTER 4

THE DATA ANALYSIS PROCEDURE

4.1 INTRODUCTION

Previous chapters have shown how EAS data are collected and are finally stored on an IBM 370/168 after satisfying various levels of checking, to be analysed at a later date. This chapter describes the analysis technique, and some preliminary results are presented.

4.2 AIMS OF THE ANALYSIS

The aim of the analysis procedure is to derive as much information about each air shower event as possible from the data contained in that event. In this experiment such parameters include:

(a) Shower arrival direction

(b) Shower core position

(c) Electron shower size.

The analysed results must be as accurate as possible, hence as many known systematic biases as possible in the data must be removed at this stage. Also a broad view of the operation of the analysis procedure is necessary to allow optimisation of the performance of the technique.

After the information is obtained from each event, bulk parameters may be ascertained from groups of events. These include the angular distribution of EAS, spectral shape measurement and structure function measurement.

4.3 METHODS OF ANALYSIS

The methods of data analysis used by other groups vary in detail, but the aim of each technique is to derive as accurate an estimate as possible of the physical parameters of interest within the statistical

limitations of the data. Williams' method of intersecting loci (Williams 1948) has been popular in the past where small amounts of data may be conveniently analysed manually. The availability of powerful computing facilities has meant that numerical minimisation techniques are now the most widely used.

Previous data from the Durham Array has been analysed using the 'Williams' method by Ashton et al (Ashton 1977). Also, Smith (Smith 1977) has used a computerised technique to obtain the shower parameters by minimisation of a weighted least squares function. The latter technique, subsequently referred to as the 1976 Analysis Programme, will now be described in detail, since this has formed the basis of the analysis programme used to obtain the results presented in this thesis.

4.4 1976 ANALYSIS PROGRAMME

The operation of the 1976 Analysis Programme is illustrated by the flow diagram shown in Figure 4.1. The analysis of the data is performed on blocks of around 1500-2000 events by a Fortran coded analysis programme running on the Northumbrian Universities IBM 370/168. A function of the form

$$F = \sum_{\substack{\text{all} \\ \text{detectors}}} (q_{obs} - q_{calc})^2 W_i$$

is minimised during both timing and density data analysis. The programme relies heavily on the CERN minimisation package MINUIT (James and Roos 1971), which performs minimisation of the appropriate function F by any of the following techniques at the users' specification.

(a) SEEK - A random minimisation starting at a user defined point and initial step size, which terminates after the maximum specified call limit on F has been exceeded.

Figure 4.1: SIMPLIFIED FLOW DIAGRAM OF 1976 ANALYSIS PROGRAMME

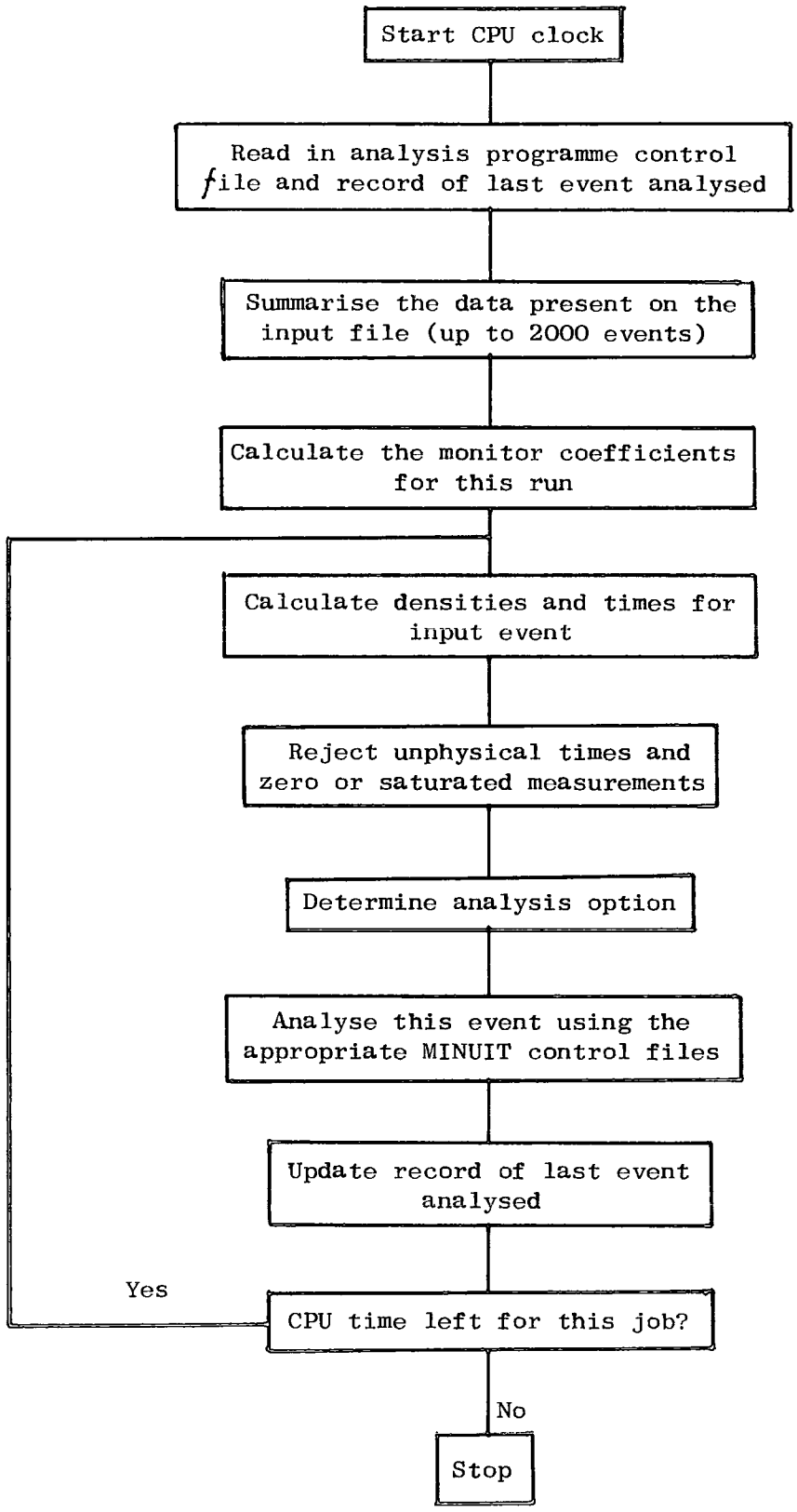

(b) SIMPLEX - A technique using the simplex method of Nelder and Meade, (Nelder and Meade 1967) which converges to the function minimum area quickly.

(c) MIGRAD - A minimisation technique using the Davidon variable matrix algorithm (Davidon 1968) which is powerful near the function minimum, providing a full error analysis.

(d) IMPROVE - This technique involves searching for the global minimum of the specified function by jumping out of a local minimum to a deeper one by a method due to Goldstein and Price (Goldstein and Price 1971).

While the user of MINUIT need not fully understand the exact operation of the above minimisation techniques, some knowledge of the suitability of each method is necessary to allow optimisation of MINUIT performance for each particular form of F, in terms of both time taken and accuracy of results returned.

The analysis of an air shower event is ideally a two stage process. First the direction of the shower front is obtained from the timing information. Then the shower size and core position are independently obtained from the density data. If either of the latter two stages is not possible through lack of information, other analysis options are performed. A table of analysis options and the data requirements that each imposes is shown in Table 4.1.

4.4.1 Timing Data

The voltages from the TAC's are first converted to positive or negative time differences representing the actual times for the shower front to pass from detector C to each timing detector. Simulations by Smith (Smith 1976) have shown that, for each timing detector, the relationship between the mode of the TAC histogram and the cable and laboratory electronics delays, is as illustrated in Figure 4.2, a result which assumes a plane shower front moving at a speed of light and a shower zenith angle distribution of the type $\cos^n \theta$ independent of shower size.

Table 4.1: THE ANALYSIS OPTION

Analysis Option	Method of Analysis of the Event
1	$\leq$ 2 times and $<$ 5 densities available: No analysis
2	$\leq$ 2 times and $\geq$ 5 densities available: θ assumed to be 0^{o}. 3 parameter fit to density data
3	$\geq$ 3 times and $<$ 3 densities available: Timing data only analysed
4	$\geq$ 3 times and $\geq$ 3 densities available: Full two stage analysis

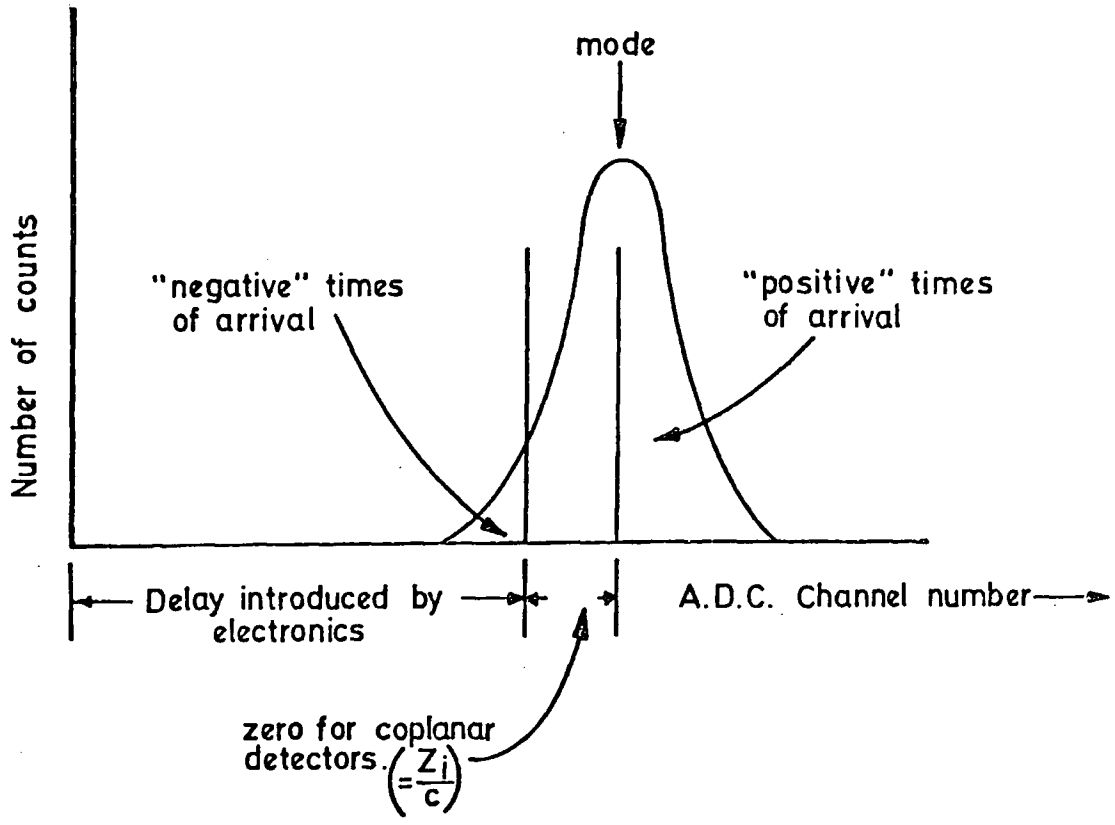

Figure 4.2: Relationship between the mode of a TAC histogram for detector i, collected during the normal operation of the array, and the delays introduced by both the detector Z oordinate, Zi, and the cable and laboratory electronics. (After Smith 1976)

The actual times at each detector, t_{obs}, may thus be obtained from the relationship shown.

A function of the form

$$F = \sum_{\substack{\text{all timing} \\ \text{detectors}}} (t_{obs} - t_{calc}(\theta,\varphi))^2$$

is minimised. t_{calc} is the calculated time at each detector, assuming a plane shower front with arrival direction (θ,φ) as shown in Figure 4.3.

4.4.2 Density Data Analysis

The data representing particle densities are first converted from ADC channels to particles/m^2. This conversion assumes that all 32 channels of the MPXR are linear and have equal gains. Data values less than 10 channels are not used in the analysis. Both the shower size and core position may now be simultaneously obtained by minimisation of a weighted least squares function of the form

$$F(x, y, N) = \sum_i \frac{A^2 (\rho_{calc} - \rho_{obs})^2}{\epsilon^2}$$

where ρ_{obs} is the measured density at detector i, and ρ_{calc} is the calculated density at that detector for a shower of size N, core location (x, y) and arrival direction (θ,φ). The structure function due to Catz (Catz 1975) has been used in this and in current versions of the analysis programme to calculate ρ_{calc}. $\frac{1}{\epsilon}$ is an approximate weight given to the observed measurement ρ_{obs}, and has been chosen as the quadrature sum of the Poissonian error on the observed number of particles and a term representing the detector response error. This slightly arbitrary weight function has been left unchanged in the current version of the analysis programme.

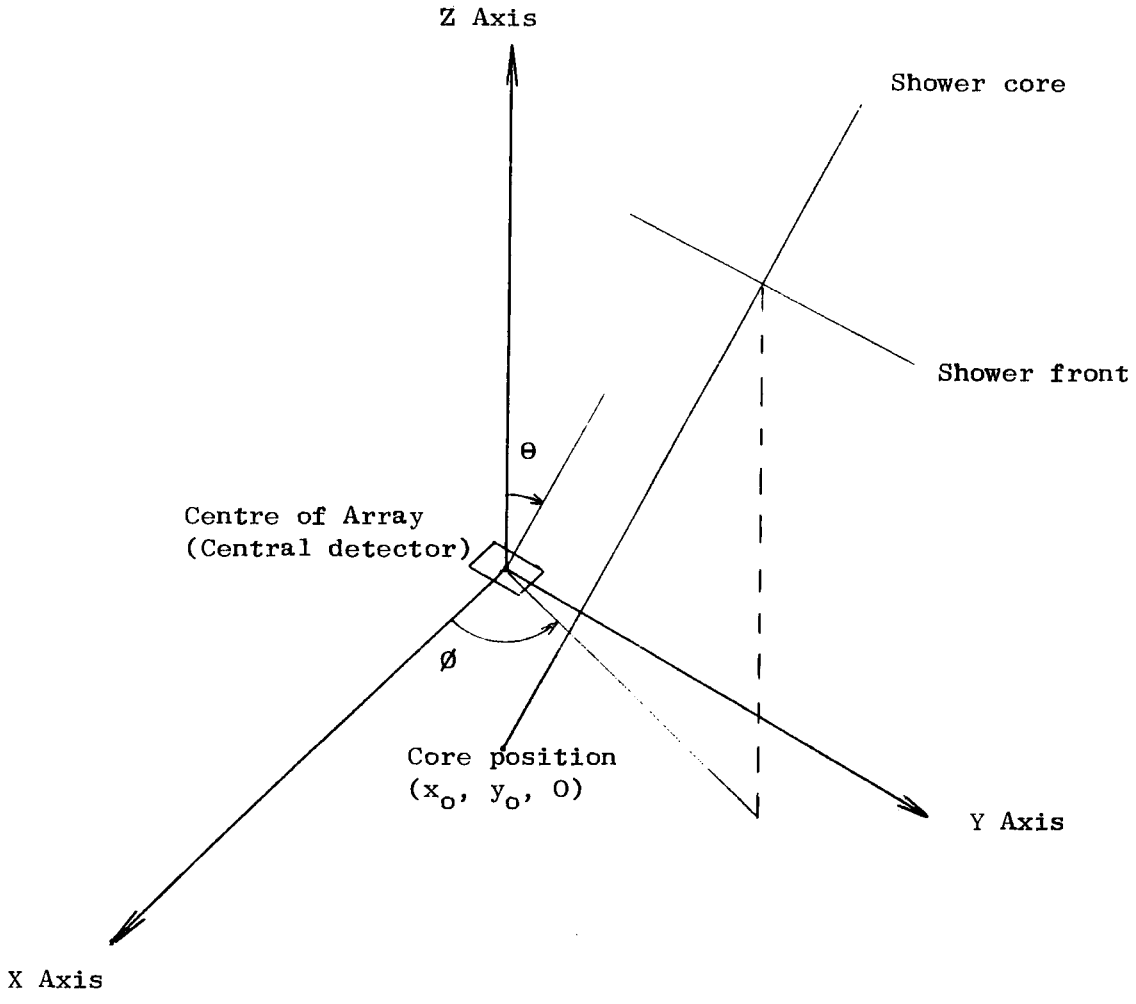

Figure 4.3: Convention for the description of the arrival direction of an extensive air shower with respect to the array axes.

4.5 MODIFICATIONS TO THE 1976 ANALYSIS PROGRAMME

Several modifications have been made to the 1976 programme. These may be conveniently grouped under two headings:

(a) Inclusion of a realistic treatment of detectors and laboratory electronics

(b) Programme performance optimisation.

4.5.1 Inclusion of Calibration Figures

The 1976 programme assumed that each detector was correctly calibrated to 100 mV/particle/m^2, that the timing electronics was calibrated on the range 500 ns = 5 V, and that all 32 MPXR inputs were perfectly linear with equal gains.

Density calibration figures, one for each detector, were added to the programme to allow conversion from voltage to particle density. Calibration figures for each TAC have been included, to relate the measured output to the time difference in nanoseconds. Each MPXR channel was individually calibrated as follows.

An accurately measured pulse height was stored sequentially through each MPXR input as an event, and the resultant set of 32 calibration events was stored in core, and transferred to magnetic disc in the normal manner. The process was repeated for the range of input pulse heights required. This method of calibration is useful , since the input pulse width may be adjusted to be of a similar time constant as real data pulses, and the timing relationships are similar to those occurring in a real event, which allows realistic measurement of droop and pickup effects in the laboratory electronics.

The resulting batch of events, perhaps up to 500 in number, are then processed by a set of calibration programmes to produce, for each MPXR input, calibration curves of input voltage versus channel number. One such curve for MPXR input 29 is shown in Figure 4.4.

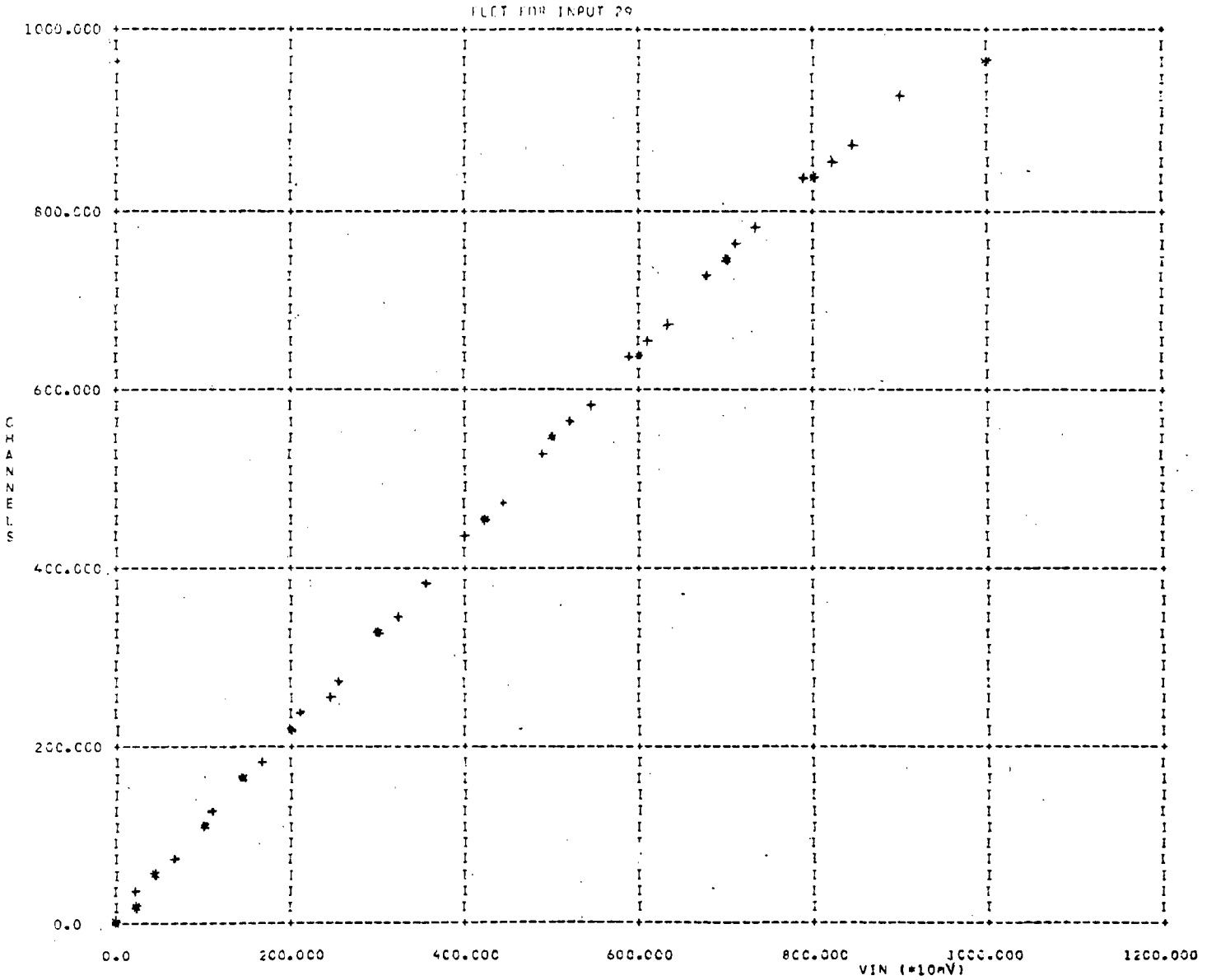

Figure 4.4: Calibration Curve for MPXR Input 29

* Calibration Data
\+ Fitted Curve

The curve fitted to the data is also shown. Several functions were considered for the representation of each input calibration curve of N points. The most convenient, a set of N-2 parabolas fitted to each group of three adjacent points, was included in the analysis programme as follows.

The function converts data in channels for each input, to a voltage, by inversion of the appropriate parabola, selected from the nearest data calibration coordinate.

4.5.2. Saturated Measurements

It is essential to determine whether the voltage from each detector is a valid measurement, or a result of the saturation of a detector head amplifier. The detector saturation values discussed in § 3.3 have been included in this version of the programme in place of the 860 channel cut present in the 1976 version. The effect of this was estimated by analysing a group of 40 events with the 860 channel cut, and then with the correct detector saturation values included in the programme. In the first analysis at least one saturation value had been assumed to be valid data in approximately 45% of events. In these events, core shifts between the two analyses of up to 65 m were found and in the first analysis, the shower size was consistently underestimated by up to a factor of 2.

4.6 PROGRAMME PERFORMANCE OPTIMISATION

An investigation was made into the performance of the analysis programme in an attempt to optimise the MINUIT control file for the core and shower size estimation of an option 4 event.

Approximately 50 outer ring trigger events were analysed four times using the MINUIT control file shown in Figure 4.5, with a core starting value of (0,0) given as a best estimate on input to the SEEK

Figure 4.5: MINUIT CONTROL FILE FOR ANALYSIS OF OPTION 4 EVENT

```
PARAMETER  DEFINITIONS      1XCRD      0.0      100.0      -100.0      100.0
                            2YCRD      0.0      100.0      -100.0      100.0
                            3SIZE     50.0       10.0        20.0       80.0

MINUIT  Commands            PRINTOUT
                            ERROR  DEF   1.0
                            SEEK         100.0
                            SIMPLEX      4000.0
                            HESSE
                            MIGRAD       4000.0
                            HESSE
                            IMPROVE      2000.0      8.0
                            END
```

command. Approximately 25% of events were found to produce different results in at least one of the analyses. In any such event, during multiple analysis, the percentage of incorrect results was found to be directly dependent on the limit of function calls by the SEEK command, as shown in Table 4.2.

In an attempt to reduce the spread of answers in any one event during multiple analysis, a more realistic first estimate of core position was given to MINUIT. The coordinates of the detector recording the maximum density, or the average combined coordinates of any saturated detectors, were calculated on entry to the analysis programme, and the result written to the MINUIT control file as a best estimate of core position for the SEEK command. Events were found to reanalyse correctly independent of the number of calls by SEEK to the user's function. The mean distance between the initial estimate and final analysed core coordinates was reduced by a factor of two to approximately 25 m. The maximum deviation found of 50 m was then used as the inital step size to define a search area for the SEEK command.

An attempt was made to analyse the average computer CPU time requirement of approximately four seconds, to analyse each event. Figure 4.6 shows the weighted least square value versus the call number to the user supplied function F for a typical option 4 event. The function F minimum is reached very quickly by commands SIMPLEX and MIGRAD, the bulk of analysis time being used by the IMPROVE command. The latter command is successful in finding a deeper minimum in approximately 15% of events with the call limits as shown in Figure 4.5. The average analysis time for these 15% of events is approximately two seconds, indicated that if CPU time were at a premium, the limit on the number of searches performed by IMPROVE may be reduced by a factor of two. It was decided, however, that further study was needed before the

Table 4.2: PERCENTAGE OF 'INCORRECT' ANALYSED RESULTS DURING MULTIPLE ANALYSIS OF EVENT 1152039

Calls To SEEK	% 'Incorrect' Results
1	30%
50	21%
100	11%
500	6%

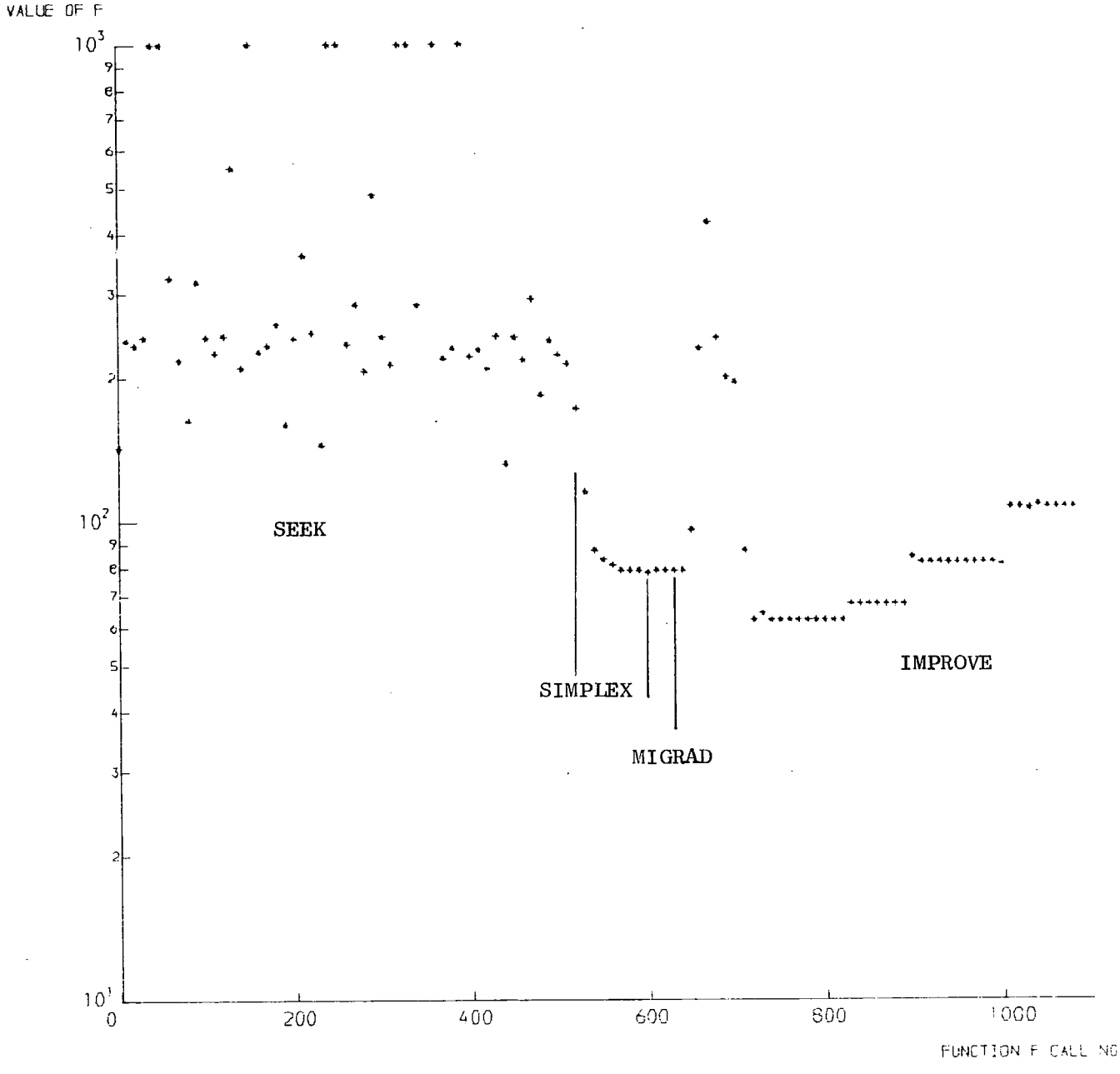

FIG 4.6 COURSE OF MINIMISATION OF EVENT NO. 1152039

IMPROVE parameters could be altered for the bulk of the analysis work. The option 4 MINUIT control file used to obtain the results presented in this thesis is as shown in Figure 4.5, with a SEEK cell limit of 100, a starting core location as described above, and an initial step size of 50 m. Figure 4.7 shows a flow diagram of the current analysis programme.

4.7 PRELIMINARY RESULTS

A full presentation of results will be given in Chapter 6, since their interpretation relies on the extensive computer simulations described in Chapter 5.

The results presented here are intended to illustrate that the analysis programme provides reasonable results on a qualitative basis only.

Figure 4.8 shows a scatter diagram of core positions of analysed showers comprising RUN 112. The limits on the core coordinates of $\pm$ 100 m imposed on MINUIT by the option 4 control file may clearly be seen.

Figure 4.9 shows a histogram of analysed θ for showers analysed within a radius of 50 m from the centre detector, and shower sizes between 5×10^5 and 10^7 particles.

Figure 4.10 shows a histogram of all shower sizes returned by the analysis programme, for inner ring triggers comprising runs 121-126, and Figure 4.11 for outer ring triggers comprising runs 112-118 indicating that the Durham array may provide information on showers with sizes between 10^4 and 2×10^7 particles.

4.8 SUMMARY

The improvements made to the 1976 analysis programme have been described under two headings. Calibration figures for particle density measuring detectors and fast timing detectors have been included and

Figure 4.7: SIMPLIFIED FLOW DIAGRAM OF THE CURRENT ANALYSIS PROGRAMME

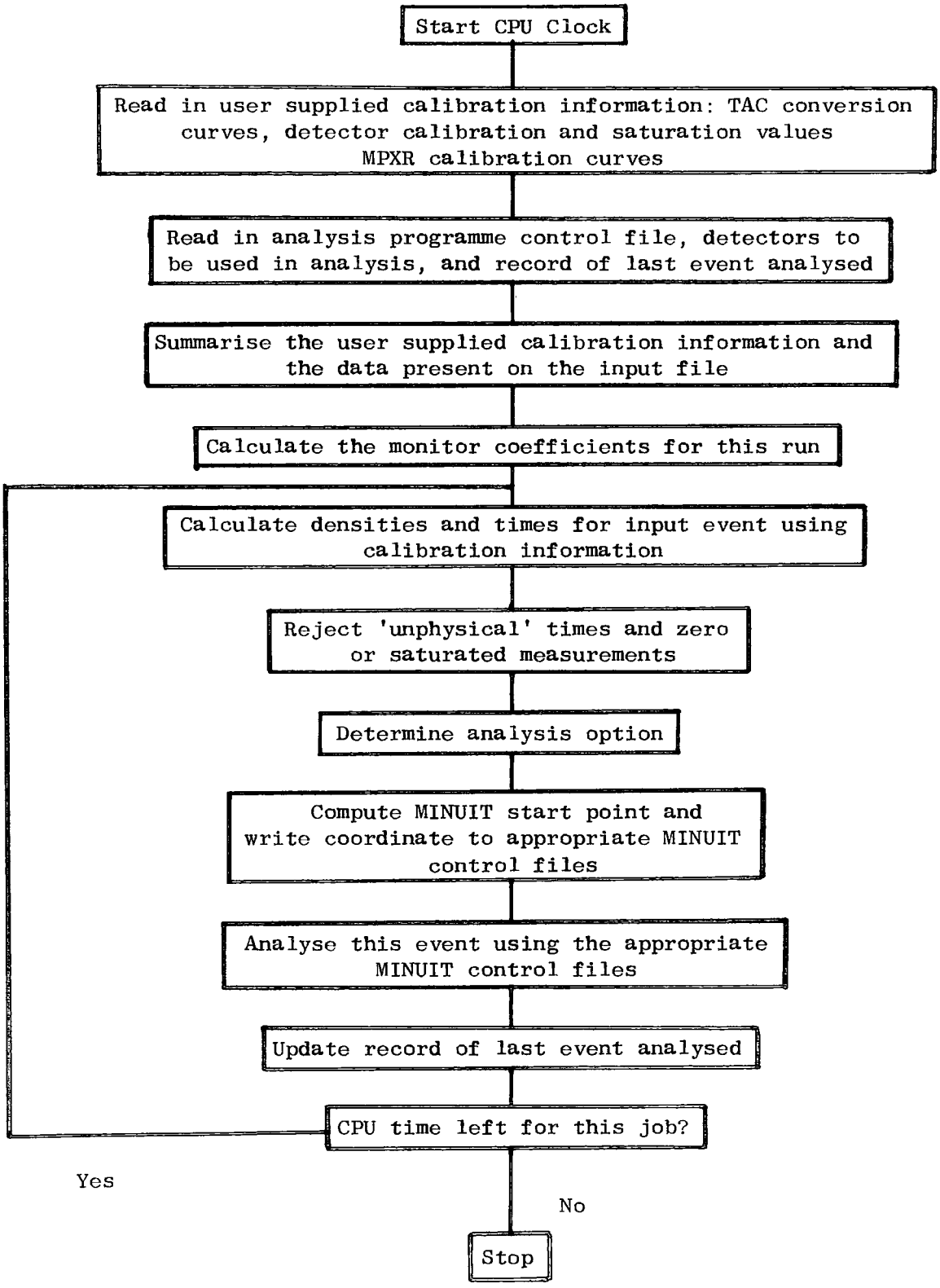

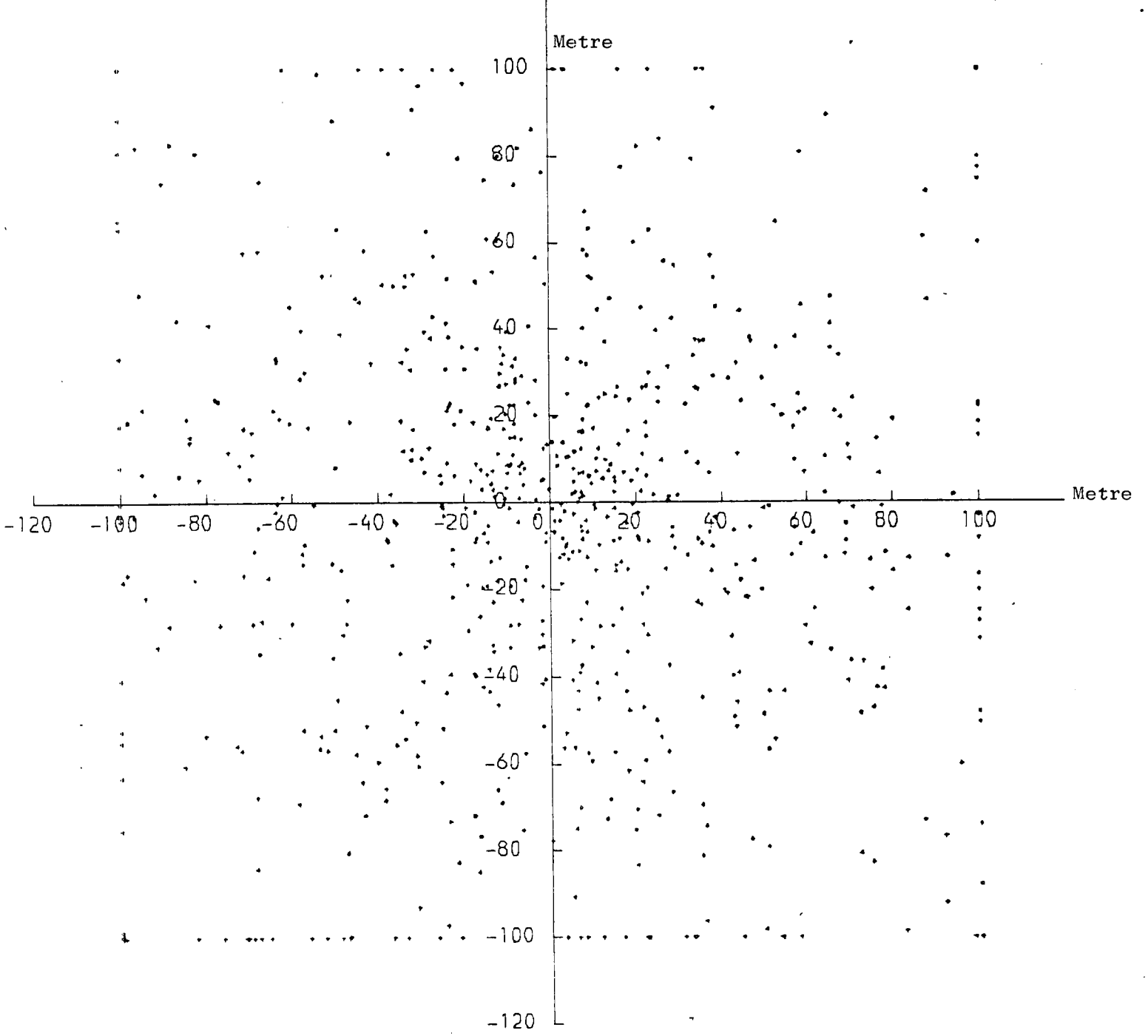

FIG 4.8 SCATTER DIAGRAM OF CORE POSITIONS RUN 112 715 EVENTS

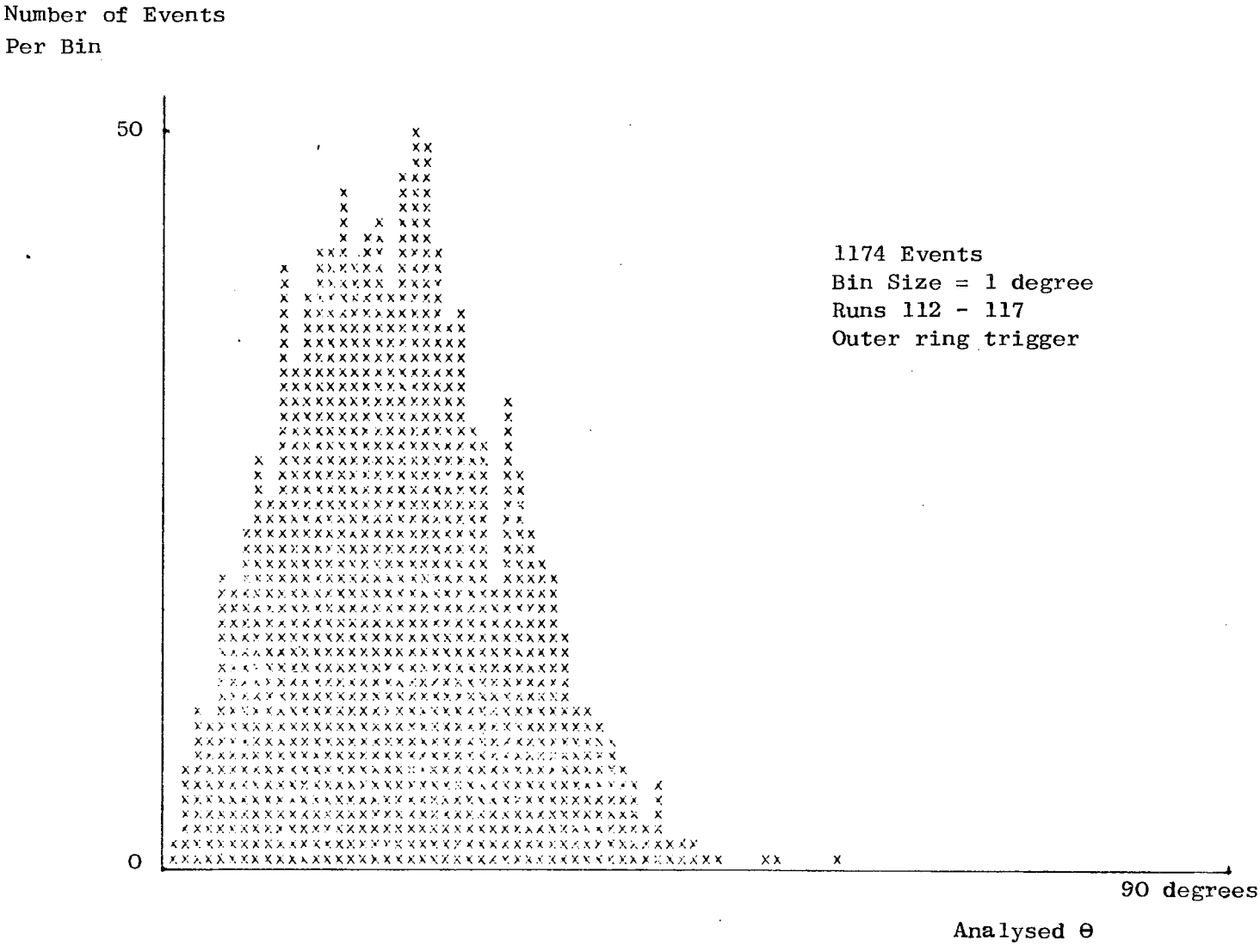

Figure 4.9: Histogram of analysed θ, for events within 50 m, 30° and analysed shower sizes between 5 x 10^5 and 10^7 particles

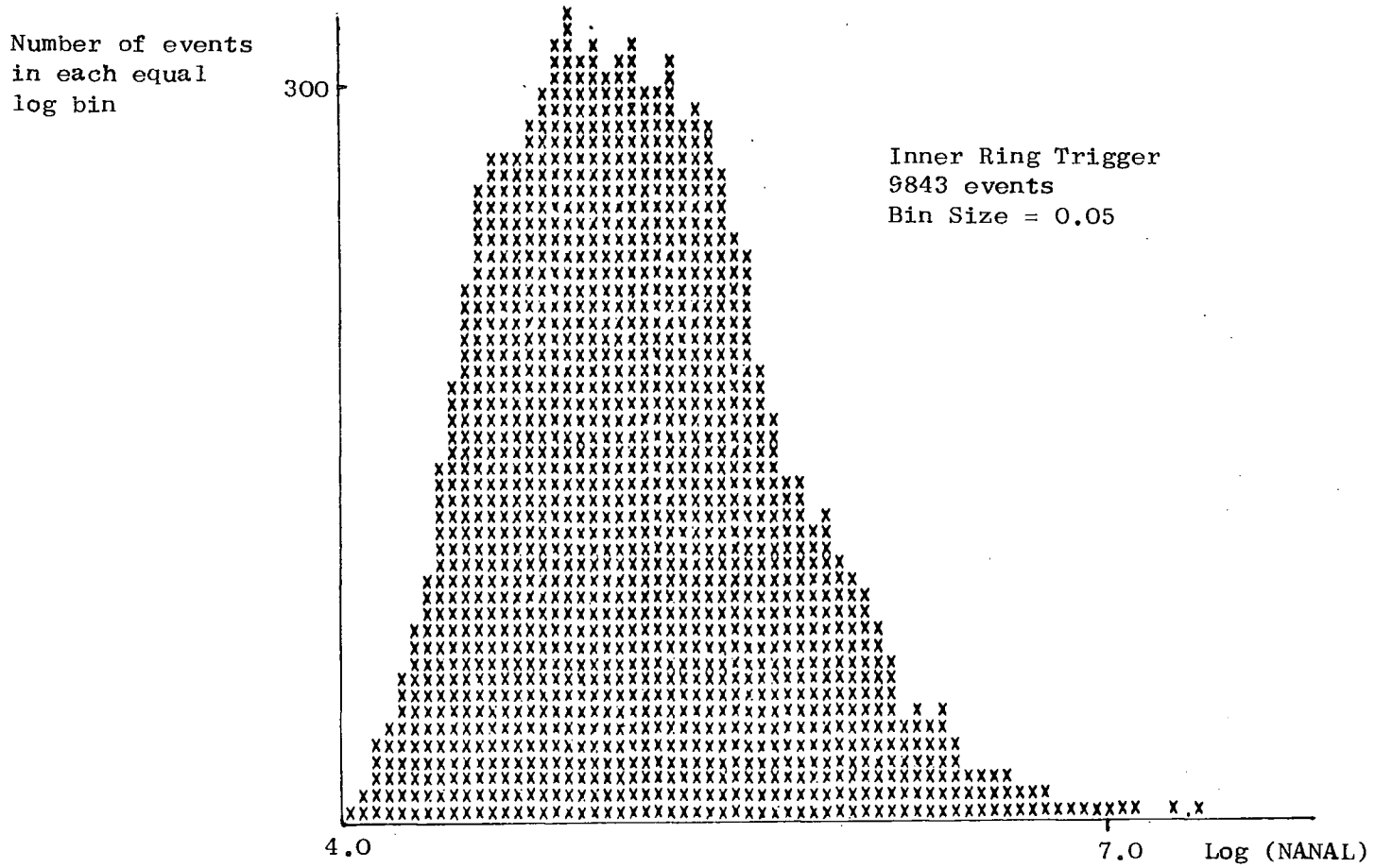

Figure 4.10: Histogram of all shower sizes returned by the analysis program for Runs 121-126

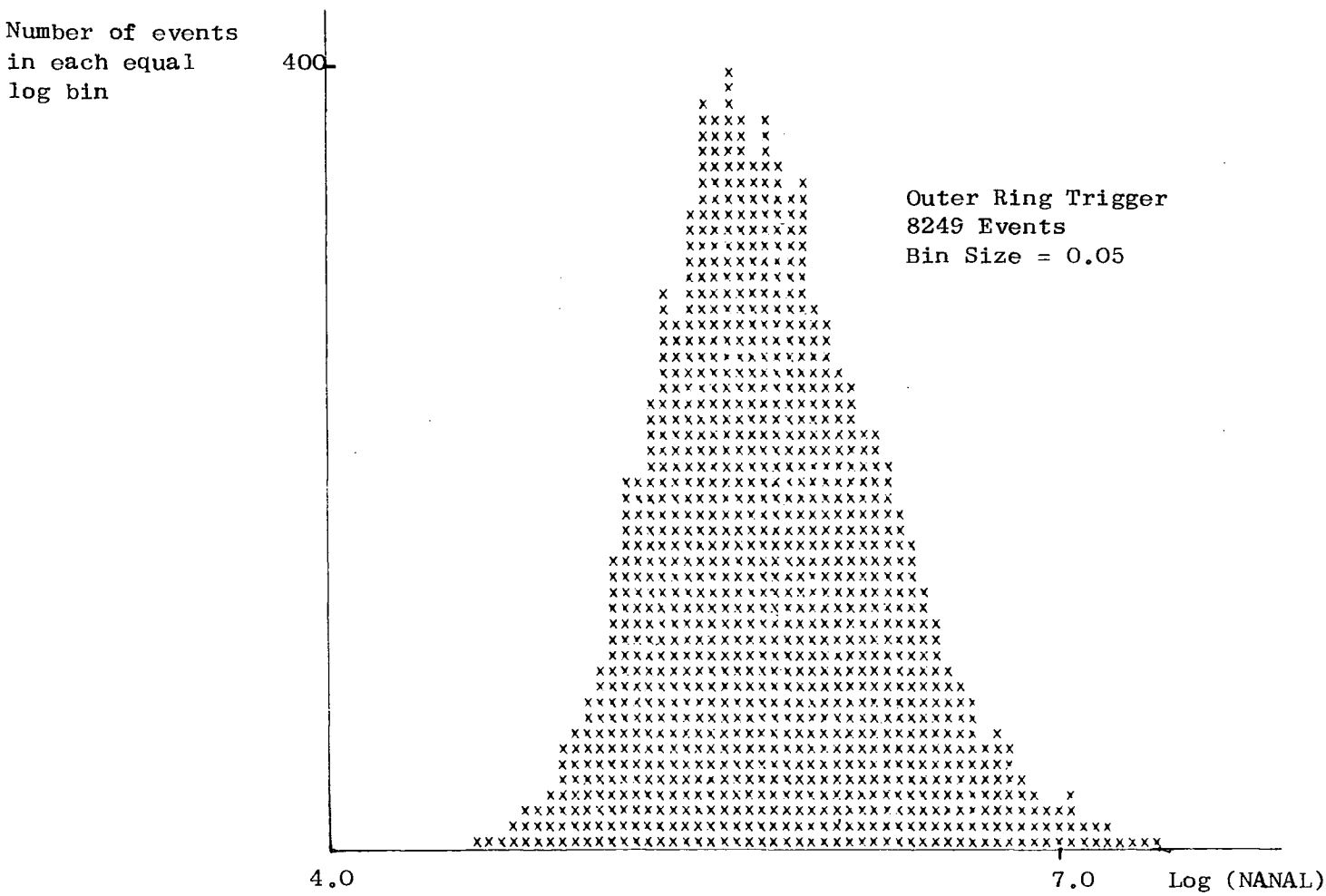

Figure 4.11: Histogram of all shower sizes returned by the analysis program for Runs 112-118

the calibration of the laboratory electronics has been described. Secondly, an outline of the approach used to validate and improve MINUIT control files is given. Finally, preliminary results serving to illustrate the operation of the current analysis programme are presented.

CHAPTER 5

THE SIMULATION PROGRAMMES

5.1 INTRODUCTION

Chapter 4 has shown that an accurate calibration of the data collection electronics, and an overall assessment of the performance of the analysis programmes, are useful in removing a certain class of biases, prior to and during, the analysis procedure. The analysed results, however, still contain biases arising from:

(a) the Array Acceptance

(b) the accuracy of the Analysis Programmes.

Each of these effects may be investigated by the simulation of air shower events on a computer, and the subsequent analysis of these data in the same manner as real data analysis. The simulation process must contain as accurate a description as possible of the real experiment, even although some of the effects included may be taken out during the subsequent analysis procedure. In addition, the simulation programme must be efficient in computer time usage, since many showers, some of small shower sizes with a low array triggering probability, may need to be generated, to adequately investigate the above biases.

5.2 THE SIMULATION PROGRAMME

A fortran coded programme, referred to as the Simulation Programme, has been written by the author to allow investigation of the post analysis biases outlined above.

Smith (Smith 1977) has presented results using the 1976 Analysis Programme to analyse simulated data in the Durham array. It was thought necessary to include a more realistic description of the laboratory electronics and array detectors in the simulation work. In addition, it was thought that improvements could be made in programme compatibility

with the current analysis programme version, programme efficiency, and flexibility of use.

Smith performed the simulation of data and subsequent analysis in a one stage process, thereby bypassing the need to include calibration effects in the simulated data, which would be taken out during the analysis. The current simulation work is a two stage process. Simulated data are generated by the programme in the same format as real data, and contains all known calibrations of both the detectors and the laboratory electronics.

Measurement errors on both timing and density data, are also included. These data may then be analysed in the same manner as real data. The pre-analysis data checking programme described in Chapter 3, may be run on the simulated raw data, allowing comparison with real data checks, and the usefulness of this technique may be investigated.

Figure 5.1 shows a flow diagram of the operation of the simulation programmes.

5.2.1 The Generation of a Shower

On entry to the programme, the user supplied data values for the simulation programme run, are read in, and any constants dependent on these data are calculated. The parameters contain the calibration information of the detectors and the laboratory electronics, the number of events required, and data specifying how the EAS are to be generated. The showers may be simulated at a constant shower size and core position, with a constant direction, or may be selected randomly from prespecified distributions describing each of the parameters (x, y, N, θ, φ) as follows.

The shower core position (x, y) is generated uniformly in a square or circular area around the array, with a shower size N selected from

Figure 5.1: Flow Diagram of the Operation of the Simulation Programmes

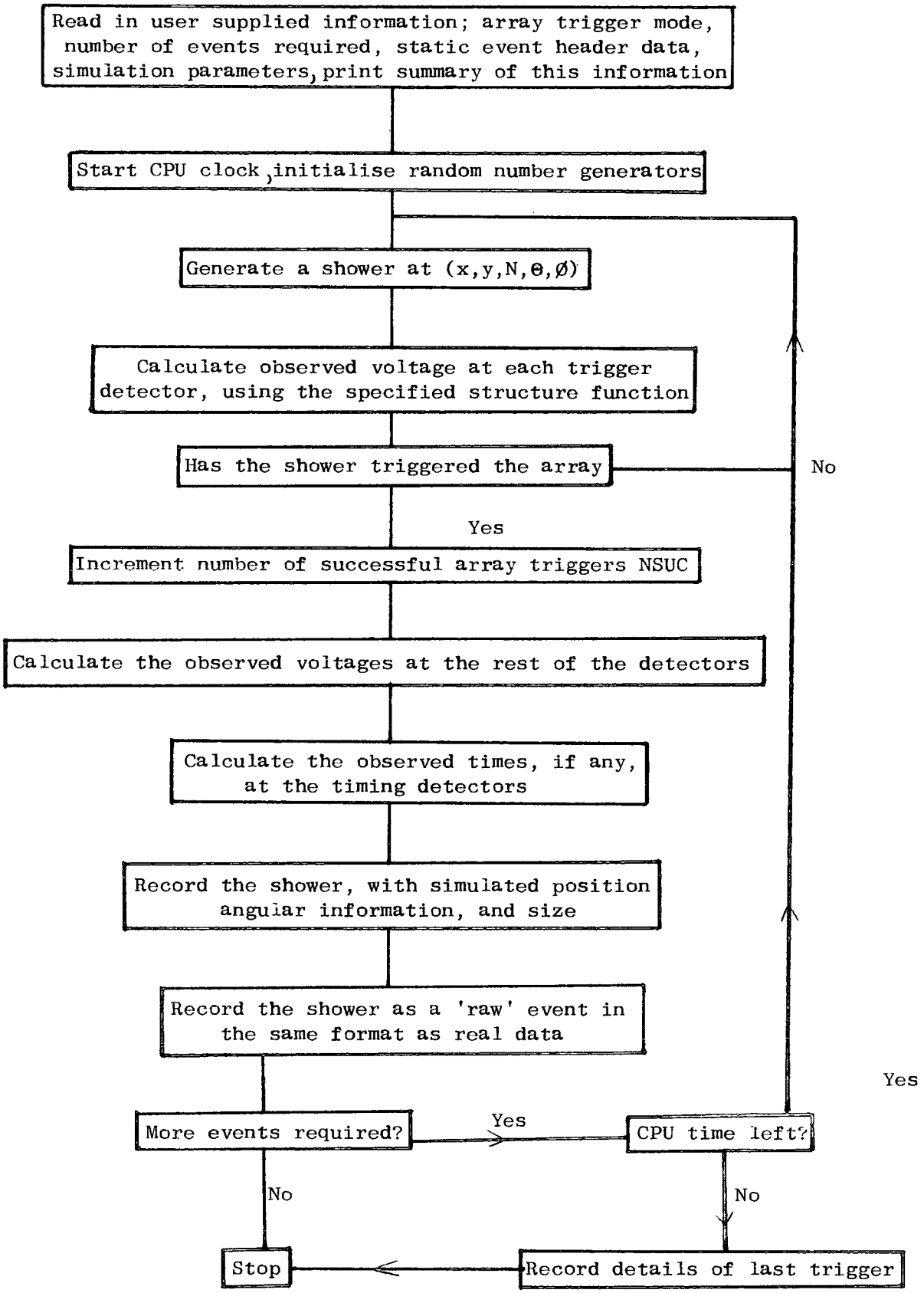

a shower size spectrum with a discrete change in slope at a prespecified break point, reflecting the 'knee' in the primary spectrum, discussed in §1.3. The zenith angle θ is selected from a probability distribution of the form $(n + 1) \sin \theta \cos^n \theta$, and the azimuthal angle φ from a uniform distribution between 0 - 2 π radians.

The technique of selection of a variable from a specified probability distribution using a computer pseudo random number generator is described in Appendix 1. The example of generating a shower size N, from a two slope shower size spectrum is given.

5.2.2 Calculation of the Observed Voltage at Each Detector

Figure 5.2 shows the sequence of calculations performed for each detector. The density at each detector site, ρ_i, is obtained by calculating the perpendicular distance between each detector and the shower axis, and using this value as input to the chosen structure function. Three well established functions have been considered for use in these simulations. The structure function due to Greisen (Greisen 1960) with an age parameter of 1.25, that due to Hasegawa (Hasegawa 1962), regarded as being appropriate for scintillator arrays, and the structure function due to Catz et al (Catz 1975).

These structure functions will be referred to as NKG, Hasegawa and Catz respectively throughout this chapter.

The actual number of particles n, passing through detector i, may then be calculated by selection of n from a poissonian distribution with a mean of $\rho_i A_i \cos \theta$, the mean number of particles passing through detector i of area A_i, at zenith angle θ. The actual voltage produced by the detector may then be selected from the appropriate 'n particle voltage distribution' for each detector. The 'Single particle distribution' discussed in Chapter 3 is represented in the simulation programmes by a Gamma type distribution

$$f(x) = e^{-x/H} x^{G-1} / H^G \Gamma(G) \qquad \text{Equation 5.1}$$

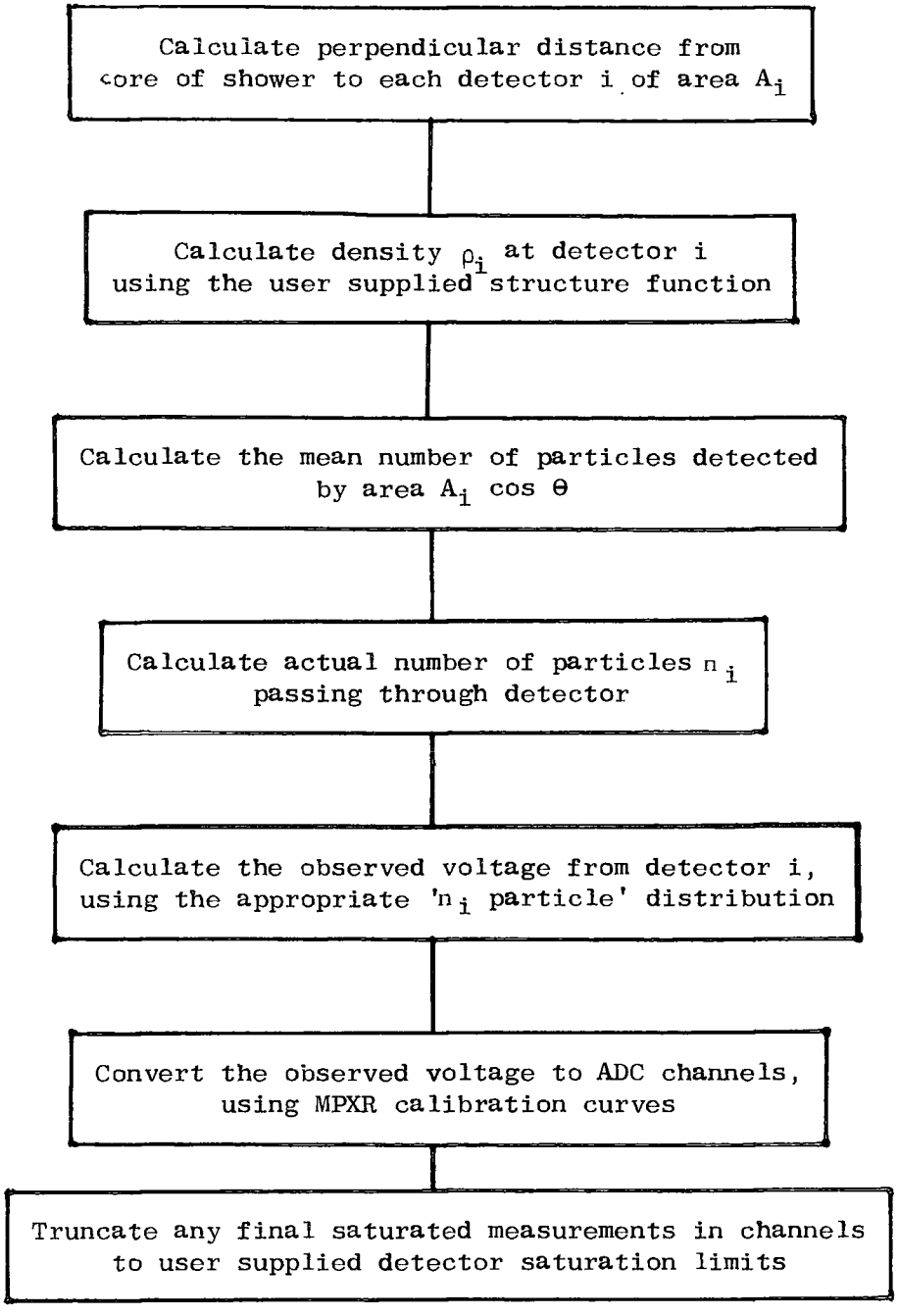

Figure 5.2: Calculation of Observed Voltage at Each Detector

where G and H are supplied by the user and determine the mean and mean/mode ratio of the resulting distribution, with an individual mean for each detector distribution according to the calibration figures discussed in Chapter 3. No attempt has been made to individually specify detector distribution shapes. An overall value for the single particle mean to mode ratio of 1.5 has been assumed, independent of detector calibration.

The 'n particle distribution' may be generated by the selection of voltages n times, from the single particle distribution, and summing the results. It was found, however, that Equation 5.1, with parameters H and nG, was an adequate representation of the 'nG particle distribution', and this was used throughout the simulations.

The measured voltages from each detector are then converted to ADC channels using the MPXR calibration curves, in a similar manner to that described in Chapter 4.

5.2.3 Timing Detector Efficiencies

Chapter 3 has discussed how an estimation of the probability of obtaining a timing pulse, versus the density measured at that timing detector, may be obtained. These probability curves, one for each timing detector, have been included in the simulation programmes to allow estimation of the effect that loss of directional information may cause in the analysis of low shower size events.

5.3 THE SIMULATIONS

The aims of the simulation work discussed in this chapter, are to investigate two broad areas:

(a) Properties of the array and biases in the data which can be investigated using the simulation programme alone, such as array acceptance and the use of bulk data checks.

(b) The performance and accuracy of the analysis programmes using simulated data as input.

A standard set of input parameter options to the simulation programme and a set of internal programme constants have been used throughout this work and are illustrated in Table 5.1.

5.3.1 The Array Acceptance Calculations

The probability of an extensive air shower triggering the array, for constant triggering conditions, is a function of the core position relative to the centre of the array, the direction of the shower and the shower size. A more useful quantity is the average probability that a shower of size N, landing within a radius R, will trigger the array. This was calculated as follows. Showers of size N were simulated with their cores uniformly distributed throughout a circular area of radius R, and their zenith angles according to a $\cos^n \theta$ distribution. The average triggering probability for this circular area and shower size, is given by the ratio of the number of successful array triggers to the total number of showers simulated. Figure 5.3 shows a graph of this triggering probability, P_{trig}, for both inner and outer ring triggers, plotted against simulated shower size N, for showers simulated within a 50 m radius of the centre of the array using the Catz structure function, and zenith angle index 8.0. The errors on the graphs are the statistical errors in the calculation of P_{trig}. Also shown for the outer ring case, is the worst case error caused by the uncertainty in the estimation of the triggering detector calibration coefficients. P_{trig} is also dependent on the structure function used in the simulation programme, the effect being most marked at low shower sizes. P_{trig} was calculated at various shower sizes, for an outer ring trigger, using the Catz, NKG and Hasegawa functions. The variation of P_{trig} with each structure function was found to increase with decreasing

Table 5.1: SIMULATION PARAMETER OPTIONS

(a) The Simulation of the Shower

Size Distribution	Constant shower size or two slope input size spectrum
Core Distribution	Constant radius or uniform core generation throughout circular or square area.
Zenith Angle Dependence (θ)	Constant θ or distribution of form $\cos^{n}\theta\ m^{-2}\ S^{-1}\ Sr^{-1}$
Azimuthal Angle Dependence (ϕ)	Constant ϕ or uniform distribution $(0, 2\pi)$
Structure Function	Catz, Hasegawa or NKG

(b) The Measurement of the Shower

Operational Units	Data for both density and timing detectors may be user specified
Trigger Criterion	'Inner' or 'Outer' ring trigger, with discrimination levels (in mV) set by user
Detector Calibrations	Detector calibration coefficients set by user
MPXR Calibration	Each channel individually calibrated
Density Measurement	Detector sampling errors assumed to be poissonian. Single particle distribution 'Mean to mode' ratio of 1.5 used
Timing Measurement	Measurement fluctuations of $\pm$ 5 ns, and each timing detector efficiency specified by user

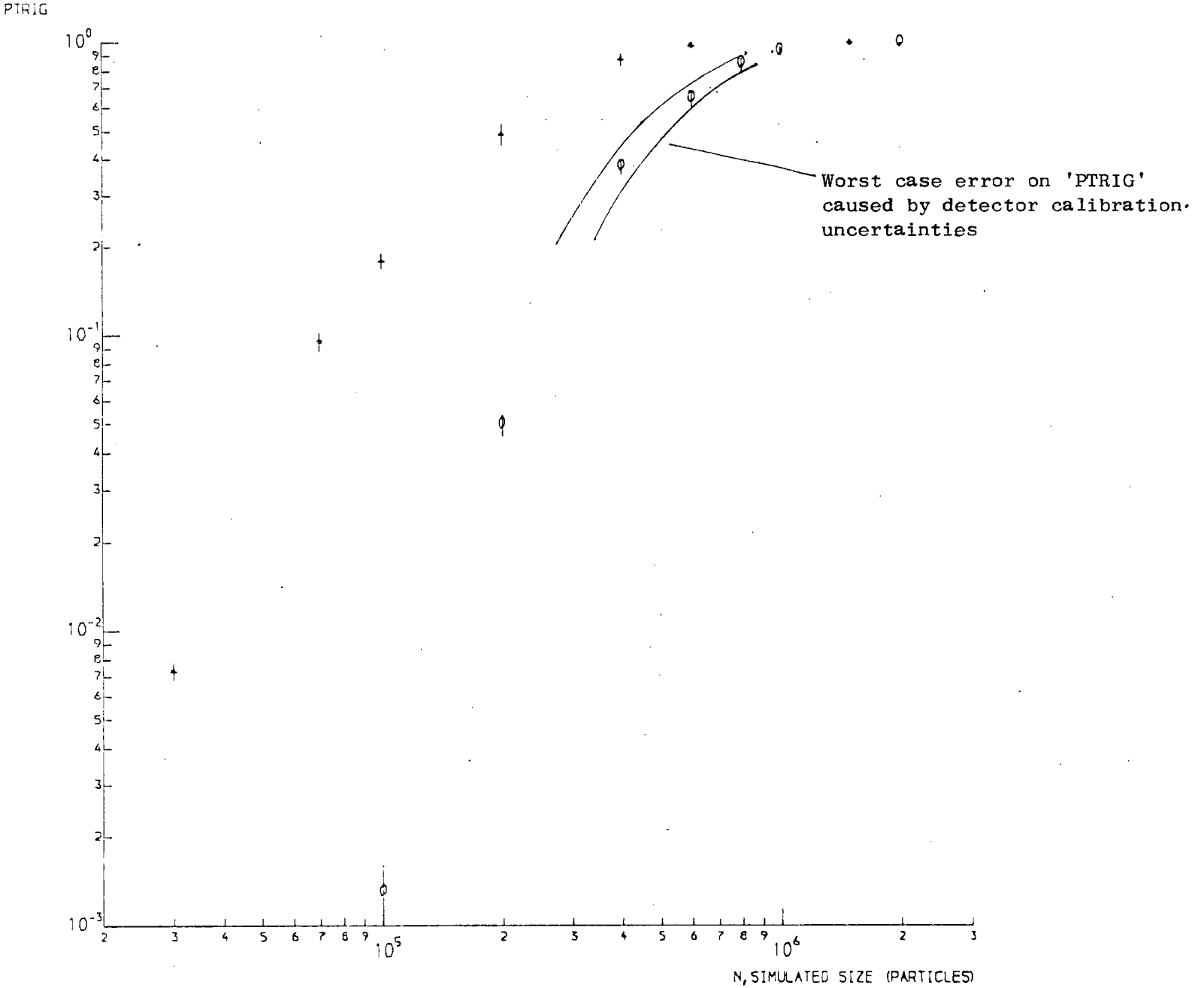

FIG 5.3 PTRIG VS N (SIMULATED SHOWER SIZE) O-OUTER RING +-INNER RING.

simulation shower size, with each of the three P_{trig} values, one calculated for each structure function, differing by a factor of 2 at a simulation shower size of 10^5 particles.

5.3.2 Simulated MPXR Input Pulse Height Distributions

Bulk data checks may be run on simulated data in the same manner as real data. The simulated data must be a result of all array triggers at all possible core positions, zenith angles, and shower sizes, as would occur in the real data case, to allow valid comparisons to be drawn. An estimation of a physically reasonable value for R, the radius of the simulation area around the array, was obtained as follows. Showers were simulated within a circular area of radius R according to the parameters outlined in Table 5.2, and the average triggering probability P_{trig} over all showers was calculated. This was repeated for various values of R. Figure 5.4 illustrates a graph of $R^2 P_{trig}$, a quantity related to the total number of successful showers, against R for both outer and inner ring triggers. The flattening of the two graphs, the inner ring case at R = 100 m, and the outer at R = 150 m, indicates that above these radii, the additional showers fired on the array have no significant effect on the final array trigger rate. These two radii, may then be used as the minimum simulation area radii, for inner and outer ring simulations respectively, in cases where simulated data must be as realistic as possible. A MPXR pulse height distribution for detector 33 obtained from data simulated under the conditions outlined in Table 5.2, with a simulation radius of 150 m is shown in Figure 5.5.

The structure function used in the simulations, was found to have little effect on the mean value or shape of any of the MPXR pulse height distributions. The MPXR pulse height distributions do, however, reflect the calibration coefficient of each detector. Figure 5.6 illustrates the variation of the mean of the MPXR pulse height distribution for detector 32, against that detector's calibration coefficient for

Table 5.2: SIMULATION PROGRAMME INPUT CONDITIONS FOR MPXR PULSE HEIGHT DISTRIBUTIONS

Spectrum	Slope 1 = -2.5 for $N < 3 \times 10^5$ particles Slope 2 = -3.5 for $N > 3 \times 10^5$ particles
Structure Function	CATZ
Trigger	Outer Ring (C, 13, 33, 53)
Calibration Information	Compatible with conditions under which runs 112-117 were collected
Index of Zenith Angle Distribution	8.0
Radius of Simulation Area	150 m

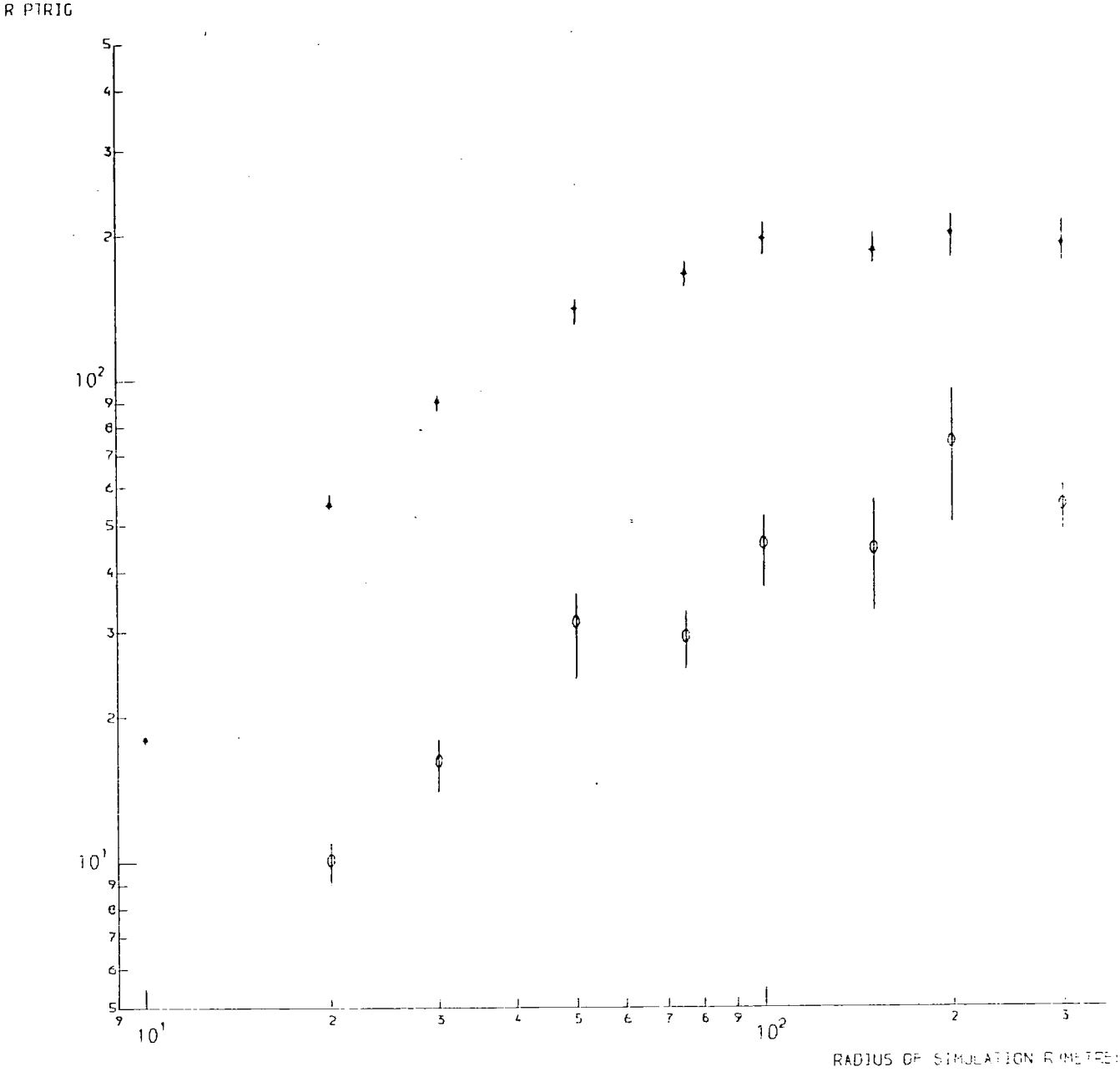

FIG 5.4 R PTRIG VS R +INNER RING TRIG O OUTER RING TRIG

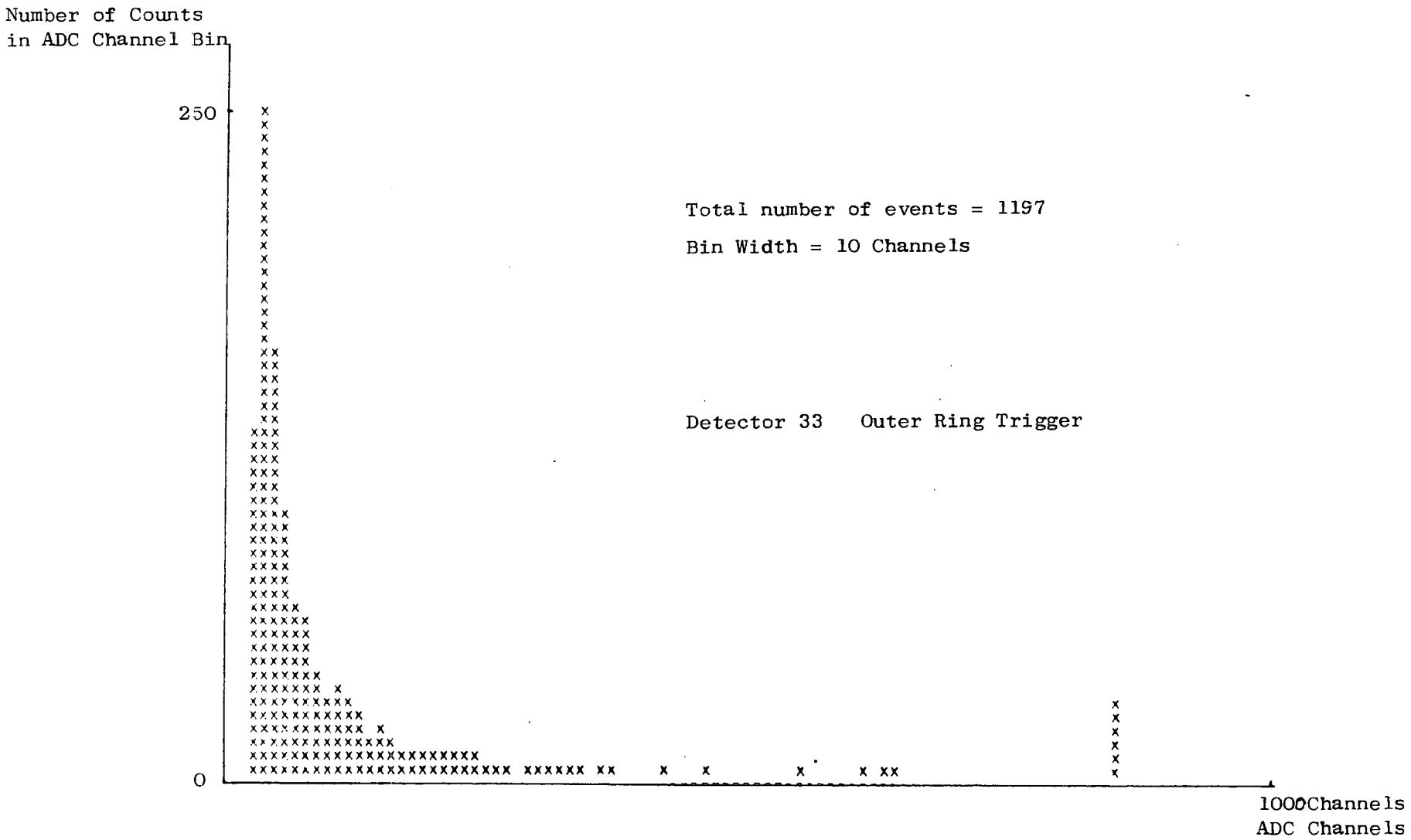

Figure 5.5: MPXR Pulse Height Distribution for Detector 33 from data simulated with the Catz Structure Function

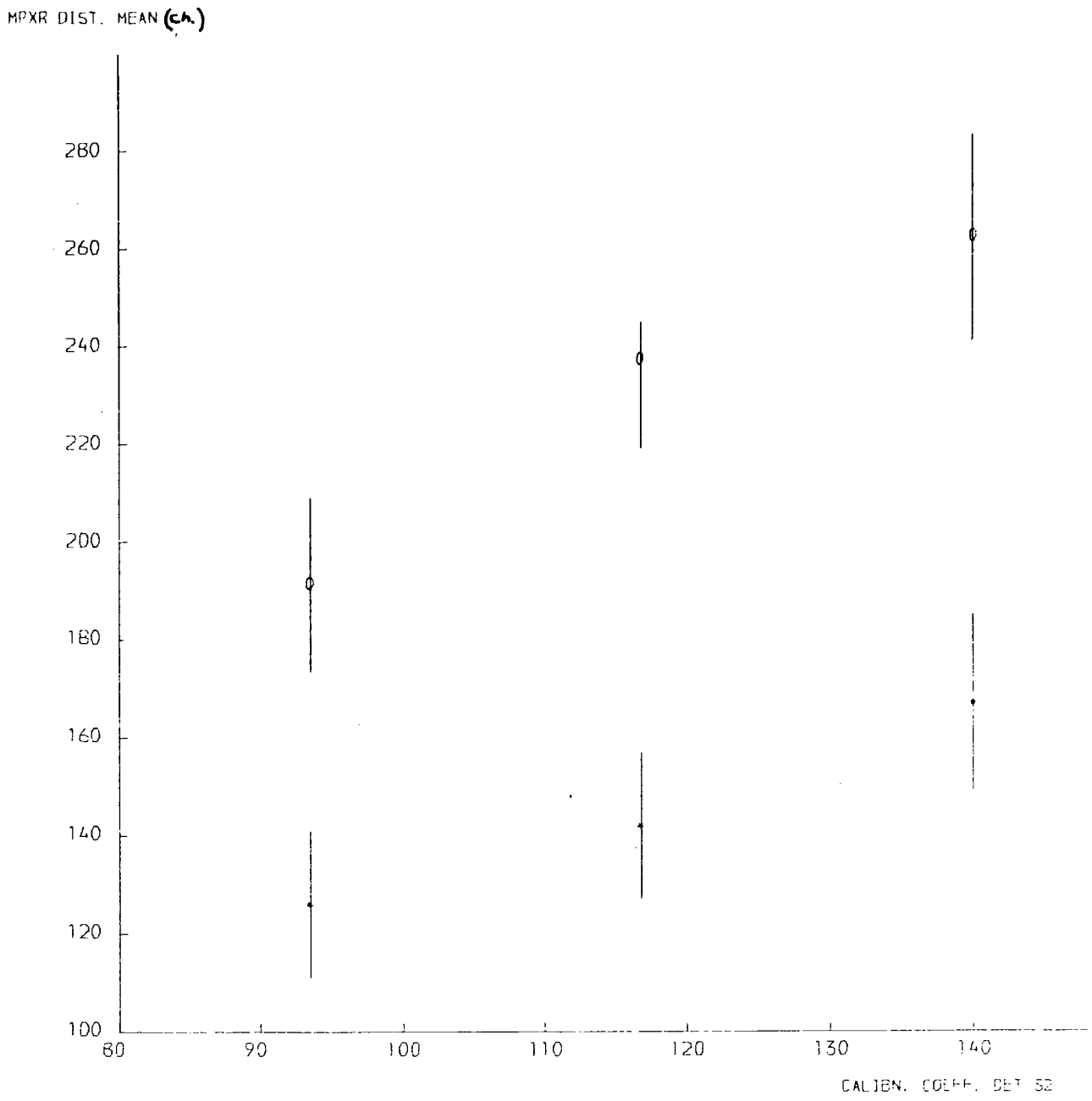

FIG 5.6 MPXR DIST. MEAN VS CALIBN. COEFF. DET 32 +INNER RING O OUTER RING

both outer and inner ring triggers. Simulations performed under similar conditions for a triggering detector, detector 33, indicate that variation of the calibration coefficient of a triggering detector produces no significant effect on the mean of the pulse height distribution of any other detector. While this result indicates that the means of the pulse height distributions may be usefully monitored throughout a long period of data collection to indicate detector calibration drift, it is felt that more detailed studies are required before the MPXR pulse height means obtained from bulk checks on real data could be used to obtain accurate estimates of the detector calibration coefficients.

5.4 ZENITH ANGLE INDEX AS A FUNCTION OF SIMULATED SHOWER SIZE

The probability that a shower will trigger the array is a function, not only of its shower size and core position, but also of its zenith angle. This effect is most marked at low shower sizes, hence the index of zenith angle distribution of array triggers, would be expected to vary with simulated shower size. This effect was measured as follows; constant size showers were simulated within a radius of 50 m of the centre of the array, with a constant zenith angle index of 8.0 using the NKG structure function. A curve of the form $(n + 1)\ \mathrm{Cos}^{n}\theta\ \sin\theta$ was fitted to the zenith angle distributions of data triggering the array, for $0^{o} < \theta < 30^{o}$, using a least squares technique. Figure 5.7 illustrates a graph of the best fit zenith angle index n versus simulated shower size NSIM. The errors on the curve reflect both the statistical error on the number of counts in the zenith angle histogram, and the accuracy of the least squares fit.

5.5 TESTING THE ANALYSIS PROGRAMME USING SIMULATED DATA

Simulated data may be used to test the accuracy of the analysis programme for both systematic and random effects. In general, showers

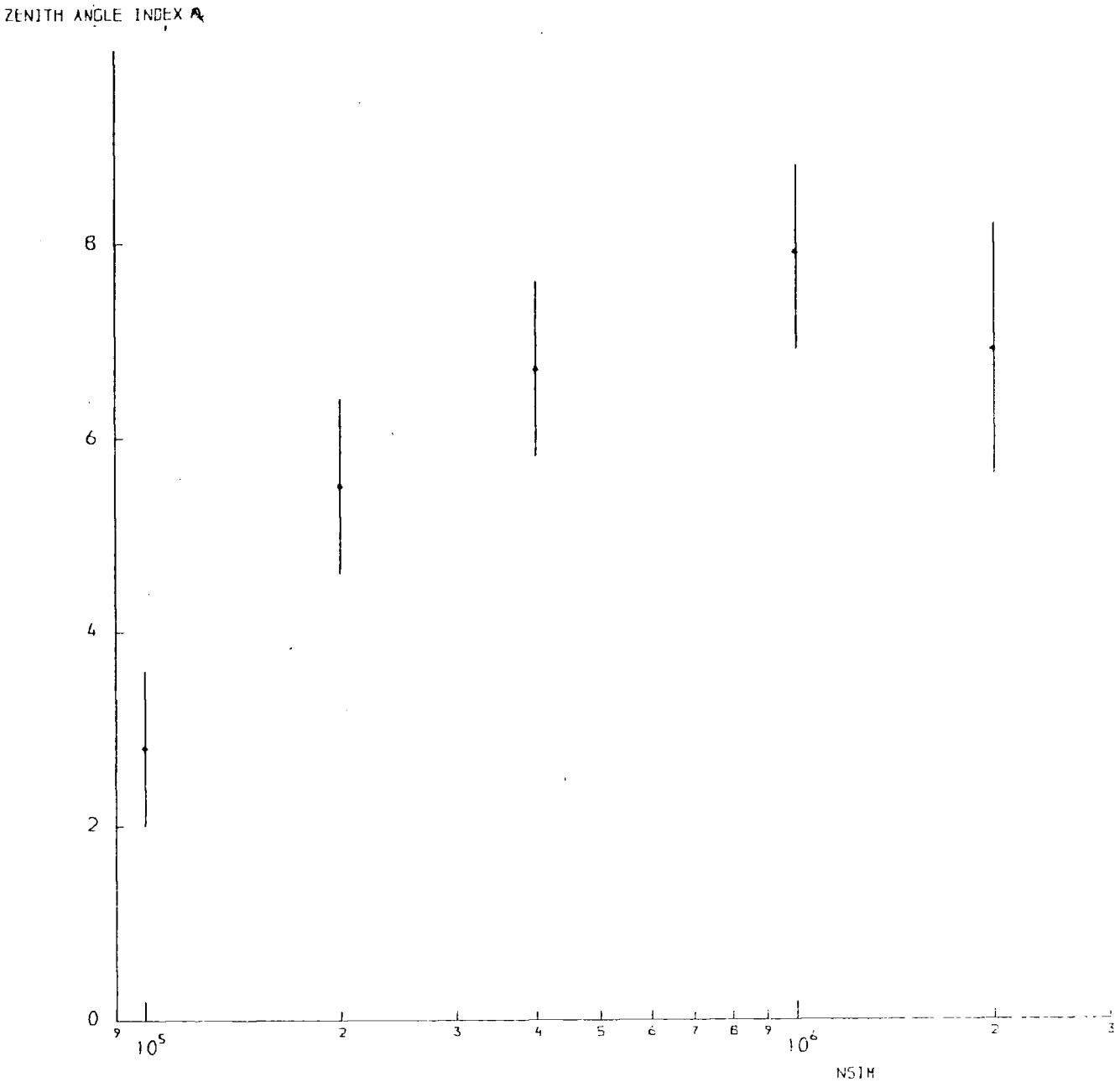

FIG 5.7 ZENITH ANGLE INDEX η VS SIMULATED SHOWER SIZE NSIM

SIMULATION ZENITH ANGLE INDEX = 8.0

THE GRAPH ILLUSTRATES THE EFFECT ON η, OF THE ARRAY TRIGGERING PROBABILITY ZENITH ANGLE DEPENDENCE, AT LOW SHOWER SIZES.

simulated with constant parameters produce a spread of analysed results, reflecting both the effect of measurement sampling errors and the performance of the analysis programmes. Data simulated under the conditions outlined in Table 5.3 have been analysed and the results used to provide information on the analysis biases, in shower direction, core position, and shower size. The estimates of these errors in analysed data, however, should be regarded as 'best case' estimates, since the technique assumes that the calibrations of all detectors and the laboratory electronics are known exactly.

5.5.1 Shower Direction

Work by Treasure (Treasure 1980) has shown that the error on the analysed zenith angle results is approximately 5^{o} for showers falling within 50 m of the centre of the array, at zenith angles less than 30^{o}, for outer ring trigger conditions. The error on the analysed azimuthal angle data is estimated to be approximately 8^{o}. There is no significant systematic bias in either case.

5.5.2 Core Location Accuracy

The core location error may be conveniently expressed as the length of the vector between a simulated and analysed core position. Figure 5.8 illustrates a graph of the mean core location error averaged over 5 m radial bias, as a function of analysed radius, for a simulated shower size of 10^{6} particles, using the Catz structure function. The results presented are for data analysed within 50 m of the centre of the array and zenith angles less than 30^{o}. Since selection has been made on the analysed radii, these figures do not include events which have been simulated within 50 m, but analysed outside this area on a MINUIT boundary. The error bars give an indication of the range of possible core location errors on any one analysed event.

Table 5.3: SIMULATION PROGRAMME INPUT CONDITIONS FOR ANALYSIS PROGRAMME TESTING

Specturm	Constant shower size, set by user
Structure Function	CATZ
Trigger	Outer Ring (C, 13, 33, 53)
Calibration Information	Compatible with conditions under which runs 112-117 were collected
Index of Zenith Angle Distribution	8.0
Radius of Simulation Area	50 m

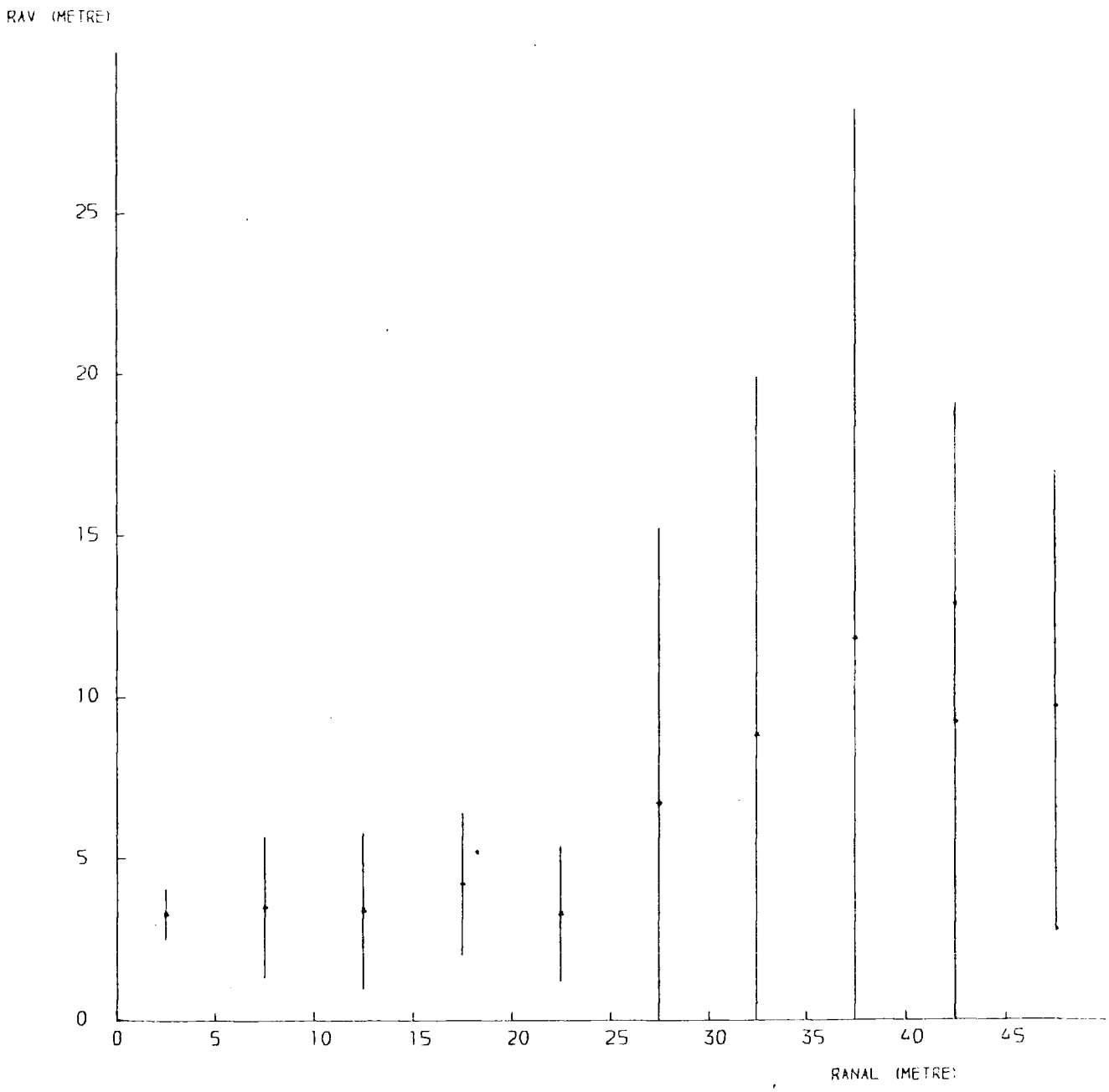

FIG 5.8 MEAN CORE LOCN. ERROR RAV, VS RADIUS RANAL FOR NSIM=10**6

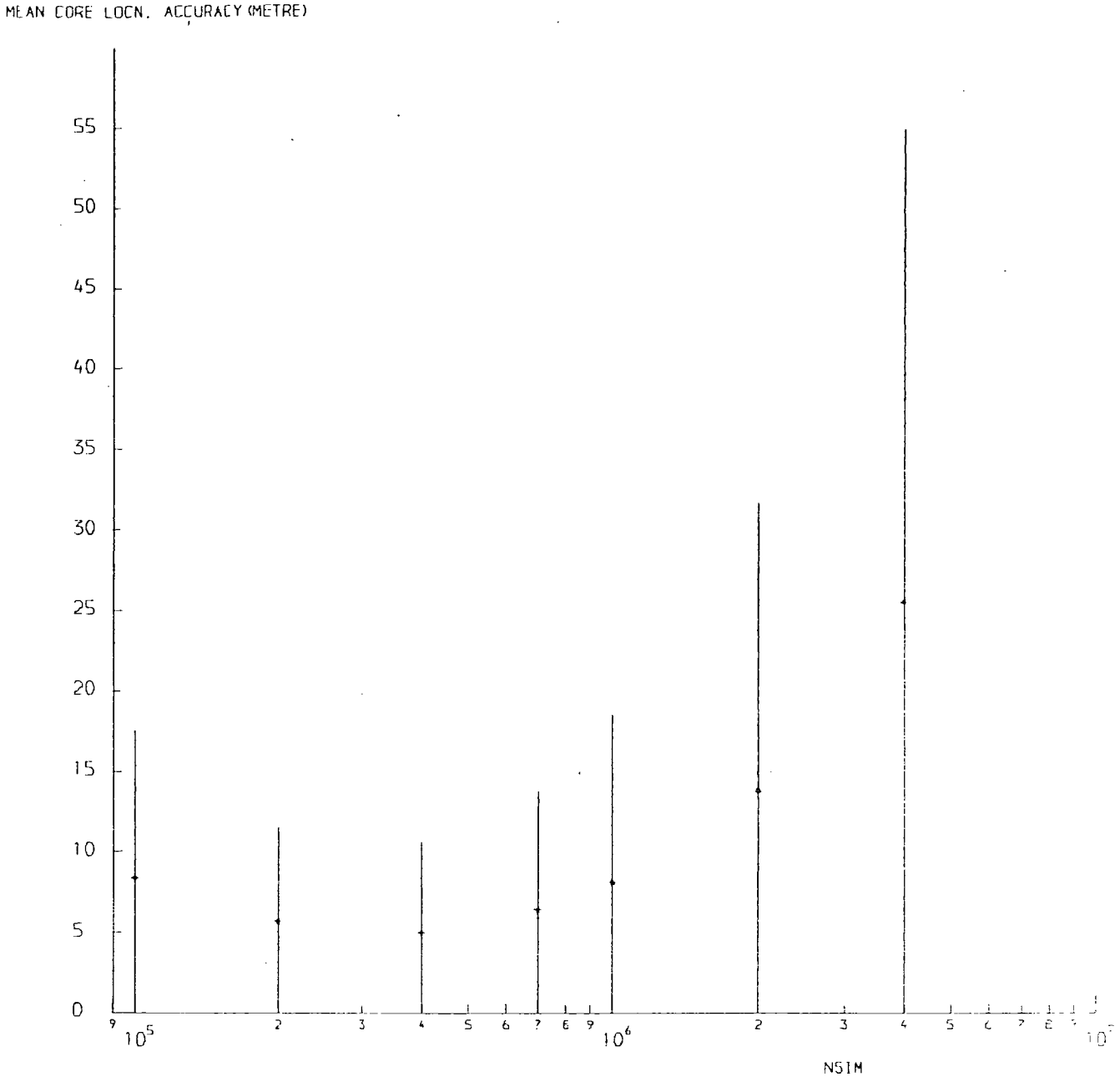

FIG 5.9 CORE LOCN ACCURACY VS SIM. SHOWER SIZE NSIM

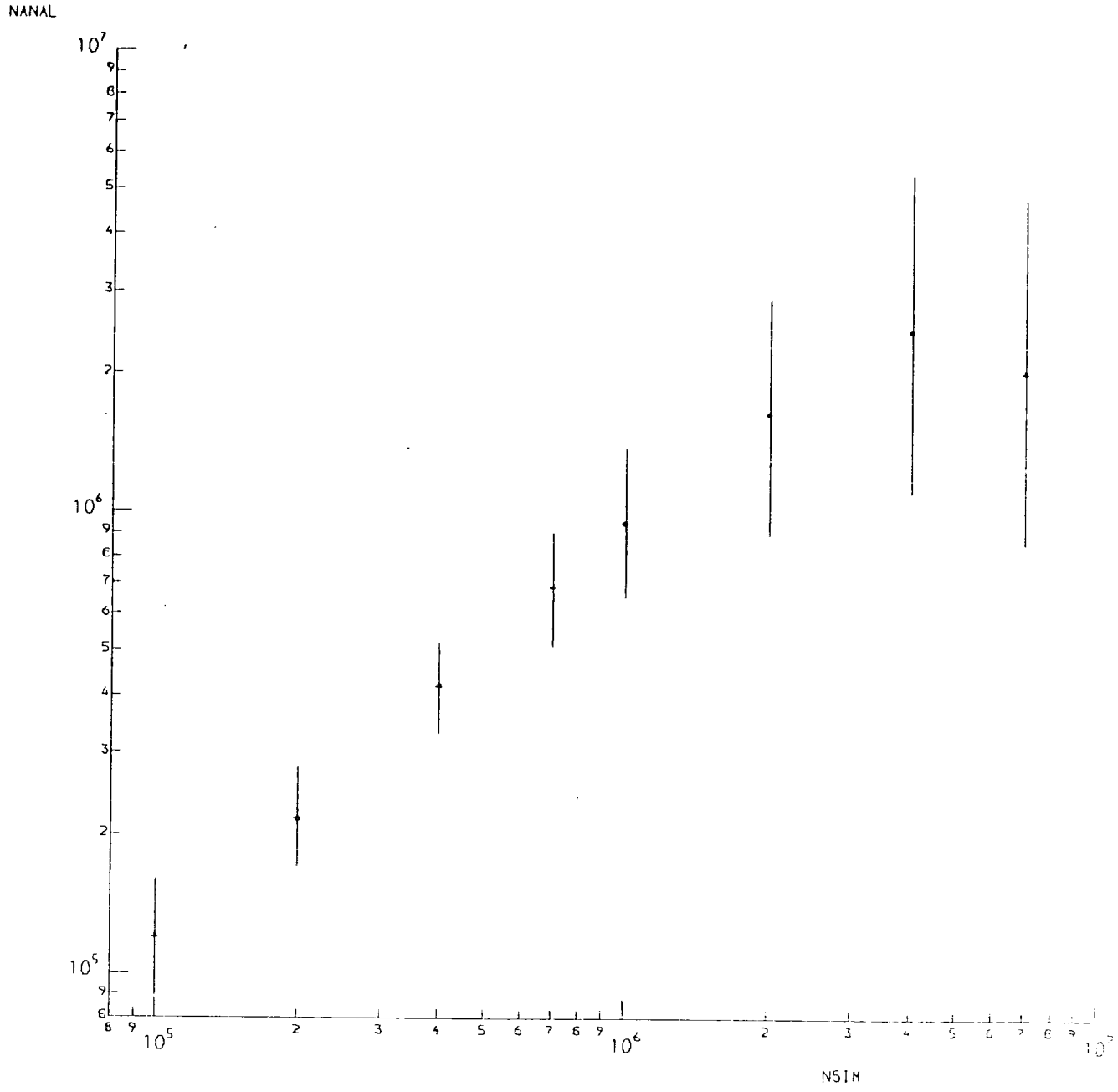

FIG 5.10 ANALYSED SHOWER SIZE NANAL VS SIMULATED SIZE NSIM

Figure 5.9 illustrates a graph of the mean core location accuracy averaged over all radii between 0 and 50 m, as a function of simulated shower size for the same selection conditions outlined above. The error bars give an indication of the core location error range in any one event, at each simulated shower size.

5.5.3 Shower Size Analysis Accuracy

A constant input simulated shower size is generally analysed to give a distribution of results with some systematic bias included. The analysis of an input shower size of 10^6 particles, simulated with the Catz structure function, results in a distribution of analysed shower sizes with a mean of 9.5×10^5 particles, and lower and upper limits of 6.5×10^5 particles and 1.4×10^6 particles respectively.

Figure 5.10 illustrates a graph of the mean analysed shower size versus input simulated shower size for data with core positions analysed within 50 m of the centre of the array, and zenith angles less than 30^o.

5.6 SUMMARY

This chapter has described how a computer simulation programme may be used to investigate the collection and analysis of data in the Durham array.

The technique of bulk data checking outlined in Chapter 3 has been investigated using simulated data. Calculations of the array acceptance have been performed and its sensitivity to the detector calibration coefficients, and simulation structure function, investigated. Finally, simulated data have been used to provide an estimate of the accuracy of the analysis programme.

CHAPTER 6
RESULTS AND CONCLUSIONS

6.1 INTRODUCTION

Chapter 5 has described how the simulation of data, and the subsequent analysis, are essential in testing the correct operation of the analysis programmes, and in giving an estimate of the accuracy of the results returned. This chapter examines the analysed air shower data in more detail in the light of the simulation work described in Chapter 5. Further simulations are used to provide an estimate of the accuracy of parameters of interest in the analysed shower data.

Finally, areas of future possible improvement, in both experimental set up, and data analysis and interpretation, are suggested.

6.2 SUMMARY OF ANALYSED DATA

The results presented in this chapter are derived from the data collected by the array between November 1976 and May 1977, which comprise a total of 8388 events collected under an outer ring trigger in a 'stand alone' mode. The total 'live' collecting time was 1761.1 hours over this period.

Certain selection conditions have been imposed on the shower data in the derivation of the parameters of interest. These conditions will be discussed in detail in the relevant sections of this Chapter. The broad restriction has been imposed that only option 4 events should be used in the derivation of all the results presented in this Chapter. This requirement reduces the number of useful analysed showers to 8274 events.

6.3 THE ANALYSIS OF TRIAL DATA

The collection and analysis of air shower data, together with the necessary selection conditions imposed on the final analysed data,

introduces biases into any derived parameters. An attempt has been made to quantify this effect as follows. Data have been simulated, using the simulation programme described in Chapter 5, under conditions which were as similar as possible to those conditions pertaining in the real data case. These simulated events were subsequently analysed using the analysis programme described in Chapter 4. The same selection conditions are applied in the derivation of parameters of interest, in the treatment of both real and simulated data, allowing an estimation of the error in the results presented.

The results in this Chapter rely heavily on the analysis of three batches of trial data, performed by Treasure (Treasure 1980). The simulation conditions for each trial, are as illustrated in Table 5.2, except that the differential shower size spectrum slope was varied between each simulation, producing analysed results referred to as SPEC 2.9, SPEC 3.0, and SPEC 3.1, from three input slopes of $\gamma = -2.9$, $\gamma = -3.0$ and $\gamma = -3.1$ respectively. A description of each of the three simulation and analysis batches is contained in Table 6.1.

6.4 THE ZENITH ANGLE INDEX

The Zenith angle dependence of EAS, caused primarily by the absorption effect by the atmosphere, is usually represented as

$$I(\theta) = I(o) \cos^n \theta \ m^{-2} \ s^{-1} \ Sr^{-1}$$

where $I(\theta)$ represents the intensity of showers at a zenith angle θ, and the index n may be a function of shower size. Care must be taken in the estimation of the index from the analysed array data, however, since the array triggering probability has a strong effect on the value of index n returned from an examination of the zenith angle distributions of showers triggering the array. This effect, illustrated in Figure 5.7 for data simulated within 50 metres of the centre of the array, is likely to be

Table 6.1: DESCRIPTION OF THE THREE TRIAL DATA RUNS

Simulation Structure Function: Catz
Index of Simulated Zenith Angle Distribution: 8.0
Array Trigger: Outer Ring

File Name	γ	Total Number of Events	Number of Option 4 Events Analysed within 50 m and 30°
SPEC 2.9	-2.9	8000	3051
SPEC 3.0	-3.0	8000	3070
SPEC 3.1	-3.1	8000	3217

present in real analysed data. It is necessary therefore to apply selection conditions to the analysed events, to provide suitable data to be used in the calculation of the zenith angle index. The requirements on the events used in these calculations are as follows:

(a) The analysed shower size NANAL, should be in the range $5 \times 10^5 < \text{NANAL} < 10^6$ particles. The lower size limit is chosen to avoid the effect caused by the array triggering probability discussed above, and the upper limit is chosen as a compromise between the desirability of presenting the result at a constant shower size, and the need to maximise the number of events in the sample.

(b) The analysed radii of showers should be less than 50 m from the centre of the array, and the analysed zenith angles in the range 0 - 30 degrees.

These conditions have also been applied to the trial data files SPEC 2.9, SPEC 3.0 and SPEC 3.1. Values of n have been calculated for the real data and each of the simulation files, using the least squares technique described in § 5.4. The values of n returned, together with an estimate of the approximate error in the fit, are illustrated in Table 6.2. These results indicate that no deductions may be made about the variation of the index with spectral slope. Assuming that the zenith angle index is independent of spectral slope, the index, based on a total of 756 outer ring trigger events, with a median analysed shower size of 6.6×10^5 particles has been calculated as:

$$n = 9.2 \pm 1.0 \text{ for } 5 \times 10^5 < \text{NANAL} < 10^6 \text{ particles.}$$

This result may be compared with the values of Ashton et al (1975) of $n = 9.3^{+1.0}_{-0.8}$ and $n = 10.0^{+1.9}_{-0.9}$ for median shower sizes of 2.7×10^5 and 5.5×10^5 particles respectively.

6.5 THE SHOWER SIZE SPECTRUM SLOPE

Chapter 5 has described how the array acceptance may be calculated as a function of simulated shower size, and that at low shower sizes, the uncertainty in the array calibrations produces a large error in the estimation of the array triggering probability. As a consequence of this, a lower limit on the range of shower sizes which may be used in the derivation of the spectral slope is imposed, of 6.3×10^5 particles, with the analysed radii and zenith angles less than 50 metres and 30 degrees respectively. These restrictions have been applied to both the real data and the three sets of trial data. The resultant events, in equal log (analysed shower size) bins, are illustrated in Table 6.3.

An attempt was made to compare the data from each of the trial spectra to the real data, using both a least squares test and a Kolmogorov-Smirnov test. (Massey 1951). These tests indicated that to observe any significant difference between each of the simulated data files, would require a data sample approximately a factor of ten greater than that available.

Preliminary simulation work indicated that the spectral slope γ may be obtained to an accuracy of $\pm$ 0.2, by a least square fit of a function of the form

$$J(N)\, dN \propto N^{-\gamma}\, dN$$

to the data available, where N represents the analysed shower size, and J(N) dN, the number of events in each shower size bin.

The value of γ obtained, however, is dependent on the upper analysed shower size limit imposed on the fit. With a lower shower size limit of Log (NANAL) = 5.8, Figure 6.1 illustrates the slopes obtained, γOUT, as a function of the upper limit, for the real data case. Each of the simulation files, SPEC 2.9 - 3.1 shows similar behaviour.

Table 6.2

VALUES OF ZENITH ANGLE INDEX RETURNED FROM LEAST SQUARES FIT ON SPEC 2.9, SPEC 3.0 AND SPEC 3.1

File Name	Simulated Index	Index Obtained From Analysed Data	Number of Events in Sample
SPEC 2.9	8.0	$6.9 \pm .7$	823
SPEC 3.0	8.0	$9.2 \pm .7$	823
SPEC 3.1	8.0	$8.3 \pm .7$	807

Table 6.3: 'SPECTRUM' EVENTS FOR REAL AND SIMULATED DATA

Log (NANAL) Log (Analysed shower size)	Number of events			
	Real data	SPEC 2.9	SPEC 3.0	SPEC 3.1
5.8 - 5.9	241	270	264	261
5.9 - 6.0	180	214	204	174
6.0 - 6.1	108	118	129	112
6.1 - 6.2	71	110	72	70
6.2 - 6.3	50	54	49	51
6.3 - 6.4	29	38	30	19
6.4 - 6.5	10	27	7	9
6.5 - 6.6	11	2	4	12
6.6 - 6.7	1	2	2	1

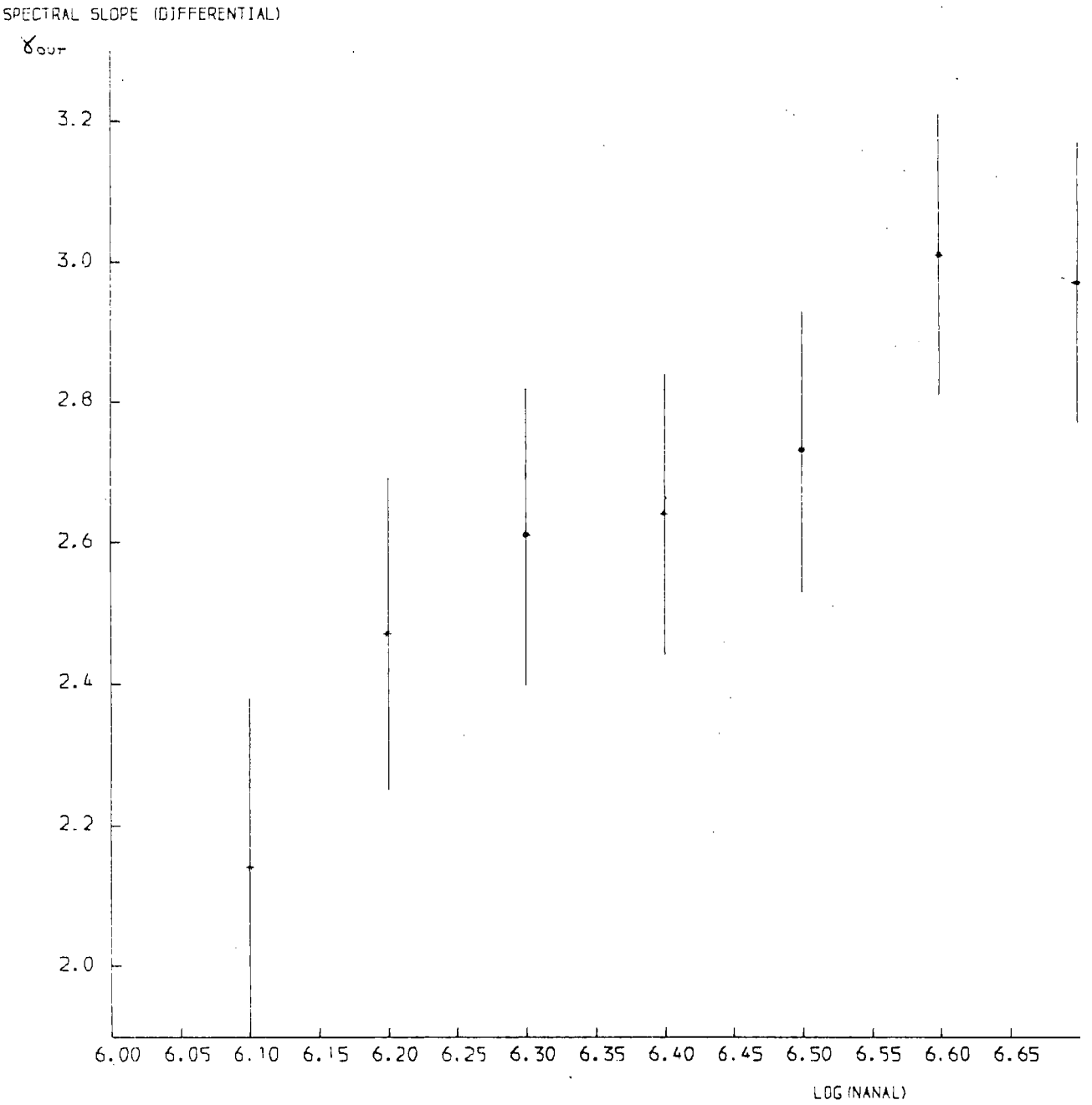

FIG 6.1 SPECTRAL SLOPE VS. UPPER SHOWER SIZE FIT LIMIT

As is illustrated in Figure 5.10, the array is not capable of the correct collection and analysis of showers larger than approximately 2×10^6 particles, due to saturation problems in the detectors caused by their limited dynamic range. The range of useful analysed shower sizes, therefore, is restricted to $5.8 < Log(NANAL) < 6.3$. Figure 6.2 illustrates the values of γ_{out} obtained for each of the trial data files SPEC 2.9 - 3.1, for this shower size range. Further simulations have shown that the error in γOUT caused by the uncertainty in the triggering probability in this range, is negligible compared to the statistical error in the fit, and that the difference between γOUT and γIN is caused primarily by the analysis programme accuracy. Using this graph, a value of

$$\gamma = 2.95 \pm 0.2$$

has been obtained for the real data, for shower sizes between 6.3×10^5 and 2×10^6, based on a sample of 650 events. Table 6.4 illustrates recent results obtained for γ by other workers.

6.6 THE WEIGHTED LEAST SQUARE DISTRIBUTION OF ANALYSED RESULTS

The distribution of the weighted least square values, returned by the analysis programme from a fit to the density data, would be expected to be similar for both real data and the trial data sets, assuming that the simulation programme is an accurate representation of the experiment. Figure 6.3 illustrates a scatter plot of least square values for real data events comprising RUNS 112-117, versus the Log of analysed shower size, NANAL, for zenith angles less than 30^o and analysed radii less than 50 m from the centre of the array. Figure 6.4 illustrates the corresponding plot for the trial data file SPEC 2.9. This plot may be taken as representative of the trial data runs, since no variation of the least square distribution was found with spectral slope. At a

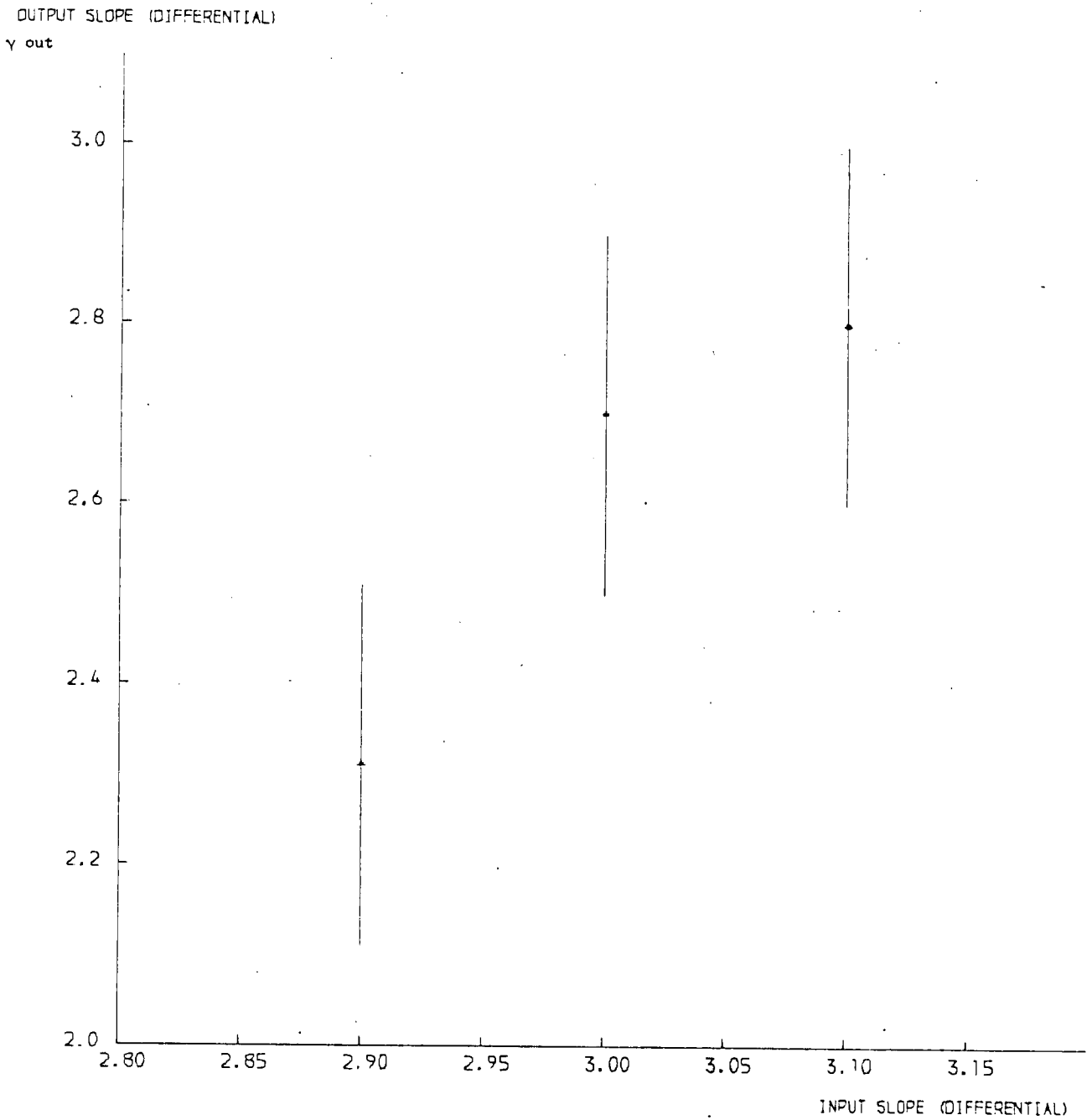

FIG 6.2 γ out, FOR SPEC2.9-SPEC3.0, 5.8 < LOG(NANAL) < 6.3

Table 6.4: Some recently reported measurements of the differential shower size spectrum slope, γ, for air showers at sea level.

Shower Size Range	γ	Reference
10^4 - 10^6	2.4 ± 0.01	Hayakawa 1969
10^6 - 10^7	3.0 ± 0.02	Hayakawa 1969
$<7 \times 10^5$	2.3 ± 0.1	Ashton et al 1975
10^5 - 10^6	2.5 ± 0.1	Khristiansen et al 1965
10^6 - 10^7	3.0 ± 0.1	Khristiansen et al 1965
10^5 - 10^6	2.59 ± 0.2	Catz et al 1975
7×10^5 - 3×10^6	2.87 ± 0.22	Rada et al 1977
10^5 - 10^6	2.61 ± 0.03	Bagge et al 1977
$>2 \times 10^6$	2.91 ± 0.03	Bagge et al 1977

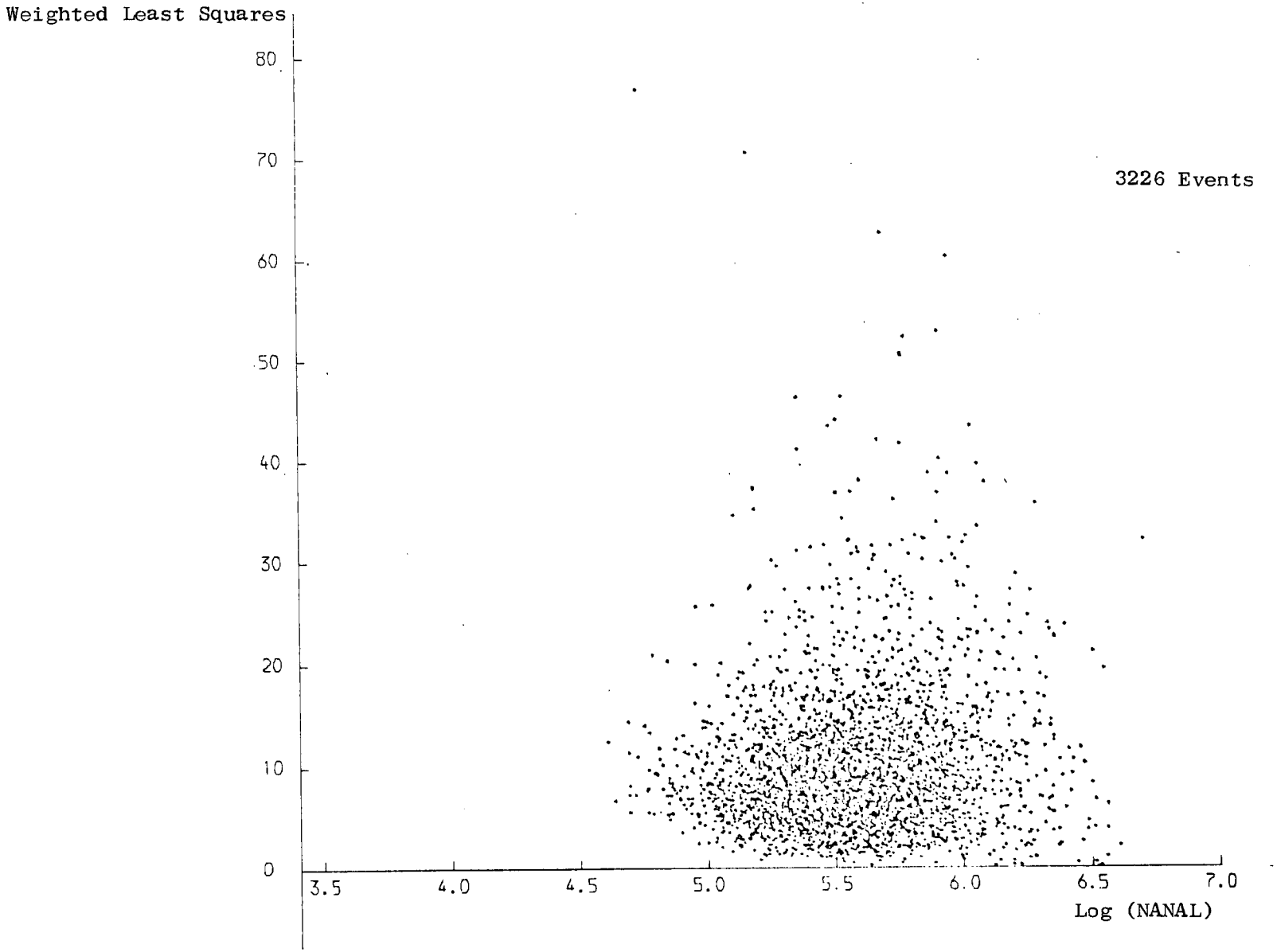

Figure 6.3: Weighted Least Square Values Vs. Log (Analysed Shower Size), for 'Selected' Real Data Events

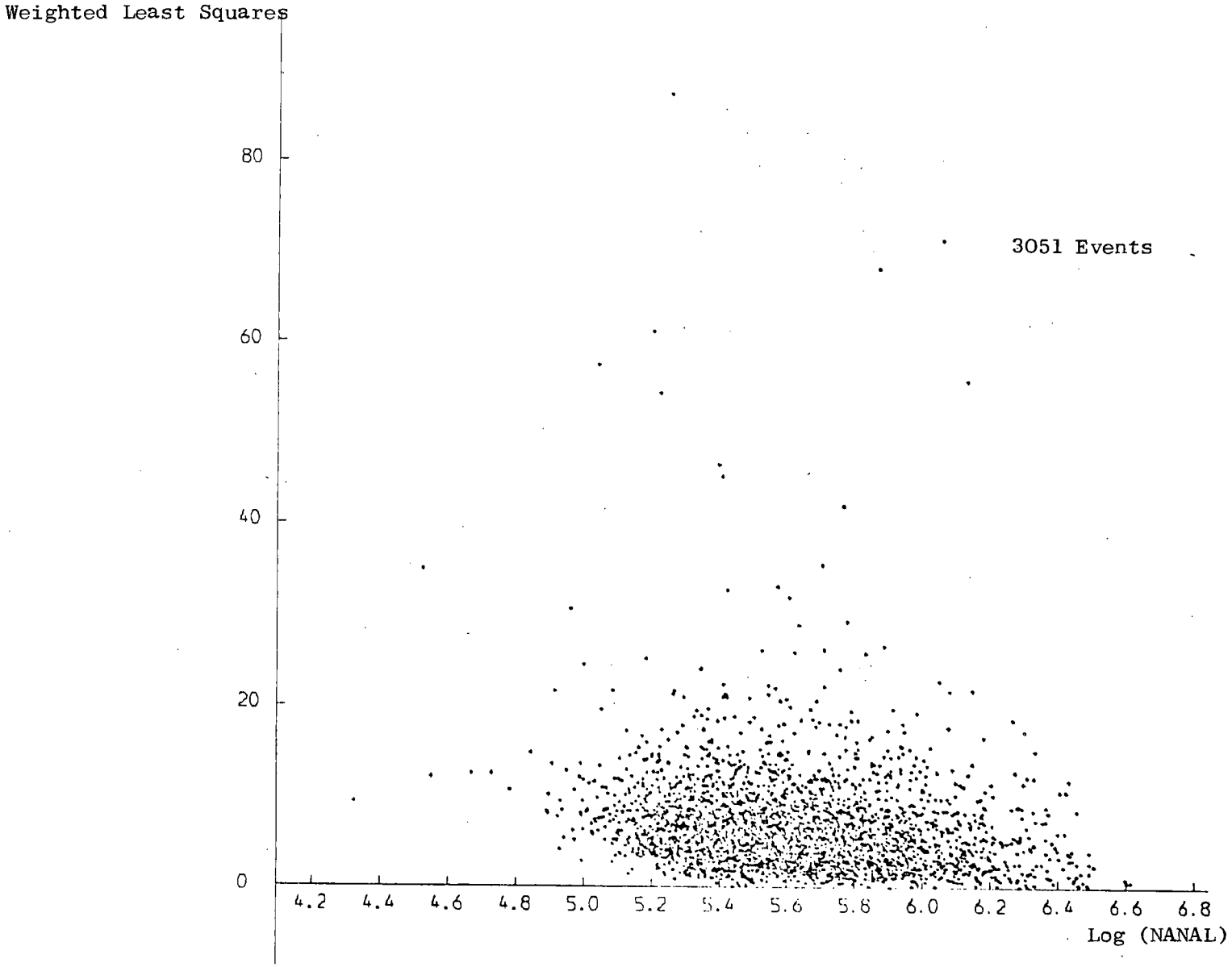

Figure 6.4: Weighted Least Square Values Vs. Log (Analysed shower size) For 'Selected' Events from SPEC 2.9

median shower size of 5.5 x 10^5 particles, for example, the mean values of the real and simulated distributions differ by a factor of 2, an indication that the simulation programme is not a realistic model of the experiment.

A limited investigation was made of the effect on the least square distribution of selected events by two factors; the structure function used for analysis, and the uncertainty in the estimation of the detector calibration coefficients.

6.6.1 The Structure Function Used For Analysis

A limitation in the simulation work described in this chapter is that the same structure function has been used for both the simulation and analysis of trial data. An attempt was made to investigate the sensitivity of the least square distribution to the structure function used in the analysis, as follows.

Approximately 300 events were simulated using the Catz structure function, at a constant shower size of 3 x 10^5 particles, under the conditions outlined in Table 5.3. These events were then analysed using the Catz, Hasegawa and NKG structure functions in turn. The resultant mean values of the least square distributions of events with analysed radii less than 50 metres and zenith angles less than 30 degrees are illustrated in Table 6.5. While there is a small variation in the distribution mean values with the structure function used in analysis, the effect is not great enough to explain the large difference observed between the real and trial data distributions.

6.6.2 The Detector Calibration Coefficients

Chapter 5 has described how the simulation programme uses as input a set of detector calibrations which are subsequently taken out during analysis. The assumption is made that the detector calibrations are

Table 6.5: DENSITY ANALYSIS, MEAN WEIGHTED LEAST SQUARE VALUES, VERSUS STRUCTURE FUNCTION AT SIMULATED SHOWER SIZE OF NSIM = 3 X 10^5 PARTICLES

Structure Function	Number of 'Selected Events'	Weighted Least Square Mean
Catz	164	6.78 $\pm$ 0.4
Hasegawa	170	7.35 $\pm$ 0.4
NKG	167	7.2 $\pm$ 0.4

	Catz	Hasegawa	NKG
Mean Analysed Shower Size (Particles)	3.2 $\pm$ .2 x 10^5	2.7 $\pm$ .2 x 10^5	3.2 $\pm$ .2 x 10^5

known exactly, for the purpose of analysis of trial data. The simulated data file described in § 6.6.1 has been analysed using 'Incorrect' calibrations, ranging from 15 and 30 per cent random errors on all the detector coefficients, to a 100 per cent error on detector C alone. While a large increase in the least square distribution was observed for all events, Table 6.6 illustrates that the likely errors in the estimation of detector calibration coefficients produces only a small increase in this mean for 'Selected' events; these events analysed within a 50 metre radius with zenith angles less than 30 degrees.

This is clearly an area of study where further simulation work would be of interest.

6.7 DISCUSSION AND CONCLUSION

This thesis deals primarily with the measures adopted to examine in detail the performance of the Durham extensive air shower experiment, from the basic hardware of the array, through to the off line analysis of the data, and to model the experiment by means of a simulation programme.

The study may be conveniently divided up into the following categories: the experiment; the analysis and simulation; and the interpretation of results. Some concluding remarks will be made about each of these in turn.

6.7.1 The Experiment

It was found during the course of the experiment that there was a clear requirement for automatic on line calibration and fault diagnosis of each detector. Other recent experiments have achieved this through varying techniques, from periodic collection of array detector pulse height distributions (Naranan 1976), to the measurement of known light output from a pulsed LED (Edge et al 1977). The simulation work,

Table 6.6: WEIGHTED LEAST SQUARE MEANS AND ANALYSED SHOWER SIZES FOR VARIOUS 'INCORRECT' DETECTOR CALIBRATIONS AT NSIM = 3.0×10^5 PARTICLES

Calibration Information	Least Square Mean	Mean Analysed Shower Size	Number of 'Selected Events'
Normal	6.78 ± 0.4	3.2×10^5	164
$\pm$ 15% random errors	6.38 ± 0.4	3.02×10^5	158
$\pm$ 30% random errors	6.76 ± 0.4	3.06×10^5	164
100% error on detector C	8.04 ± 0.4	3.02×10^5	150

described in Chapter 5 has shown that the MPXR pulse height distributions are useful and provide essential data as input to both the analysis and simulation programmes, and in addition provide a long term detector calibration check. Since, however, a minimum of approximately 2000 events are required to achieve useful accuracy, this technique may not be regarded as a replacement for on line detector calibration measurement.

Computer technology has advanced considerably since the original design in 1973 of the data collection electronics used in the array. Computers are now being used more frequently in the design and construction of EAS experiments, from simple replication of hardware functions, through the use of small but powerful programmable calculators (Orford et al 1976), to the use of medium size minicomputers for on line recording of events, the performance of diagnostic checks of both the detectors and the data collection electronics, and some preliminary processing of data, (Naranan 1976). Table 6.7 illustrates tasks which could conveniently be handled by a computer in real time, for an experiment similar to that in Durham. The range of tasks performed by the computer depends on the device chosen. A single board microcomputer with limited memory may only be required as a flexible replacement for some hardware units, whereas a multi-language interrupt driven minicomputer may be required for the servicing of the experiment in real time, operator interfaces, and some formalisation of the data checking procedures discussed in Chapter 3.

6.7.2 Data Simulation and Analysis

Chapter 4 has illustrated that the analysis programme may successfully make use of a sophisticated minimisation package, employing a variety of minimisation techniques, including that of a random search, provided care is taken in the specification of any parameters supplied as input. These

Table 6.7: DIVISION OF TASKS SUITABLE FOR REALTIME IMPLEMENTATION

Current Technique: Hardware	1130 Minicomputer	IBM Mainframe
Coincidence Monitor Event Counter 'Static' data Event clock Trigger mode Control of MPXR and ADC conversion	Daily MPXR pulse height distributions. Trigger flag analysis Service of buffer memory.	EAS rates vs. time All facilities offered by bulk data checks.

Additional Features: Programmed startup/stop procedures
Data checking formalisation
Automatic online detector/electronics calibration
Automatic runtime monitoring

parameters may be the data describing the array electronics, such as detector calibrations and saturation limits, or the control information supplied to direct the course of the minimisation procedure. Careful consideration must be given to the total computer time requirement for analysis of both real and simulated data. Where large amounts of data are to be processed, it may be necessary to consider the use of a slower dedicated minicomputer, rather than a larger time shared machine.

The technique of simulation and data analysis in a two stage process has been shown to be superior to previous techniques employed in the Durham array, and is particularly useful in the evaluation of the power of pre-analysis data checks.

6.7.3 Data Interpretation

Some limited results have been presented in this Chapter for both the simulation files and the real data file under carefully specified selection conditions. The size of the data sample clearly does not allow the use of the relaxation technique, which compares the results of the simulated shower size spectra, to the real data. Some limited results have been presented of the dependence of the shower size on the structure function used for analysis; but further work is necessary to allow an estimation of the effect that this produces in the spectral slope measured.

The poor precision of the results presented for the outer ring trigger data, is due primarily to the small number of events in the data sample, caused by the limited range of useful showers collected by the array. The triggering of the array on both the inner and outer ring detectors, will increase the collection rate of useful showers by a factor of 5, extending the lower shower size limit, imposed by the triggering probability requirement, down to approximately 2.5×10^5 particles.

Finally, the distribution of weighted least squares of analysed events is shown to be one area of discrepancy between real and simulated data. Some possible causes investigated were found to be inadequate in explaining this difference, indicating an area where further simulation and analysis of data would be of interest.

A P P E N D I X 1

(a) Computer simulation programmes using the 'Monte Carlo' technique, often require the generation of a series of random numbers, modulated according to a user specified distribution. Some common distributions are available under MTS on public disc. (See for example the *NAG manual on NUMAC). However, it is occasionally necessary for a specific distribution to be generated using as a starting point, the uniform computer random number generator F(s), $0 \leq F \leq 1$. Previous work by Smith (Smith 1976) has used the so called Laplace Method of selection of a random variable from a prespecified distribution. This was rejected as too inefficient, since every random number supplied to the generating subprogramme is not used.

The technique adopted by the author is described below. The normalised integral J(x) of the required function y(t) is formed as shown

$$J(x) = \int_0^x y(t)\,dt \Big/ \int_0^\infty y(t)\,dt \qquad \text{..... Equation (A1)}$$

A value of J(x) is generated by selection from the uniform distribution F, and x, a random variable modulated by y(t) is obtained by inversion of equation A1.

(b) Shower size spectrum example.

For a shower size spectrum of the form

$$Y(N)\,dN = AN^{-\gamma}\,dN$$

the normalised integral is given by

$$J(x) = \int_{N_L}^{x} y(N)\, dN \Big/ \int_{N_L}^{N_U} Y(N)\, dN$$

$$= \frac{N_L^{-(\gamma-1)} - x^{-(\gamma-1)}}{N_L^{-(\gamma-1)} - N_U^{-(\gamma-1)}}$$

where N_L and N_U are the smallest and largest shower sizes of interest. A spectrum with two slopes γ_1 and γ_2 and break point N_{BK}, may be treated in a similar manner. The normalised integral J(x) becomes

$$J(x) = \int_{N_L}^{x} y(N)\, dN \Big/ \text{XORM} \qquad \text{..... Equation A2}$$

where

$$\text{XORM} = \int_{N_L}^{N_{BK}} A_1 N^{-\gamma_1}\, dN + \int_{N_{BK}}^{N_U} A_2 N^{-\gamma_2}\, dN$$

x may be found by inversion of equation A2, where y(N) has the appropriate form depending on the value of x relative to N_{BK}.

R E F E R E N C E S

(PICCR = Proceedings of the International Conference on Cosmic Rays)

ADCOCK, C., et al, J. Phys. A;Gen. Phys.,3, (1970), 697

ADCOCK, C., et al, J. Phys. A;Gen. Phys.,4, (1971), 276

ANDERSON, C., and NEDDERMEYER, S.H., Phys. Rev., (1936), 50, 263

ASHTON, R., et al, PICCR Munich, 8, (1976), 2719

ASHTON, R., et al, PICCR Plovdiv, 8, (1977), 1

AUGER, P., et al, Revs. Mod. Phys., 11, (1939), 288

AYRE, C.A., Ph.D. Thesis, University of Durham, (1971)

BAGGE, E.R., et al, PICCR Plovdiv, 8, (1977), 34

BELL, C.J., et al J. Phys. A,7, (1974), 990

BOTHE, W., and KOLHÖRSTER, W.,S., Phys., 56, (1929), 751

CATZ, P.H., et al, PICCR Munich, 12, (1975), 4329

CLAY, J., Proc. Roy. Acad. Amsterdam, 30,(1927), 1115

COCCONNI, G., KOESTER, L.J., and PERKINS, D.H., URCL High Energy Phys. Study Seminars, 28, Part 2, UCID, (1961), 1444

COOPER, D.A., Ph.D. Thesis, University of Durham, (1974)

DAKE, S., et al, PICCR Hobart, 3, (1971), 948

DAVIDON, D., et al, Computer Journal, 6, (1963), 163

EDGE, D.M., et al, J. Phys. A,6, (1973), 1612

EDGE, D.M., et al, PICCR Plovdiv, 9, (1977), 137

ELSTER, J., and GEITEL, H., Physik, Z., 1,(1899), 11

ELBERT, J.W., et al, J. Phys. A;Math. Gen., 8,1, (1975), L13

FROMAN, D.K., and Stearns, J.C., Revs Mod. Phys., 10, (1938), 133

GOLDSTEIN, A.A., and PRICE, J.F., Math. Comp., 25, (1971), 569

GREIDER, P.K.F., PICCR Plovdiv, 8, (1977), 376

GREISEN, K., Ann. Rev. Nucl. Science, 10, (1960), 63

GREISEN, K., Phys. Rev. Lett., 16, (1966), 748

HASEGAWA, H., et al, J. Phys. Soc. Japan, 17, A111, (1962), 189

HAYAKAWA, S., Cosmic Ray Phys. (Monographs and Texts in Phys. and Astronomy Vol. XXII, Wiley Interscience), (1969), 467

HESS, V.F., Physik Z., 13, (1912), 1084

JAMES, F., and ROOS, M., Comp. Phys. Comm., 10, (1975), 343

JULIUSSON, E., PICCR Munich, 8, (1975), 2689

KARAKULA, S., et al, J. Phys. A;Math, Nucl. Gen., 7, (1974), 437

KEMPA, J., WDOWCZYK, J., Wolfendale, A.W., J. Phys. A, 7, (1974),1213

KOLHÖRSTER, W., et al, Naturwissenschaften, (1938), 26, 1721

KHRISTIANSEN, G.B., et al, PICCR London, 2, (1965) 799.

MALHOTRA, P.K., et al, Nature, 209, (1966), 567

MASSEY, F.J., J. American Statistical Assoc., 46, (1951), 68)

MILLIKAN, R.A., and CAMERON, G.H., Phys. Rev., 28, (1926), 851

NARANAN, S., et al, PICCR Munich, 9, (1975), 3346

NELDER, J.A., and MEAD, R., Computer Journal, 7, (1964), 308

ORFORD, K.J., STUBBS, R.J., PICCR Munich, 9, (1975), 3406

RADA, W.S., et al PICCR Plovdiv, 8, (1977), 13

ROLL, P.G., and WILKINSON, D.T., Phys. Rev. Lett., 16, (1966), 405

SHAAT, E.A.M., Ph.D. Thesis University of Durham, (1979)

SMITH, A.C., Ph.D. Thesis, University of Durham, (1976)

SMITH, A.C., Nucl. Inst., Meth., 145, (1977), 289.

STRONG, A.W., WDOWCZYK, J., Wolfendale, A.W., J. Phys. A, 7, (1974), 1489

TREASURE, M.W., Ph.D. Thesis, University of Durham, (1980)

WHALLEY, M.R., Ph.D. Thesis, University Durham, (1974)

WILLIAMS, R.W., Phys. Rev., 74, (1948), 1689

WOLFENDALE, A.W., Cosmic Rays, at ground level, (Ed. Wolfendale, A.W., The Institute of Physics, London), (1973).

Addenda

JOHNSON, T.H., and STREET, J.C., Phys. Rev., 43, (1933), 381

BELL, M.C., Ph.D. Thesis, University of Durham, (1974 (6))

WDOWCZYK, J., WOLFENDALE, A.W., J. Phys. A, 6, (1973), 1594

FEYNMAN, R.P., Phys. Rev. Lett., 23, (1969), 1415

A C K N O W L E D G E M E N T S

The author would like to thank Professor A. W. Wolfendale for the use of the Physics Department's well equipped laboratories and for continued interest in the project.

The author is grateful to his supervisor, Dr. M. G. Thompson, for guidance throughout the work. Members of the MARS group are thanked for their constant help and advice. In particular, Mr. M. W. Treasure is thanked for his frequent detailed discussions at all stages of the development of the project.

Mr. K. Tindale is especially thanked for his assistance and advice in the technical matters of the experiment.

Thanks go to Miss C. Plummer for the typing of this thesis.

Finally, the Science Research Council is thanked for the provision of computing facilities and a studentship.